Physics 373
April 2005

α-Particle Spectroscopy with Si

Purpose: Learn about α-particle spectroscopy techniques using solid-state Si detectors. Understand α-particle decays and how levels are how daughter products can also be a source of α particles.

Overview: We will be studying α particles from a source which was originally pure ^{226}Ra.

Goals:

- Understand the α-particle decay of ^{226}Ra and its daughter products.
- Understand the logic of the electronics used, the purpose of each module employed, and the setup of timing, gates, gains.
- Understand the features of the energy spectrum.
- Perform an energy calibration for the detector using the energies of known peaks.
- Determine the energy resolution for the detector.
- Determine the activity of the source.
- Identify the daughter products from their Q-values and intensity.
- Determine the age of source, relative to the time when it was pure ^{226}Ra.
- Keep a detailed logbook of all relevant details.
- Access the literature to determine the expected properties of each isotope.
- Prepared a detailed formal laboratory report on these investigations.

For the first day in the lab:

- Read all of the background material beforehand.
- Understand the list of goals.
- Begin to familiarize yourself with the experimental setup.
- Try to understand each part of the system.
- Become familiar with the the oscilloscope and use it to look at the linear and logical signals and various points in the setup.
- Learn about how the digitized signals are stored in the computer.

Your Brief Technical Report Should Include:

- A plot of the α spectrum.
- A table of Energies and Channels for the peaks observed.
- A plot of Energy versus Channel for the peaks observed.
- Identification of the peaks observed.
- Determine the energy calibration of the detection system.
- Determine the energy resolution of the detection system.
- Determine the number of ^{226}Ra atoms present in the source.
- Determine the age of source, relative to the time when it was pure ^{226}Ra.

Appendix 1: Decay of ^{226}Ra

88-Ra-226 Radium-226
Half-life: 1600 years
Mode of decay: alpha into Rn-222
Decay energy: 4.871 MeV ← to excited state
Subsequently γ radiation of Rn-222 at 186 keV possible

86-Rn-222 Radon-222, noble gas
Half-life: 3.8235 days
Mode of decay: alpha into Po-218
Decay energy: 5.590 MeV

84-Po-218 Polonium-218 (Historically Po-218 is also called radium A)
Half-life: 3.10 minutes
Mode of decay: alpha into Pb-214
Probability: 99.98 %
Decay energy: 6.115 MeV
Mode of decay: beta into At-218
Probability: 0.02 %
Decay energy: 0.265 MeV

85-At-218 Astatine-218
Half-life: 1.5 seconds
Mode of decay: alpha into Bi-214
Probability: 99.90 %
Decay energy: 6.874 MeV
Mode of decay: beta into Rn-218
Probability: 0.1 %
Decay energy: 2.883 MeV

86-Rn-218 Radon-218
Half-life: 35 milliseconds
Mode of decay: alpha into Po-214
Decay energy: 7.263 MeV

82-Pb-214 Lead-214 (Historically Pb-214 is also called radium B)
Half-life: 26.8 minutes
Mode of decay: beta into Bi-214
Decay energy: 1.024 MeV
Subsequently γ radiation of Bi-214 at 352 keV, 295 keV, 242 keV, 53 keV possible

83-Bi-214 Bismuth-214 (Historically Bi-214 is also called radium C)
Half-life: 19.9 minutes
Mode of decay: beta into Po-214
Probability: 99.98 %
Decay energy: 3.272 MeV
Subsequently γ radiation of Po-214 at 609 keV possible
Mode of decay: alpha into Tl-210
Probability: 0.02 %
Decay energy: 5.617 MeV

84-Po-214 Polonium-214 (Historically Po-214 is also called radium C')
Half-life: 164.3 ms
Mode of decay: alpha into Pb-210
Decay energy: 7.833 MeV

81-Tl-210 Thallium-210 (Historically Tl-210 is also called radium C")
Half-life: 1.3 Minutes
Mode of decay: beta into Pb-210
Decay energy: 5.484 MeV

82-Pb-210 Lead-210 (Historically Pb-210 is also called radium D)
Half-life: 22.3 years
Mode of decay: beta into Bi-210
Decay energy: 0.064 MeV
Mode of decay: alpha into Hg-206
Probability: 1.9E-6 %
Decay energy: 3.792 MeV

83-Bi-210 Bismuth-210 (Historically Bi-210 is also called radium E)
Half-life: 5.013 days
Mode of decay: beta into Po-210
Decay energy: 1.163 MeV
Mode of decay: alpha into Tl-206
Probability: 0.00013 %
Decay energy: 5.037 MeV

84-Po-210 Polonium-210 (Historically Po-210 is also called radium F)
Half-life: 138.376 days
Mode of decay: alpha into Pb-206
Decay energy: 5.407 MeV

82-Pb-206 Lead-206 (Historically Pb-206 is also called Radium G)
Pb-206 is the final product of the U-238 radioactive series. It is stable. This lead is dead!

The entries are taken from the NUDAT database, see:

R.R.Kinsey, et al.,The NUDAT/PCNUDAT Program for Nuclear Data, paper submitted to the 9th International Symposium of Capture Gamma-ray Spectroscopy and Related Topics, Budapest, Hungary, October 1996. Data extracted from NUDAT database (Dec.18, 1997).

Physics 373
May 2005 / May 2007

Some Remarks on Determining the "age" of a ^{226}Ra Source

Assuming that one starts with pure ^{226}Ra, it is possible to determine its "age" (defined here to be the time since it started life in a pure state) by observing the decays of its daughter products. First note that all the decay half-lives are very short (less than one week), except for two: the initial ^{226}Ra decay ($t_{1/2} = 1600$ years) and the the ^{210}Pb decay ($t_{1/2} = 22.3$ years).

The number of ^{226}Ra atoms N_A present in the source is a function of time t and is described by

$$N_A = N_0 \exp(-t/\tau_A), \tag{1}$$

where $N_0 = N_A(0)$ and τ_A is the mean lifetime of ^{226}Ra given by $t_{1/2}/\ln 2$. The decay rate of ^{226}Ra is given by

$$-\frac{dN_A}{dt} = N_A/\tau_A. \tag{2}$$

I will assume $t = 0$ when the source was made. Note that $\frac{dN_A}{dt}$ is a quantity that you can measure in the laboratory and can be used to determine N_A.

Once the source is several weeks old, an equilibrium is established. Consider for example ^{222}Rn. In equilibrium, this isotope is produced at essentially the same rate as which is it decays – this must be the case because every ^{222}Rn which is created decays shortly thereafter. This same argument can be applied to all of the other isotopes in the decay chain which have short half-lives (i.e. less than one week). Unfortunately, these decays don't tell us anything about the age of the source.

For ^{210}Pb and ^{206}Pb we have to be a little bit more careful. Once the source is several weeks old, ^{210}Pb is produced at the same rate as ^{226}Ra decays. However, ^{210}Pb decays with a 22.3-year half-life. We can describe the number of ^{210}Pb atoms N_B as a function of time via:

$$\frac{dN_B}{dt} = -\frac{dN_A}{dt} - \frac{N_B}{\tau_B} \tag{3}$$

$$= \frac{N_0}{\tau_A}\exp(-t/\tau_A) - \frac{N_B}{\tau_B}. \tag{4}$$

The first term in this equation describes the creation of N_B by the decays of parent nuclei and the second term describes the decay of N_B due to its own half-life (τ_B is the mean lifetime of ^{210}Pb).

This is a differential equation. It can be solved by "guessing" the answer:

$$N_B = A\exp(-t/\tau_A) + B\exp(-t/\tau_B), \tag{5}$$

Where A and B are arbitrary constants. If we start with a pure ^{226}Ra source that means we have zero ^{210}Pb initially so we have $N_B(t = 0) = 0$, i.e. $A = -B$. We can determine A by substituting in Eq. (4); the final result is:

$$N_B = \frac{N_0}{\tau_A/\tau_B - 1}\left[\exp(-t/\tau_A) - \exp(-t/\tau_B)\right]. \tag{6}$$

The quantity N_B *does* tell us something about the age of the source. Unfortunately neither N_B or its decay rate can be measured directly with our setup (^{210}Pb decays by β emission).

We can apply the equilibrium argument to decays following ^{210}Pb. In particular, the decay rate of ^{210}Po is equal to the decay rate of ^{210}Pb once the source is several weeks old. The nucleus ^{210}Po decays by α emission – something which we can measure. In addition the ^{210}Po decay rate is just given by $\frac{N_B}{\tau_B}$ – something we can calculate from Eq. (6)! The comparison can be used to determine t – the age of the source.

Electronics Setup

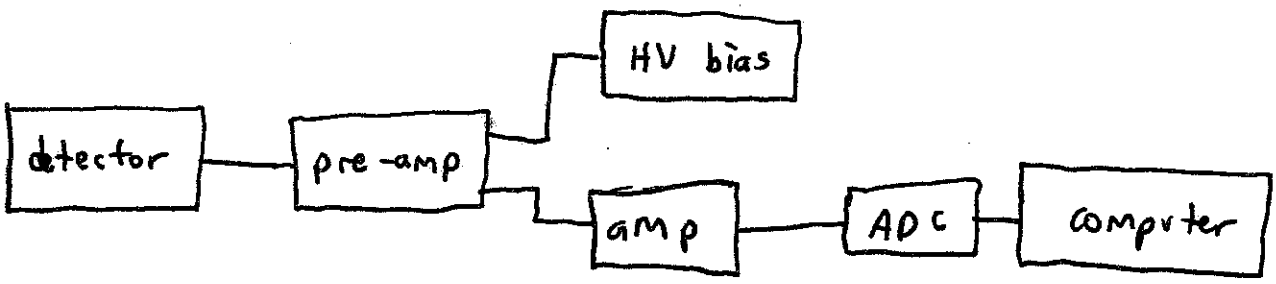

- The chamber must be evacuated before starting the measurements. Do not leave the high-voltage bias on when either pumping out or venting the chamber. Any ideas why?
- The bias voltage for BA-024-300-500 is 250 V.
- The detector is connected to a pre-amplifier by a single coaxial cable.
- The high-voltage bias for the detector is supplied to the preamp.
- The pre-amp output is sent to an amplifier.
- The amplifier output is sent to an ADC.
- The digital data from the ADC is stored in the computer.

Germanium Detectors

Discrete-line γ-ray spectroscopy requires a detection system that offers excellent energy resolution. Today, practically all γ ray spectroscopy experiments employ high-resolution germanium (Ge) detectors. The germanium detector, similar to other semiconductor detectors, is a large reverse-biased p-n junction diode. At the junction between the p-type and the n-type material, the migration of electrons from the n-type material and holes from the p-type material gives rise to a region of net zero charge. This region is known as the *depletion region.* The net positive charge on one side of the junction, and the net negative charge on the other, sets up an electric field gradient across the depletion region. Any γ rays interacting with the germanium (through the photoelectric effect, Compton scattering, or pair production) will produce electron-hole pairs in the depletion region, which will then be swept to the edges of the detector because of the electric field gradient, constituting an electric current. Since the depletion region is the active part of the Ge detector, the active volume is required to be as large as possible. If a reverse-bias is applied, the width of the depletion region can be increased. The width is proportional to $(V/n)^{1/2}$. Here, V is the bias voltage applied and n is the impurity concentration of the germanium. Natural purity germanium can only maintain a depletion region of a few millimeters before electrical breakdown occurs. Therefore at a given bias voltage, the only way to increase the width of the depletion region is to reduce the impurity concentration, N. This fact led to the introduction of *lithium-drifted* germanium detectors known as Ge(Li) detectors. These detectors are manufactured by adding lithium donor atoms to the Ge material. The donor lithium atoms exactly balance the acceptor impurities, resulting in a very low net impurity level. This allows the depletion region to be extended over the whole of the lithium-drifted region. Advances in manufacturing techniques have, however, allowed extremely pure Ge crystals to be grown. This *high-purity germanium*, or HPGe, has impurity concentrations of around one part in 10^{12}, allowing depletion depths of several centimeters to be achieved. High-purity germanium also has the advantage over Ge(Li), in that it can be stored at room temperature. Ge(Li) detectors must be stored at 77K, to avoid a redistribution of the drifted lithium, which effectively destroys the detector.

The energy required to create an electron-hole pair in Ge is approximately 3 eV, thus an incident γ ray, with an energy of several hundred keV, produces a large number of such pairs, leading to good resolution and low statistical fluctuations. These are desirable properties. HPGe detectors are operated at temperatures of around 77 K, in order to reduce noise from electrons that may be thermally excited across the small band gap in Ge (0.67 eV) at room temperature. This is achieved through thermal contact of the Ge crystal with a dewar of liquid nitrogen, using a copper rod, known as a cold finger.

The contribution from the detector to the overall resolution can be calculated from the formula:

$$\text{system resolution} = \sqrt{[R(d)]^2 + [R(E)]^2}, \tag{1}$$

where $R(d)$ is the detector resolution and $R(E)$ is the electronic resolution. These resolutions add in quadrature. There is a lower limit to $R(d)$ that is energy dependent. The production

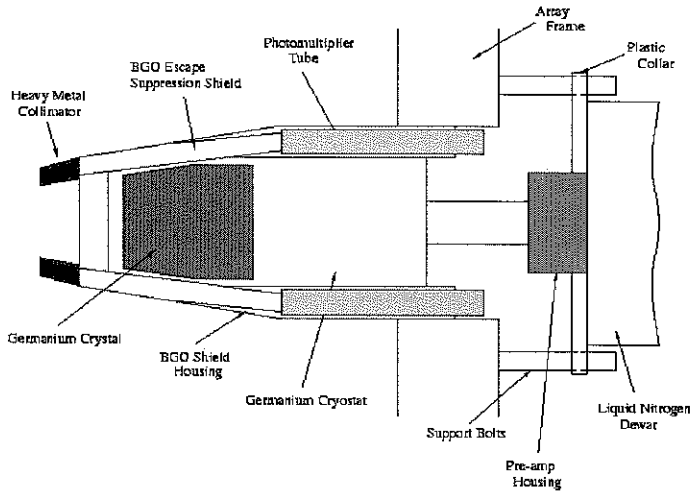

Figure 1: Schematic diagram of a typical germanium detector showing the germanium crystal, the photomultiplier tube, and the liquid nitrogen cooling system.

where $R(d)$ is the detector resolution and $R(E)$ is the electronic resolution. These resolutions add in quadrature. There is a lower limit to $R(d)$ that is energy dependent. The production of electron-hole pairs is a process that is statistical in nature, and hence there are fluctuations in the actual number produced. When the proper statistics are used, the theoretical lower limit to $R(d)$ is given by:

$$R(d) = K\sqrt{F \cdot E}, \tag{2}$$

where K is a constant, E is the energy of the photon in MeV, and F is the statistical Fano factor (a measure of the magnitude of the statistical fluctuations). To a very good approximation, this equation reduces to:

$$R(d) \text{ in keV} = 1.44\sqrt{E \text{ (in MeV)}}. \tag{3}$$

Acknowledgements

The material in this document has been extracted from a thesis from P.T. Greenless at the University of Liverpool and Ortec Application Note AN-34.

CHAPTER 15

Radioactive-series Decay

The exponential laws which govern the decay and growth of radioactive substances were first formulated by Rutherford and Soddy in 1902 (R52) in order to explain their experiments on the thorium series of radioactive substances. Useful mathematical generalizations were made in 1910 by Bateman (B20). The more general forms of the decay and growth equations are therefore often referred to as "the Bateman equations." For three decades the applicability of the equations governing series decay was confined to the uranium, actinium, and thorium series of naturally occurring radioactive substances. With the discovery of nuclear fission a vast number of cases of radioactive-series decay appeared among the fission products. The behavior of all these can be understood with the help of the original Bateman equations.

1. *Decay of a Single Radioactive Nuclide*

a. Radioactive Decay Constant λ. Consider a group containing a large number A of identical radioactive atoms. Let the probability that any particular atom will disintegrate in unit time be λ, the *total radioactive decay constant.* Then the *activity* of these atoms, i.e., the total number of disintegrations per unit time (in a time which is short compared with $1/\lambda$), will be simply $A\lambda$. The rate of depletion, dA/dt, of the group of atoms is equal to the activity, so long as we do not provide any new supply of radioactive atoms. Because A decreases as time increases, we insert a minus sign and write

$$\frac{dA}{dt} = -A\lambda \tag{1.1}$$

Rewriting this fundamental relationship in integral form, with the variables separated, we have

$$\int \frac{dA}{A} = -\int \lambda\, dt \tag{1.2}$$

We now make the fundamental assumption that *the probability of decay of an atom is independent of the age of that atom.* Then if λ is independent of t and is constant, we can integrate Eq. (1.2) simply. If

there were A_0 atoms at $t = 0$, while A atoms remain at time $t = t$, then Eq. (1.2) becomes

$$\ln\left(\frac{A}{A_0}\right) = -\lambda t \tag{1.3}$$

or, in the usual exponential form,

$$A = A_0 e^{-\lambda t} \tag{1.4}$$

Recalling that $A_0\lambda$ is the activity at $t = 0$, Eq. (1.4) can be written in terms of the ratio of the activities at t and at $t = 0$. Because λ is independent of t, we can write

$$\frac{A\lambda}{A_0\lambda} = e^{-\lambda t} \tag{1.5}$$

in agreement with the empirical law of radioactive decay and the associated disintegration hypothesis of Rutherford and Soddy (R52).

The exponential law, Eq. (1.4), of radioactive decay can also be derived from the laws of chance† without any knowledge of the mechanism of disintegration. The only assumptions needed are that:

1. The probability of decay λ is the same for all atoms of the species.
2. The probability of decay λ is independent of the age of the particular atom.

These conditions are mathematically "sufficient," as was first shown by von Schweidler (S20). They are also mathematically "necessary" conditions, as is most readily seen from the experimental fact that the statistical fluctuations in α-ray emission obey the Poisson distribution (Chap. 26), for the derivation of which assumptions analogous to those given above are both necessary and sufficient. Ruark (R38) has developed an analytical proof that these conditions are mathematically necessary. The point is of importance because the wave-mechanical theories of α-ray and β-ray radioactive decay involve the basic assumption that the probability λ of decay in unit time is independent of the age of the particular atom in question.

The most direct experimental proof that the decay constants of a number of naturally occurring radioactive substances have not changed in the last 10^9 yr comes from the sharpness of individual rings in uranium and thorium pleochroic halos in mica (H32, H33, H34).

The disintegration law of Eq. (1.4) applies universally to all radio-

† If ϑ is a time interval which is very small compared with $1/\lambda$, then $\lambda\vartheta$ is the chance that a particular atom will decay in the time ϑ. Its chance of survival for a time ϑ is then $(1 - \lambda\vartheta)$, for a time 2ϑ is $(1 - \lambda\vartheta)^2$, . . . , and for any arbitrary time $t = n\vartheta$ is $(1 - \lambda\vartheta)^n = (1 - \lambda\vartheta)^{t/\vartheta}$. It can be verified easily by series expansion that, if the arbitrary time interval ϑ is taken as very small, then in the limit of $\vartheta/t \to 0$

$$\lim_{\vartheta/t \to 0} (1 - \lambda\vartheta)^{t/\vartheta} = e^{-\lambda t}$$

Thus the chance of survival is $e^{-\lambda t}$ *for each atom.* Hence the *average fraction* which survives a time t is also $e^{-\lambda t}$. We must expect statistical fluctuations in the *actual fraction* which survives, such that the average value is $e^{-\lambda t}$.

active nuclides, but the constant λ is different for each nuclide. The known radioactive nuclides extend between $\lambda = 3 \times 10^{6}$ sec^{-1} (for ThC') and $\lambda = 1.58 \times 10^{-18}$ sec^{-1} (for Th), a range of over 10^{24}. The decay constant λ is one of the most important characteristics of each radioactive nuclide; it is essentially independent of all physical and chemical conditions such as temperature, pressure, concentration, or age of the radioactive atoms. Among the more than 800 known radioactive nuclides, no two have exactly the same decay constant. The identification of some radioactive samples can be made simply by measuring λ, which can serve as a type of qualitative chemical analysis.

b. Partial Decay Constants. Many nuclides have at risk several alternative modes of decay. For example, Cu^{64} can decay by electron capture or by positron β-ray emission or by negatron β-ray emission. If the competing modes of decay of any nuclide have probabilities λ_1, λ_2, λ_3, . . . per unit time, then the total probability of decay is represented by the total decay constant λ, where

$$\lambda = \lambda_1 + \lambda_2 + \lambda_3 + \cdots \tag{1.6}$$

The "partial activity" of a sample of A nuclei, if measured by a particular mode of decay characterized by λ_i, is then

$$\frac{dA_i}{dt} = \lambda_i A = \lambda_i A_0 e^{-\lambda t} \tag{1.7}$$

and the total activity is

$$\frac{dA}{dt} = \sum_i \frac{dA_i}{dt} = A \sum_i \lambda_i = \lambda A_0 e^{-\lambda t} \tag{1.8}$$

Note that partial activities, such as positron β rays from Cu^{64}, are proportional to total activities at all times. Each partial activity falls off with time as $e^{-\lambda t}$, not as $e^{-\lambda_i t}$. Physically, this is because the decrease of activity with time is due to the depletion of the stock of atoms A, and this depletion is accomplished by the combined action of all the competing modes of decay.

c. Units of Radioactivity. The curie unit was redefined in 1950 by action of the international Joint Commission on Standards, Units, and Constants of Radioactivity (P3) in such a way that it applies to all radioactive nuclides and is no longer tied to the presumed activity of 1 g of radium. This definition is *"The curie is a unit of radioactivity defined as the quantity of any radioactive nuclide in which the number of disintegrations per second is* 3.700×10^{10}." The "number of disintegrations" is the sum of all competing modes of disintegration. Therefore the full decay scheme of a nuclide has to be known, including the electron-capture branching, before the quantity of any sample can be expressed in curies as a result of measurements on any particular mode of disintegration, such as β rays or α rays. In practical use, the "quantity of" any radionuclide is usually nearly synonymous with the "total activity of" the nuclide.

d. Half-period T. The half-period T is the time interval over which the chance of survival of a particular radioactive atom is exactly one-half. Then, if λ is the total decay constant, Eq. (1.3) gives

$$T = \frac{\ln 2}{\lambda} = \frac{0.693}{\lambda} \tag{1.9}$$

In a large initial stock of A_0 atoms, with initial activity $A_0\lambda$, the expectation value of the activity $A\lambda$, one half-period later, is $A\lambda = A_0\lambda/2$.

For mnemonic reasons, the half-period T (or $T_{\frac{1}{2}}$ whenever there is any ambiguity about symbols) is much more frequently employed than the decay constant λ. The *half-period* is sometimes also called the *half-value time* or, with less justification, the *half-life.*

Two related periods which are useful in the laboratory are the nine-tenths period and the one-tenth period. Nine-tenths of the atoms survive longer than the *nine-tenths period* $T_{\frac{9}{10}}$ whose value is

$$T_{\frac{9}{10}} = \frac{\ln \left(\frac{10}{9}\right)}{\lambda} = 0.1520 T_{\frac{1}{2}} \simeq \frac{3}{20} T_{\frac{1}{2}} \tag{1.10}$$

One-tenth of the atoms survive longer than the *one-tenth period*, given by

$$T_{\frac{1}{10}} = \frac{\ln 10}{\lambda} = 3.322 T_{\frac{1}{2}} \simeq \frac{10}{3} T_{\frac{1}{2}} \tag{1.11}$$

Cruder but handier approximations are $T_{\frac{9}{10}} < \frac{1}{6} T_{\frac{1}{2}}$ and $T_{\frac{1}{10}} > 3 T_{\frac{1}{2}}$.

e. Mean Life τ. The actual life of any particular atom can have any value between 0 and ∞. The average life of a large number of atoms is, however, a definite and important quantity.

If there are A_0 atoms present initially, then the number remaining undecayed at a subsequent time t is $A = A_0 e^{-\lambda t}$. Each of these atoms has a life longer than t. Those which decay between t and $t + dt$ each have a life span t. The absolute number of atoms having a life t is therefore $A\lambda\, dt = A_0 \lambda e^{-\lambda t}\, dt$. The total lifetime L of all the atoms is therefore

$$L = \int_0^\infty tA\lambda\, dt = \int_0^\infty tA_0\lambda e^{-\lambda t}\, dt = \frac{A_0}{\lambda} \tag{1.12}$$

Then the average lifetime L/A_0, which is called the *mean life* τ, is simply

$$\tau = \frac{1}{\lambda} \tag{1.13}$$

Thus the mean life exceeds the half-period and is always given by

$$\tau = \frac{T}{0.693} = 1.44T \tag{1.14}$$

Substitution in Eq. (1.4) shows that the mean life is the time required for the number of atoms, or their activity, to fall to $e^{-1} = 0.368$ of any initial value.

f. Total Number of Radioactive Atoms. The total *number of radioactive atoms* A present at any time is simply the product of the total activity $A\lambda$ and the mean life, because

$$(A\lambda)\tau = \frac{A\lambda}{\lambda} = A \tag{1.15}$$

The relationships of A_0, A, t, λ, T, and τ are illustrated graphically in Fig. 1.1. It will be noted that the area under the *decay curve* of activity

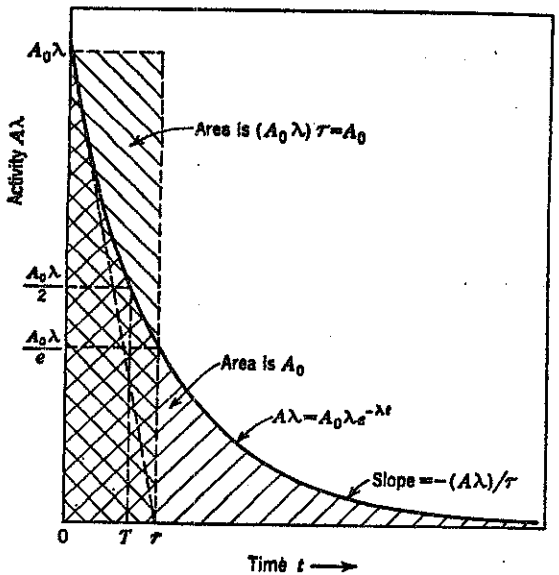

Fig. 1.1 Graphical relationships in the decay of a single radioactive nuclide. $T = 0.693/\lambda = 0.693\tau$; $\tau = 1.44T$; $\tau = 1/\lambda$. T = half-period; τ = mean life; λ = decay constant; A_0 = number of atoms at time $t = 0$; A = number of atoms at t. The slope of the activity curve at any time t is $d(A\lambda)/dt = -(A_0\lambda)\lambda e^{-\lambda t} = -\lambda(A\lambda) = -(A\lambda)/\tau$. The initial slope, at $t = 0$, is $-\lambda(A_0\lambda) = -(A_0\lambda)/\tau$. If the initial slope is extrapolated (dotted line), it intersects the time axis at the mean life τ.

vs. time equals the total number of atoms which were present initially; thus,

$$\text{Area} = \int_0^\infty A\lambda\, dt = \int_0^\infty \lambda A_0 e^{-\lambda t}\, dt = A_0 \tag{1.16}$$

This area is the same as that within the rectangle $A_0\lambda\tau$. Thus, if the initial activity $A_0\lambda$ could remain constant for a mean life τ, all the atoms would have been transformed.

g. Aids in the Computation of Radioactive Decay. Computations of $e^{-\lambda t}$ can be tedious if a few simple aids are ignored. Some of the most useful elementary techniques (K24) follow.

Semilogarithmic Graph Paper. If relative activities $A\lambda/A_0\lambda$ or relative amounts A/A_0 are plotted on the logarithmic axis, against time t on the linear axis, then $e^{-\lambda t}$ is a straight line passing through the points $A/A_0 = 1$ at $t = 0$ and $A/A_0 = 0.5$ at $t = T$. Depending on the scale of the graph paper, two- or three-place accuracy is obtainable, as illustrated in Fig. 12.1*b*.

Common (Base 10) Logarithm Tables, or Slide Rules. It may be noted that Eq. (1.3) or (1.4) can be expressed equally well using the base 10, instead of the base e. Thus

$$\frac{A_0}{A} = e^{\lambda t} = e^{\lambda T(t/T)} = 2^{(t/T)} \tag{1.17}$$

$$\ln\left(\frac{A_0}{A}\right) = \left(\frac{t}{T}\right)\ln 2 = \frac{0.693t}{T} \tag{1.18}$$

$$\log_{10}\left(\frac{A_0}{A}\right) = \left(\frac{t}{T}\right)\log_{10} 2 = \frac{0.301t}{T} \tag{1.19}$$

or

$$\frac{A}{A_0} = e^{-\lambda t} = \left(\tfrac{1}{2}\right)^{t/T} = e^{-0.693(t/T)} = 10^{-0.301(t/T)} \tag{1.20}$$

Thus, on slide rules, the value of the mantissa of $0.301(t/T)$ can be set on the L scale, and A_0/A can be read on the C scale, or A/A_0 read directly on the CI scale.

Log-Log Slide Rules. These rules have scales of e^x and of e^{-x}. At the risk of being gratuitous, it should be said that the student will be amply rewarded by becoming familiar with their range and uses. When 0.5 on the log-log scale is set opposite the half-period T, A/A_0 can be read directly for all other values of t. Analytically, the operation of the exponential scales can be illustrated by the following expressions

$$e^{-\lambda t} = \left(\frac{1}{2}\right)^{t/T} \qquad \log e^{-\lambda t} = \frac{t}{T}\log\left(\frac{1}{2}\right)$$

$$\log\log e^{-\lambda t} = \log\log\left(\frac{1}{2}\right) + \log\left(\frac{t}{T}\right) \tag{1.21}$$

Approximate Forms. For values of t which are small compared with the half-period, use of the exponential expansion

$$e^{-\lambda t} = e^{-(t/\tau)} = 1 - (t/\tau) + \frac{(t/\tau)^2}{2} - \cdots \tag{1.22}$$

is often the most accurate procedure.

Problems

1. The relative intensities of negatron β decay, electron-capture decay, and positron β decay of Cu^{64} are approximately $(\beta^-):(EC):(\beta^+) = 2.0:2.0:1.0$. The half-period of Cu^{64} is 12.8 hr.

(*a*) Calculate the total decay constant λ and the partial decay constants λ_{β^-}, λ_{EC}, λ_{β^+} in sec^{-1}.

(*b*) What is the "partial half-period" for negatron β decay, i.e., the half-period for a Cu^{64} nucleus in which the possibility of other modes of decay has been turned off?

(*c*) Evaluate in millicuries a source of Cu^{64} which emits 3.7×10^7 negatron β rays per second.

Ans.: (*b*) 32.0 hr; (*c*) 2.5 mc.

2. Determine the half-period of K^{40}, knowing that ordinary potassium (*a*) is a mixture of K^{39}, K^{40}, and K^{41} containing 0.0119 atom per cent K^{40}; (*b*) emits 31 β rays/sec per gram in transitions of $K^{40} \xrightarrow{\beta^-} Ca^{40}$; and (*c*) emits 3.4 γ rays/sec per gram in electron-capture transitions $K^{40} \xrightarrow{EC} A^{40}$, and every EC transition is accompanied by just one photon. *Ans.:* 1.15×10^9 yr.

3. Compute the number of grams and the number of radioactive atoms contained in 1 mc of (*a*) radiosodium (Na^{24}, $T = 14.8$ hr); (*b*) radiophosphorus (P^{32}, $T = 14.5$ days); and (*c*) radium (Ra^{226}, $T = 1{,}620$ yr). *Ans.:* mass, 1.1×10^{-10} g of Na^{24}; 3.5×10^{-9} g of P^{32}; 0.0010 g of Ra.

4. (*a*) A radioactive substance has a mean life τ sec, an activity of a_1 disintegrations per second at time t_1, and an activity of a_2 at time t_2. Show that the number of atoms $(A_1 - A_2)$ disintegrating between t_1 and t_2 is

$$A_1 - A_2 = \tau(a_1 - a_2)$$

(*b*) If the average energy per β ray of 12.6-hr iodine I^{130} is 0.29 Mev, determine the β-ray energy in ergs liberated in 24 hr by an iodine source whose initial strength is 1 mc.

(*c*) If this iodine is present in 2 g of thyroid tissue, determine the radiation dose absorbed in 24 hr by the tissue, remembering that 1 rep (roentgen equivalent physical) corresponds to the absorption of 94 ergs per gram of tissue. *Ans.:* (*b*) 8.2×10^5 ergs; (*c*) 4,400 rep.

5. In 1 g of natural uranium,

(*a*) What is the activity of U^{238}, UX_1, UX_2, and U^{234}, in μc?

(*b*) What is the ratio of the activity of U^{235} to that of U^{238}?

(*c*) What is the number of spontaneous fissions per hour?

DATA: The decay series of U^{238} and U^{235} and half-periods are

$$_{92}U^{238} \xrightarrow[4.51 \times 10^9 \text{ yr}]{\alpha} UX_1 \xrightarrow[24.1 \text{ d}]{\beta} UX_2 \xrightarrow[1.14 \text{ min}]{\beta} U^{234} \xrightarrow[2.35 \times 10^5 \text{ yr}]{\alpha} Io \longrightarrow Io \xrightarrow[8.0 \times 10^4 \text{ yr}]{\alpha} Ra^{226} \xrightarrow[1{,}620 \text{ yr}]{\alpha} Rn \xrightarrow[3.82 \text{ d}]{\alpha} \cdots$$

$$_{92}U^{235} \xrightarrow[7.1 \times 10^8 \text{ yr}]{\alpha} UY \xrightarrow[25.6 \text{ hr}]{\beta} Pa \xrightarrow[3.43 \times 10^4 \text{ yr}]{\alpha} Ac \xrightarrow[22 \text{ yr}]{\beta} RdAc \xrightarrow[18.9 \text{ d}]{\alpha} AcX^{223} \xrightarrow[11.2 \text{ d}]{\alpha} \cdots$$

In natural uranium, there is 1 atom of U^{235} per 139 atoms of U^{238}. The partial half-periods for spontaneous fission are

U^{238}	8.0×10^{15} yr
U^{235}	1.9×10^{17} yr
U^{234}	2×10^{16} yr

Ans.: (*a*) 0.33 μc per gram U for each; (*b*) 0.046; (*c*) 25 fissions per hour per gram U (these are generally useful numbers, worth memorizing).

6. If an atom is known to exist at $t = 0$, what is its probability of decaying in the time interval Δt between t and $t + \Delta t$, if its decay constant is λ? Under what restrictions does this general relationship reduce to simply $\lambda\,\Delta t$?

Ans.: $(1 - e^{-\lambda\,\Delta t})e^{-\lambda t}$; reduces when $\lambda t \ll 1$ and $\lambda\,\Delta t \ll 1$.

2. *Radioactive-series Decay. Growth of a Daughter Product*

In a number of cases a radioactive nuclide A decays into a nuclide B which is also radioactive. Let the initial part of such a series be represented by

$$A \xrightarrow{\lambda_A} B \xrightarrow{\lambda_B} C$$

where λ_A is the decay constant of atoms of type A and λ_B is the decay constant of atoms of type B, and where the symbols A and B represent the number of atoms of each type which are present at any time t. The limiting case in which B is stable is represented then by $\lambda_B = 0$.

a. The General Differential Equation for a Daughter Product. At any time t, the activity of A is $A\lambda_A$ and the activity of B is $B\lambda_B$. The rate of change dB/dt, in the number of atoms of type B, is then equal to the supply of new atoms of type B due to the decay of A, diminished by the rate of loss of B through its own decay, or

$$\frac{dB}{dt} = A\lambda_A - B\lambda_B \tag{2.1}$$

If the only source of atoms of type A is from an initial supply $A = A_0$ at $t = 0$, then

$$A = A_0 e^{-\lambda_A t}$$

and, with these initial conditions on A, Eq. (2.1) becomes

$$\frac{dB}{dt} = A_0\lambda_A e^{-\lambda_A t} - B\lambda_B \tag{2.2}$$

From this differential equation, we wish to obtain an explicit solution for B as a function of time. We proceed, as usual, by a seasoned guess that the general solution will be of the form

$$B = A_0(h_A e^{-\lambda_A t} + h_B e^{-\lambda_B t}) \tag{2.3}$$

In order to evaluate the coefficients h_A and h_B, we substitute B and dB/dt from Eq. (2.3) into Eq. (2.2) and collect terms, obtaining

$$e^{-\lambda_A t}(-h_A\lambda_A - \lambda_A + h_A\lambda_B) = 0 \tag{2.4}$$

If this is to be valid for all values of t, the parentheses must equal zero, and therefore we have

$$h_A = \frac{\lambda_A}{\lambda_B - \lambda_A} \tag{2.5}$$

The coefficient h_B depends on the value of B at $t = 0$. For the important special case in which $B = 0$ at $t = 0$, we have at once from Eq. (2.3)

$$h_A + h_B = 0 \tag{2.6}$$

Hence $h_B = -h_A$, and we have for the *amount* of B

$$B = A_0 \frac{\lambda_A}{\lambda_B - \lambda_A}(e^{-\lambda_A t} - e^{-\lambda_B t}) \tag{2.7}$$

as the important general solution for the initial conditions $A = A_0$, and $B = 0$, at $t = 0$.

Then the *activity* of B is $B\lambda_B$ [*not* dB/dt; see Eq. (2.1)], where

$$B\lambda_B = A_0\lambda_A \frac{\lambda_B}{\lambda_B - \lambda_A} (e^{-\lambda_A t} - e^{-\lambda_B t}) \tag{2.8}$$

or, since the activity of A at t is $A\lambda_A = A_0\lambda_A e^{-\lambda_A t}$,

$$B\lambda_B = (A\lambda_A) \frac{\lambda_B}{\lambda_B - \lambda_A} (1 - e^{-(\lambda_B - \lambda_A)t}) \tag{2.9}$$

Various special cases, depending on the relative magnitudes of λ_A and λ_B, will be discussed and plotted in Sec. 5 below.

3. *Accumulation of Daughter Atoms*

The most fundamental physical concepts underlying the entire mathematical theory of radioactive-series decay are embodied in Eq. (2.1). The same concepts will reappear as Eq. (7.1) and Eq. (8.1) in the more general treatment of a long series of substances. This is the principal justification for having presented here the classical method of deriving Eq. (2.7).

Another viewpoint is highly instructive and also lends itself directly to other problems which are mathematically similar (such as to the secondary radiation produced when γ rays pass through an absorbing barrier).

At time $t = 0$, let $A = A_0$ and $B = 0$. Then at a later time, $t = x$, there will remain $A = A_0 e^{-\lambda_A x}$ atoms of A. In the time interval between x and $x + dx$, the number of new atoms of B formed will be $A\lambda_A\, dx$. The fraction of these atoms of B which survive until a later time $t = t$ is $e^{-\lambda_B(t-x)}$. Then the total stock of B at $t = t$ is given by an integral over all values of the time x between $t = 0$ and $t = t$ and is

$$B = \int_0^t (A\lambda_A\, dx)(e^{-\lambda_B(t-x)}) \tag{3.1}$$

$$\begin{aligned} B &= \int_0^t A_0\lambda_A e^{-\lambda_A x} e^{-\lambda_B(t-x)}\, dx \\ &= A_0\lambda_A e^{-\lambda_B t} \int_0^t e^{-(\lambda_A - \lambda_B)x}\, dx \\ &= A_0\lambda_A e^{-\lambda_B t} \left[\frac{1}{\lambda_B - \lambda_A} (e^{-(\lambda_A - \lambda_B)t} - 1)\right] \\ &= A_0 \frac{\lambda_A}{\lambda_B - \lambda_A} (e^{-\lambda_A t} - e^{-\lambda_B t}) \end{aligned} \tag{3.2}$$

The result, Eq. (3.2), of this entirely different approach is, of course, the same as Eq. (2.7). The same concept can be successively reapplied in order to derive the expressions for the amounts of C, D, . . . , N, produced in time t from A_0 at $t = 0$. This is left as an exercise. We shall

follow the more conventional methods based on analogues of the basic idea, $dB/dt = A\lambda_A - B\lambda_B$, in developing later the general expressions for C, D, . . . , N.

4. *Time of Maximum Activity of Daughter Product. Ideal Equilibrium*

We note at once from Eq. (2.7) that the amount of B is zero both at $t = 0$ and at $t = \infty$, when all the atoms of both A and B have decayed. At some intermediate time t_m the amount of B, and hence its activity $B\lambda_B$, passes through a maximum value. This is the time t_m for which $dB/dt = 0$. The differential of B, Eq. (2.7), with respect to time is zero when

$$\lambda_A e^{-\lambda_A t_m} = \lambda_B e^{-\lambda_B t_m}$$

from which it follows that the time t_m of maximum activity of B is

$$t_m = \frac{\ln (\lambda_B/\lambda_A)}{(\lambda_B - \lambda_A)} \tag{4.1}$$

if, at $t = 0$, $A = A_0$ and $B = 0$.

Equation (4.1) may be easily transformed to read directly in terms of mean life τ and half-period T; thus

$$\begin{aligned} t_m &= \frac{\ln (\tau_A/\tau_B)}{(1/\tau_B) - (1/\tau_A)} = \tau_B \left(\frac{\tau_A}{\tau_A - \tau_B}\right) \ln \frac{\tau_A}{\tau_B} \\ &= \tau_B \left(\frac{T_A}{T_A - T_B}\right) \ln \left(\frac{T_A}{T_B}\right) \end{aligned} \tag{4.2}$$

This important result shows that t_m is positive and real for either $T_A > T_B$ or $T_A < T_B$. No physical cases are known for which $T_A = T_B$. But if the two half-periods are nearly equal, we may write

$$T_A = T_B(1 + \delta) \qquad \text{where } \delta \ll 1$$

Making use of the expansion of the logarithm

$$\ln (1 + \delta) = \delta - \frac{\delta^2}{2} + \frac{\delta^3}{3} - \cdots$$

we have

$$\begin{aligned} t_m &= \tau_B \frac{1 + \delta}{\delta} \left(\delta - \frac{\delta^2}{2} + \cdots\right) \\ &= \tau_B(1 + \delta) \left(1 - \frac{\delta}{2} + \cdots\right) \\ &\simeq \tau_B \left(1 + \frac{\delta}{2}\right) \simeq \tau_B \left(\frac{T_A}{T_B}\right)^{\frac{1}{2}} \\ &= \sqrt{\tau_A \tau_B} \end{aligned} \tag{4.3}$$

Thus, in the limiting case where parent A and daughter B have substantially the same half-period, the maximum activity of B occurs about one mean life after the accumulation of B is begun.

At t_m, we have from Eq. (2.1)

$$A\lambda_A = B\lambda_B \tag{4.4}$$

Thus the activity of the residual parent A and of the accumulated daughter B are *equal only at* t_m, at which time each is equal to

$$\begin{aligned} A\lambda_A &= A_0\lambda_A e^{-[\lambda_A \ln(\lambda_B/\lambda_A)]/(\lambda_B-\lambda_A)} \\ &= A_0\lambda_A \left(\frac{\lambda_A}{\lambda_B}\right)^{\lambda_A/(\lambda_B-\lambda_A)} \\ &= A_0\lambda_A \left(\frac{T_B}{T_A}\right)^{T_B/(T_A-T_B)} \end{aligned} \tag{4.5}$$

The situation in which the activities of the parent and daughter are equal is called *ideal equilibrium* and exists only at the moment t_m. It is to be emphasized that from $t = 0$ to $t = t_m$ the activity of the parent always exceeds the activity of the daughter, that is, dB/dt is positive. Conversely, *from* $t = t_m$ to $t = \infty$ *the activity of the daughter continuously exceeds the activity of its parent*, that is, dB/dt is negative.

Problems

1. On a single curve for the decay of parent activity, to a scale such as Fig. 1.1, draw accumulation curves of daughter activity $B\lambda_B$, if (*a*) $T_B \ll T_A$, (*b*) $T_B < T_A$, (*c*) $T_B \simeq T_A$, and (*d*) $T_B > T_A$.

2. Consider the decay scheme: $A \longrightarrow B \longrightarrow C$, with $\lambda_A < \lambda_B$. After transient equilibrium is established between A and B, show that the interval of time Δt such that (activity of A at $t - \Delta t$) = (activity of B at t) is given by

$$\Delta t = \tau_A \ln\left(\frac{\lambda_B}{\lambda_B - \lambda_A}\right)$$

and that this approaches $\Delta t = \tau_B$ as τ_B/τ_A approaches zero.

5. *Ratio of Activity of Parent and Daughter. Transient Equilibrium*

The ratio of the activities of the parent and daughter, under the initial conditions $B = 0$ at $t = 0$, is given at once by Eq. (2.9). This activity ratio $B\lambda_B/A\lambda_A$ is zero for $t = 0$, unity for $t = t_m$, and has its maximum value for large values of t. Several distinct cases arise, depending on the relative half-periods of A and B.

a. Daughter Longer-lived Than Parent. If $T_A < T_B$, then the activity ratio $B\lambda_B/A\lambda_A$ increases continuously as t increases. Thus, when $\lambda_A > \lambda_B$, Eq. (2.9) may be written

$$\frac{B\lambda_B}{A\lambda_A} = \frac{\lambda_B}{\lambda_A - \lambda_B}\left(e^{(\lambda_A-\lambda_B)t} - 1\right) \tag{5.1}$$

Such a case is illustrated by Fig. 5.1 which represents the well-known series

$$\mathrm{Te}^{131} \xrightarrow[T_A = 1.25\ \mathrm{d}]{} \mathrm{I}^{131} \xrightarrow[T_B = 8.0\ \mathrm{d}]{} \mathrm{Xe}^{131}$$

In the extreme case when $T_A \ll T_B$, the activity of the daughter substance finally becomes effectively independent of the residual activity of

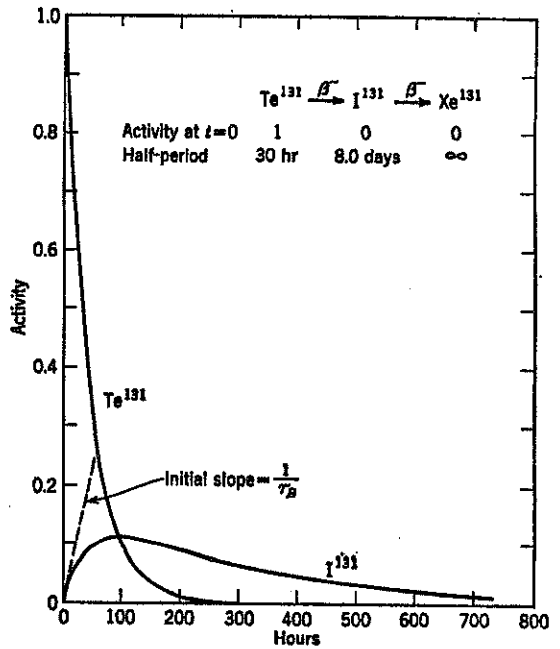

Fig. 5.1 Decay of the activity of an initially pure source of Te^{131} (T = 1.25 days) and growth of its decay product I^{131} (T = 8.0 days) produced in the Te^{131} source. The maximum activity of I^{131} occurs at t_m = 3.96 days = 95.0 hr, in accord with Eq. (4.1). The ratio of activity of I^{131} to that of its parent Te^{131} increases continuously with time, Eq. (5.1).

the parent. Thus, for $t \gg T_A$, Eq. (5.1) or Eq. (2.7) becomes

$$B\lambda_B \simeq A_0\lambda_B e^{-\lambda_B t} \tag{5.2}$$

Thus the initial stock of short-lived atoms A_0 has, in effect, quickly become an initial stock of long-lived atoms B_0, with $A_0 \simeq B_0$, which decay exponentially like $e^{-\lambda_B t}$.

b. Daughter and Parent of Nearly Equal Half-period. If T_A and T_B are nearly equal, such that $T_A = T_B(1 + \delta)$, where $\delta \ll 1$, then Eq.

(2.9) for the ratio of activities of daughter to parent becomes

$$\frac{B\lambda_B}{A\lambda_A} = \frac{1+\delta}{\delta}\left(1 - e^{-\frac{\delta}{1+\delta}\frac{t}{\tau_B}}\right)$$
$$= \frac{t}{\tau_B}\left(1 - \frac{\delta}{1+\delta}\frac{t}{2\tau_B} + \cdots\right)$$
$$\simeq \frac{t}{\tau_B} \tag{5.3}$$

Thus the activity ratio would increase approximately linearly with time, so long as $t \ll 2\tau_B/\delta$.

c. Daughter Shorter-lived Than Parent. If $T_A > T_B$, then the ratio of the activities increases with time at first and then approaches a constant value. Thus Eq. (2.9) can be written as

$$\frac{B\lambda_B}{A\lambda_A} = \frac{T_A}{T_A - T_B}\left(1 - e^{-[(T_A - T_B)/T_A]\lambda_B t}\right) \tag{5.4}$$

For all values of t which are large compared with $\tau_B T_A/(T_A - T_B)$, Eq. (5.4) becomes simply

$$\frac{B\lambda_B}{A\lambda_A} = \frac{T_A}{T_A - T_B} \qquad \text{for large } t \tag{5.5}$$

When the ratio of the activities of daughter to parent is constant, a particular type of radioactive equilibrium exists. This is spoken of as *transient equilibrium* when the ratio $T_A/(T_A - T_B)$ is clearly greater than unity. Such cases are very common.

If $A\lambda_A$ is the activity of the parent at some time t, which is long enough so that equilibrium has been established between A and B, then we may ask what additional time Δt must elapse before the activity $B\lambda_B$ of the daughter will fall to the value $A\lambda_A$. It can be shown that the activity $B\lambda_B$ at $t + \Delta t$ is the same as the activity $A\lambda_A$ at t, if

$$\Delta t = \tau_B\left[1 + \frac{1}{2}\left(\frac{T_B}{T_A}\right) + \frac{1}{3}\left(\frac{T_B}{T_A}\right)^2 + \cdots\right]$$
$$\simeq \tau_B \qquad \text{if } T_B \ll T_A \tag{5.6}$$

An important classical example is the transient equilibrium between mesothorium-1 ($MsTh_1$) and radiothorium (RdTh). Pure $MsTh_1$ (which is isotopic with radium) can be separated from thorium minerals and has a half-period of 6.7 yr. The decay series can be written

$$_{88}MsTh_1 \xrightarrow[T_A = 6.7\ yr]{\beta^-} {}_{89}MsTh_2 \xrightarrow[T = 6\ hr]{\beta^-} {}_{90}RdTh \xrightarrow[T_B = 1.90\ yr]{\alpha} {}_{88}ThX \xrightarrow{\alpha}$$

The first decay product $MsTh_2$ has a half-period of only 6.13 hr and decays promptly into RdTh. The accumulation of RdTh is controlled by its own half-period of 1.90 yr. When viewed on a time scale measured in years, the half-period of the intermediate product $MsTh_2$ is so short that its activity can be taken as always equal to that of $MsTh_1$.

Analytically, this corresponds to ignoring the presence of $MsTh_2$ as an intermediate product and can be justified easily from Eq. (8.2a). We see from Eq. (5.5) that the equilibrium activity ratio will be

$$\frac{RdTh}{MsTh_1} = \frac{B\lambda_B}{A\lambda_A} = \frac{6.7}{6.7 - 1.9} = 1.39 \tag{5.7}$$

This is clearly a case of transient equilibrium, because the constant-activity ratio is significantly greater than unity. Figure 5.2 shows the decay of an originally pure source of $MsTh_1$ and the growth in it of RdTh.

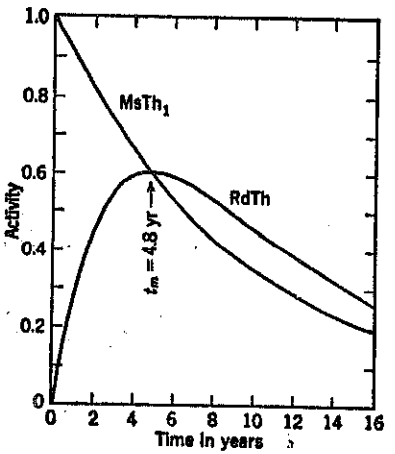

Fig. 5.2 The activity of an originally pure $MsTh_1$ source and of the RdTh produced in it. The maximum activity of the RdTh occurs at 4.8 yr in accord with Eq. (4.1), at which time its activity is the same as its parent. At larger values of the time coordinate, the activity of RdTh approaches its transient equilibrium value of 1.39 times the residual activity of $MsTh_1$, Eq. (5.7).

Its importance lies in the fact that mesothorium is the most refinable, commercially important, long-lived member of the thorium series. Mesothorium is used to replace radium in some self-luminous paints. In the laboratory, mesothorium sources are used primarily as a convenient source of the 2.62-Mev γ rays of ThC″. These γ rays have the highest quantum energy available from any naturally occurring sources. The half-periods of all the decay products of RdTh are relatively short, so that ThC″ is essentially in equilibrium with RdTh. Accordingly, an originally pure $MsTh_1$ source will *increase* in γ-ray activity up to a time $t_m = 4.8$ yr, Eq. (4.1); then the activity will begin to decline with an apparent half-period which varies with time, in accord with Eq. (2.8).

The observation that the rate of emission of disintegration particles from a radioactive product permanently exceeds the activity of its parent substance, when the two are in equilibrium, is not the paradox which it may seem at first sight. This condition can be visualized in two ways. First, reference to Eq. (2.1) reminds us that, if the amount of the product B is decreasing with time, then dB must be negative, and hence the rate of its decay $B\lambda_B$ must exceed the rate of its formation by the decay $A\lambda_A$ of its parent. Secondly, the area under a curve such as those in Fig. 5.2 for $t = 0$ to $t = \infty$ represents the total number of disintegrations, hence the total number of radioactive atoms originally available. The area under the two curves must be equal for the two because the same nuclei are involved, only at different stages in their disintegration series. From $t = 0$ to $t = t_m$ the activity of the parent exceeds

that of its product. After t_m the activity of the product must therefore exceed that of its parent.

d. Daughter Much Shorter-lived Than Parent. When the half-period of the daughter product is negligible compared with that of its parent, then Eq. (2.9) takes on a particularly simple form. Then $\lambda_A \ll \lambda_B$, and Eq. (2.9) becomes

$$B\lambda_B = A\lambda_A(1 - e^{-\lambda_B t}) \tag{5.8}$$

The daughter activity $B\lambda_B$ increases according to the simple exponential growth curve governed by *its own decay constant* λ_B. This was the historically important case discovered by Rutherford and Soddy (R52) in the growth of ThX ($T = 3.64$ days) from thorium (actually from RdTh, $T = 1.90$ yr). Other important examples include the growth of radon in radium sources, etc. In these cases the equilibrium ratio of activities becomes substantially unity. Note then that

$$B\lambda_B = A\lambda_A \qquad \text{for } t \gg T_B \tag{5.9}$$

only if $T_A \gg T_B$. This condition is spoken of classically as *secular equilibrium.*

6. *Yield of a Radioactive Nuclide Produced by Nuclear Bombardment*

Consider any nuclear reaction which results in the production of a radioactive nuclide, e.g.,

$$_{11}\mathrm{Na}^{23} + \mathrm{H}^2 \rightarrow \mathrm{H}^1 + {}_{11}\mathrm{Na}^{24}$$

In this reaction the number of target atoms of Na^{23} which are accessible to the deuteron beam can be called A_0. The probability of transforming one of these atoms into Na^{24} in unit time can be called λ_A. Then $A_0\lambda_A$ is the rate at which new atoms of Na^{24} are produced. We see that the target is to be treated mathematically as though it were a parent source, having an activity $A_0\lambda_A$, and producing a radioactive substance B. Thus the scheme

$$A \underset{\lambda_A}{\rightarrow} B \underset{\lambda_B}{\rightarrow} C$$

represents the reactions

$$\mathrm{Na}^{23} \xrightarrow[\lambda_A]{(d,p)} \mathrm{Na}^{24} \xrightarrow[\lambda_B]{\beta^-} \mathrm{Mg}^{24}$$

The probability λ_A of producing the (d,p) reaction is very small, but the number of target atoms A_0 is very large. Hence, mathematically,

$$A_0\lambda_A \text{ is finite} \qquad \lambda_A \rightarrow 0 \qquad A_0 \rightarrow \infty$$

Usually, a negligible fraction of the atoms of the target is transformed so that the number of residual target atoms, $A = A_0e^{-\lambda_A t}$, is effectively equal to A_0. However, in some exceptional instances a measurable fraction of the target may be consumed, such as in the production of plutonium through intense and prolonged neutron irradiation of uranium.

In the $Na^{23}(d,p)Na^{24}$ example, the activity $B\lambda_B$ of Na^{24} produced after a uniform bombardment of duration t will be given by Eq. (5.8) for the growth of activity of a daughter product from an effectively long-lived parent.

The *yield* Y of such a nuclear reaction is the rate of production of activity (*not* atoms) of the radioactive nuclide, under specified bombardment conditions of deuteron energy and current, etc. For example, the yield of Na^{24} from the reaction $Na^{23}(d,p)Na^{24}$ is 11.1 mc/(hr)(μa) of 14-Mev deuterons bombarding a thick target of metallic sodium (C24).

The yield is the rate at which new activity is formed. In the important but special case of a first daughter product, the *yield* is a constant and is equal to *the initial slope of the growth curve of the activity formed,* or

$$Y = \left[\frac{d(B\lambda_B)}{dt}\right]_{\text{at } t=0} \tag{6.1}$$

For $B\lambda_B$ we can take Eq. (5.8) when $\lambda_A \ll \lambda_B$. For greater generality let us use instead the more fundamental expression of Eq. (2.8). Then, in general, the yield of B is

$$\begin{aligned} Y &= A_0\lambda_A \frac{\lambda_B}{\lambda_B - \lambda_A}(-\lambda_A e^{-\lambda_A t} + \lambda_B e^{-\lambda_B t})_{t=0} \\ &= A_0\lambda_A\lambda_B \end{aligned} \tag{6.2}$$

Thus in the growth equations, Eq. (2.8) or (5.8), the effective activity of the "parent" target, or the rate of production of *atoms* of B, is

$$A_0\lambda_A = Y/\lambda_B = Y\tau_B \tag{6.3}$$

Note that the yield, Y, does not have the dimensions of activity, but of *activity per unit time.* The net activity accumulated during a time t is then written as

$$B\lambda_B = Y\tau_B(1 - e^{-\lambda_B t}) \tag{6.4}$$

The maximum activity which can be produced is then $Y\tau_B$. For example, the maximum Na^{24} ($\tau_B = 1.44T = 1.44 \times 14.8$ hr $= 21.3$ hr) activity under the conditions mentioned above would be, per microampere of deuterons,

$$Y\tau_B = 11.1 \frac{\text{mc}}{\text{hr}} \times 21.3 \text{ hr} = 236 \text{ mc} = 0.236 \text{ curie}$$

and this is the "effective activity," $A_0\lambda_A$, of the parent target while under bombardment, by Eq. (6.3). In one half-period T (= 14.8 hr for Na^{24}), one-half this ultimate maximum activity can be accumulated. Figure (6.1) shows that it is evidently inefficient to accumulate activity for much more than one or two half-periods. The activity already accumulated decays almost as rapidly as new activity is produced. The rates of production and of decay become substantially equal after about six half-periods ($e^{-\lambda t} = 0.01$ when $t = 6.6T = 4.6\tau$).

Any particular target, when under nuclear bombardment, may be the source of several radioactive substances. For example, when Al^{27} is bombarded by fast neutrons, the following three reactions occur competitively:

$$Al^{27} \xrightarrow{(n,\gamma)} Al^{28} \qquad T = 2.4 \text{ min}$$
$$Al^{27} \xrightarrow{(n,p)} Mg^{27} \qquad T = 10.2 \text{ min}$$
$$Al^{27} \xrightarrow{(n,\alpha)} Na^{24} \qquad T = 14.8 \text{ hr}$$

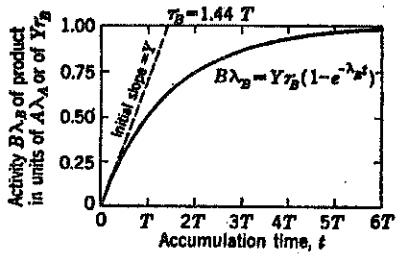

Fig. 6.1 Growth of activity in a target irradiated under constant-bombardment conditions. T is the half-period, and τ_B is the mean life of the radioactive nuclide which is being produced. The rate of production of radioactive *atoms* of B is $A_0\lambda_A$, which can be visualized as the "effective activity" of the target under the conditions of bombardment. The rate of production of *activity* of B is then $A_0\lambda_A\lambda_B$ and is called the *yield* Y. The slope of the growth curve at $t = 0$ is the yield Y. If the initial slope is extrapolated (dotted line), it intersects at a time τ_B with the maximum attainable activity of B, which is $1.0\ A_0\lambda_A = 1.0\ Y\tau_B$.

Similarly, the fission of U^{235} leads competitively to many fission chains. Each of these reactions will have its own characteristic yield. In other cases, the same radioactive nuclide may be produced by two different nuclear reactions occurring in the same target. For example, among the reactions when tin is bombarded by deuterons, there are

$$Sn^{118} \xrightarrow{(d,n)} Sb^{119} \qquad T = 39 \text{ hr}$$
$$Sn^{119} \xrightarrow{(d,2n)} Sb^{119} \qquad T = 39 \text{ hr}$$

The yield of each reaction will depend on the conditions of bombardment.

Problem

Under bombardment of sodium by 10 μa of 14-Mev deuterons, the yield of the reaction $_{11}Na^{23}(d,p)_{11}Na^{24}$ is 110 mc per hour. The half-period of Na^{24} is 14.8 hr.

(*a*) What is the maximum activity of Na^{24} which can be produced under these bombardment conditions?

(*b*) What activity of Na^{24} will be produced in 8 hr of continuous bombardment?

(*c*) Eight hours after the conclusion of an 8-hr bombardment, what activity of Na^{24} will remain?

Ans.: (*a*) 2.34 curies; (*b*) 734 mc; (*c*) 504 mc.

7. *Growth of a Granddaughter Product*

We can write the expressions for the amount and activity of C, accumulated in time t, from an initial supply of A_0 atoms of type A. In the series

$$A \xrightarrow[\lambda_A]{} B \xrightarrow[\lambda_B]{} C \xrightarrow[\lambda_C]{}$$

let there be B atoms of type B and C atoms of type C present at time t. Then the rate of increase in C is, by analogy with Eq. (2.1),

$$\frac{dC}{dt} = B\lambda_B - C\lambda_C \tag{7.1}$$

The solution for C will have the form

$$C = A_0(h_A e^{-\lambda_A t} + h_B e^{-\lambda_B t} + h_C e^{-\lambda_C t}) \tag{7.2}$$

where the coefficients h_A, h_B, h_C depend on the initial conditions. The most important case is for the initial conditions $A = A_0$, $B = 0$, $C = 0$, at $t = 0$. Then Eq. (2.7) gives B as a function of time, and the solution for C can be obtained by substituting Eq. (7.2) into Eq. (7.1) and evaluating the coefficients. In this way it is found that if, at $t = 0$, $A = A_0$, and $B = 0$, then

$$h_A = \frac{\lambda_A}{\lambda_C - \lambda_A}\frac{\lambda_B}{\lambda_B - \lambda_A} \tag{7.3a}$$
$$h_B = \frac{\lambda_A}{\lambda_A - \lambda_B}\frac{\lambda_B}{\lambda_C - \lambda_B} \tag{7.3b}$$

If also $C = 0$, at $t = 0$, then

$$h_A + h_B + h_C = 0$$

and it follows that

$$h_C = \frac{\lambda_A}{\lambda_A - \lambda_C}\frac{\lambda_B}{\lambda_B - \lambda_C} \tag{7.3c}$$

Then the activity $C\lambda_C$ under the initial conditions $A = A_0$, $B = 0$, $C = 0$, at $t = 0$, is

$$C\lambda_C = A_0\lambda_A\left(\frac{\lambda_B}{\lambda_B - \lambda_A}\frac{\lambda_C}{\lambda_C - \lambda_A}e^{-\lambda_A t} + \frac{\lambda_B}{\lambda_A - \lambda_B}\frac{\lambda_C}{\lambda_C - \lambda_B}e^{-\lambda_B t} + \frac{\lambda_B}{\lambda_B - \lambda_C}\frac{\lambda_C}{\lambda_A - \lambda_C}e^{-\lambda_C t}\right) \tag{7.4}$$

For numerical work it is often convenient to use the identity

$$\frac{\lambda_1}{\lambda_1 - \lambda_2} = \frac{T_2}{T_2 - T_1} \tag{7.5}$$

The residual activity of the parent radioactive substance is

$$A\lambda_A = A_0\lambda_A e^{-\lambda_A t}$$

which can be factored out of the right-hand side of this equation if desired.

For large values of t, the ratio of the activity $C\lambda_C$ to the residual activity of the parent depends on the relative half-periods of all three substances. If the parent is longer-lived than both B and C, then Eq. (7.4)

becomes

$$\frac{C\lambda_C}{A\lambda_A} = \frac{\lambda_B}{\lambda_B - \lambda_A}\frac{\lambda_C}{\lambda_C - \lambda_A} = \frac{T_A}{T_A - T_B}\frac{T_A}{T_A - T_C} \tag{7.6}$$

for $\lambda_A < \lambda_B$ and $\lambda_A < \lambda_C$ and $t \gg \tau_B$ or τ_C. Equation (7.6) then gives the activity ratio corresponding to *transient equilibrium*, or to *secular equilibrium* (unity) if $\lambda_A \ll \lambda_B$ and $\lambda_A \ll \lambda_C$.

The well-known $Te^{131} \rightarrow I^{131}$ series will serve as a practical illustration of the behavior of Eq. (7.6). One method of producing these radioactive nuclides is by bombardment of stable Te^{130} with deuterons. The reaction $Te^{130}(d,p)Te^{131}$ is then the effective long-lived parent of Te^{131}. Then in the scheme

$$Te^{130} \xrightarrow[\lambda_A]{(d,p)} Te^{131} \xrightarrow[\lambda_B]{\beta^-} I^{131} \xrightarrow[\lambda_C]{\beta^-} Xe^{131}\ \text{(stable)}$$

the activity $C\lambda_C$ of I^{131} accumulated after an irradiation of duration t will be given by Eq. (7.4). Recalling from our discussion of the $Na^{23}(d,p)$ reaction that we can put $\lambda_A \rightarrow 0$, while $A\lambda_A$ remains finite and constant, Eq. (7.4) becomes

$$C\lambda_C = A\lambda_A\left[1 - \frac{\lambda_C}{\lambda_C - \lambda_B}\left(e^{-\lambda_B t} - \frac{\lambda_B}{\lambda_C}e^{-\lambda_C t}\right)\right] \tag{7.7}$$

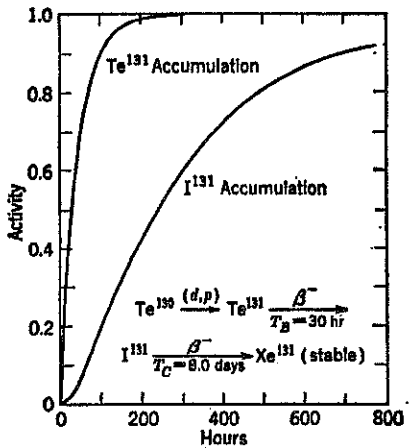

Fig. 7.1 Accumulation of Te^{131} activity [$B\lambda_B$ of Eq. (6.4)] and of I^{131} activity [$C\lambda_C$ of Eq. (7.7)] in terms of the effective activity $A\lambda_A$ of the reaction $Te^{130}(d,p)Te^{131}$ taken as unity.

for any finite values of λ_B, λ_C, and t.

The growth of Te^{131} activity, $B\lambda_B$, and of I^{131} activity, $C\lambda_C$, as a function of irradiation time is shown in Fig. 7.1. It will be noted that *the initial slope of the growth curve for the activity $C\lambda_C$ is zero.* Physically, this is because at $t = 0$ there has been no B produced, and so there is no initial production of C by decay of B. Mathematically, we note the same result from Eq. (7.1) in which both terms on the right-hand side are zero at $t = 0$. Similarly, differentiation of Eq. (7.7) gives also $d(C\lambda_C)/dt = 0$ when $t = 0$. We shall return to this concept and to Fig. 7.1 in another connection in Sec. 10.

a. General Initial Conditions. If at $t = 0$ there was an amount B_0 of substance B present, then at any later time there will be an additional activity of C, due to the C produced by decay of B_0. This *additional* activity of C can be written at once from Eq. (2.8) by appropriate *upgrading of all subscripts* and is

$$C\lambda_C = B_0\lambda_B\frac{\lambda_C}{\lambda_C - \lambda_B}(e^{-\lambda_B t} - e^{-\lambda_C t}) \tag{7.8}$$

for the activity of C at time t due to B_0 at $t = 0$. This activity is, of course, additional to the activity of Eq. (7.4), which represents the activity of C grown only from A_0.

If, at $t = 0$, there was also an amount C_0 of substance C present, then at any later time the *additional* activity due to the residue of this initial stock will be

$$C\lambda_C = C_0\lambda_C e^{-\lambda_C t} \tag{7.9}$$

Problems

1. On a single schematic diagram, show the basic relationships between $A\lambda_A$, $B\lambda_B$, and $C\lambda_C$ as functions of time, if A experiences appreciable decay, for example, $T_A = 5T_B = 3T_C$. Does the $C\lambda_C$ curve cross over $B\lambda_B$ as well as over $A\lambda_A$? Where does the $C\lambda_C$ curve have zero slope? Does the ultimate transient-equilibrium activity ratio $C\lambda_C/B\lambda_B$ depend on T_B?

2. Derive the general expression for the activity $C\lambda_C$ in the series $A \rightarrow B \rightarrow C \rightarrow$, with initial conditions $A = A_0$, $B = C = 0$ at $t = 0$. Use the method based on the production of $B\lambda_B\,dx$ atoms of C during the time interval between x and $x + dx$ and their subsequent decay for the remaining time $(t - x)$.

3. Consider the isomeric transition:

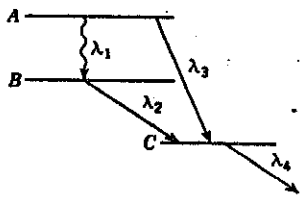

(*a*) Derive expressions for the *activity* of B and of C, if at $t = 0$: $A = A_0$, $B = C = 0$.

(*b*) Show that these expressions collapse into the simpler standard form, Eqs. (2.8) and (7.4), when the crossover transition λ_3 is absent.

4. A thorium mineral contains the entire Th series of radioactive nuclides, in secular equilibrium with Th. The series begins as follows:

$$_{90}Th^{232} \xrightarrow[1.39\times10^{10}\,yr]{\alpha} MsTh_1 \xrightarrow[6.7\,yr]{\beta^-} MsTh_2 \xrightarrow[6.1\,hr]{\beta^-} {}_{88}RdTh^{228} \xrightarrow[1.9\,yr]{\alpha} ThX \xrightarrow[3.6\,d]{\alpha}$$

RdTh is seen to be an isotope of Th. When Th is separated chemically from a mineral, it is accompanied by the equilibrium activity of RdTh, but by no $MsTh_1$.

(*a*) Derive an expression for the activity of RdTh in a thorium salt, as a function of time elapsed after separation of Th, and hence also RdTh, from the mineral. Show graphically the character of the variation with time of the activity of both RdTh and $MsTh_1$ in the Th fraction.

(*b*) Show that the activity of RdTh passes through a *minimum* value several years after the separation. Find the time of this minimum and the minimum activity of RdTh relative to its equilibrium value. *Ans.:* 4.8 yr; 0.392.

5. From an old and unaltered uranium mineral, the entire ionium and radium content are quantitatively separated into two residues by chemical methods. The radium produced per year in the ionium separate ($\Delta Ra/\Delta t$) is then compared with the quantity of radium (Ra) originally in the mineral and hence in equi-

librium with this amount of ionium. Show that the mean life τ of radium is given directly by a measurement of the ratio of the two radium samples, Ra/ΔRa, and observation of a calendar for Δt, that is, $\tau = (\text{Ra}/\Delta\text{Ra})\,\Delta t$. [Gleditsch and Foyn, *Am. J. Sci.*, **24**: 387 (1932)].

8. *General Equations of Radioactive-series Growth and Decay*

Equations (1.4), (2.7), and (7.4), which refer to one, two, or three radioactive substances, have been generalized and put into a symmetrical form for any number of products by Bateman (B20).

a. Accumulation of Decay Products. Suppose that, at time $t = 0$, there are A_0 atoms of A present and no atoms of its series of decay products $B, C, \ldots, M, N$. Let the decay constants of A and its products be $\lambda_A, \lambda_B, \lambda_C, \ldots, \lambda_M, \lambda_N$. Then, at any time t, the number of atoms of N present will be given by the integral of

$$\frac{dN}{dt} = M\lambda_M - N\lambda_N \tag{8.1}$$

where M is evaluated from a series of equations similar to Eq. (8.1) for the amounts of the preceding products. The result of this integration is

$$N = A_0(h_A e^{-\lambda_A t} + h_B e^{-\lambda_B t} + \cdots + h_M e^{-\lambda_M t} + h_N e^{-\lambda_N t}) \tag{8.2a}$$

in which the coefficients are dimensionless functions of the decay constants and have the following systematic values

$$\begin{aligned}
h_A &= \frac{\lambda_A}{\lambda_N - \lambda_A}\,\frac{\lambda_B}{\lambda_B - \lambda_A}\,\frac{\lambda_C}{\lambda_C - \lambda_A}\cdots\frac{\lambda_M}{\lambda_M - \lambda_A} \\
h_B &= \frac{\lambda_A}{\lambda_A - \lambda_B}\,\frac{\lambda_B}{\lambda_N - \lambda_B}\,\frac{\lambda_C}{\lambda_C - \lambda_B}\cdots\frac{\lambda_M}{\lambda_M - \lambda_B} \\
h_M &= \frac{\lambda_A}{\lambda_A - \lambda_M}\,\frac{\lambda_B}{\lambda_B - \lambda_M}\,\frac{\lambda_C}{\lambda_C - \lambda_M}\cdots\frac{\lambda_M}{\lambda_N - \lambda_M} \\
h_N &= \frac{\lambda_A}{\lambda_A - \lambda_N}\,\frac{\lambda_B}{\lambda_B - \lambda_N}\,\frac{\lambda_C}{\lambda_C - \lambda_N}\cdots\frac{\lambda_M}{\lambda_M - \lambda_N}
\end{aligned} \tag{8.2b}$$

The initial condition, that $N = 0$ at $t = 0$, requires that the sum of the coefficients be zero, and these coefficients do satisfy the condition that

$$h_A + h_B + h_C + \cdots + h_M + h_N = 0 \tag{8.2c}$$

Although the solutions for A, B, C are contained as special cases in the general *Bateman equation*, Eqs. (8.2), it is usually simpler to use the explicit formulations of Eqs. (1.4), (2.7), and (7.4) for these three simplest cases.

The activity of the product N is, of course, $N\lambda_N$, and the values $A_0, A, \ldots, N$ refer to the number of atoms present. To obtain relative weights of the substances, each of these values must be multiplied by the atomic weight of the substance in question.

An important example of the application of Eqs. (8.2) is the equilibrium activity of the short-lived decay products of radon when at $t = 0$ only radon is present. Then in Eqs. (8.2) the symbols $A, B, \ldots$ and $\lambda_A, \lambda_B, \ldots$ represent the radioactive substances and their decay constants as given in Table 8.1. For $t > 4$ hr, equilibrium exists as is

TABLE 8.1. THE SHORT-LIVED DECAY PRODUCTS OF RN

The type of radioactive transition is indicated for each substance. The last row gives the per cent by which the activity of the product exceeds the activity of the parent Rn, when transient equilibrium exists.

Substances:	$_{86}Rn^{222}$ $\xrightarrow{\alpha}$	RaA $\xrightarrow{\alpha}$	RaB $\xrightarrow{\beta}$	RaC $\xrightarrow{\substack{0.9996\beta \\ 0.0004\alpha}}$	RaC′ $\xrightarrow{\alpha}$
T:	3.82 days	3 min	26.8 min	19.7 min	150 μsec
Symbols:	$A \longrightarrow$	$B \longrightarrow$	$C \longrightarrow$	$D \longrightarrow$	E
λ in 10^{-4} sec^{-1}:	$\lambda_A = 0.021$	$\lambda_B = 37.9$	$\lambda_C = 4.31$	$\lambda_D = 5.86$	$\lambda_E = 4 \times 10^{11}$
Per cent excess activity:		0.054	0.54	0.89	0.85

shown by the fact that in the expressions from Eqs. (8.2) for $A, B, \ldots$ all the exponentials reach values which are negligible compared with the term in $e^{-\lambda_A t}$. Thus the number of atoms of D (that is, RaC) present is

$$D = \frac{\lambda_A}{\lambda_D - \lambda_A}\,\frac{\lambda_B}{\lambda_B - \lambda_A}\,\frac{\lambda_C}{\lambda_C - \lambda_A}\,(A_0 e^{-\lambda_A t}) \tag{8.3}$$

the term in parentheses being equal to A. Then the activity of D is $D\lambda_D$ and of A is $A\lambda_A$, and rearranging Eq. (8.3) we have the ratio of these activities

$$\begin{aligned}
\frac{D\lambda_D}{A\lambda_A} &= \frac{\lambda_B}{\lambda_B - \lambda_A}\,\frac{\lambda_C}{\lambda_C - \lambda_A}\,\frac{\lambda_D}{\lambda_D - \lambda_A} \\
&= \frac{T_A}{T_A - T_B}\,\frac{T_A}{T_A - T_C}\,\frac{T_A}{T_A - T_D} = 1.0089
\end{aligned} \tag{8.4}$$

The activity of RaC is therefore 0.89 per cent greater than its parent Rn, and transient equilibrium exists. Similarly the excess activity of the other products in this series is as shown in Table 8.1. The activity of RaC′, because of its almost immeasurably short life, is the same as that of its parent RaC, except for a deficiency of 0.04 per cent of the RaC disintegrations which skip the RaC′ step by traversing an alternative, or branch, disintegration through RaC″ to RaD.

The solution of Eqs. (8.2) for the α-ray decay products Rn, RaA, and RaC′ is shown in Fig. 8.1 as a function of t for 0 to 4 hr, when equilibrium becomes essentially established. Note that the curve for RaC′ is appreciably different from a simple accumulation curve, because of the effects of the intermediate products.

b. Decay of a Series of Products. The amount and activity of each radioactive product, due to a nuclear bombardment or a radioactive accumulation of any duration t, have been obtained through Eqs. (8.2). If now the primary source of radioactivity is removed, the amount and

activity of each product at any subsequent time can also be calculated with the aid of a group of equations, each having the form of Eqs. (8.2). It is only necessary to remember that the amount of N, for example, remaining at any later time is made up of (1) supply from $A, B, \ldots,$ each acting independently as an originally pure source of $A, B, \ldots,$ and producing the substance N in accord with Eqs. (8.2); and (2) the residual of the original amount of N present, which decays exponentially. Analytically,

$$N\lambda_N \equiv (\text{activity of } N) = (\text{growth from } A_0) + (\text{growth from } B_0) + \cdots + (\text{growth from } M_0) + (\text{residue of } N_0) \quad (8.5)$$

Thus, no matter how complicated the conditions of bombardment, accumulation, and decay, Eqs. (8.2) may be successfully applied because

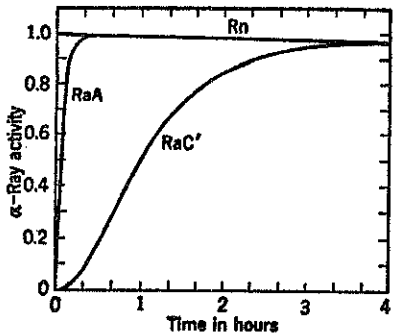

Fig. 8.1 The α-ray activity of Rn ($A\lambda_A$) and its accumulating decay products RaA ($B\lambda_B$) and RaC' ($E\lambda_E$), in terms of the α-ray activity of Rn at $t = 0$.

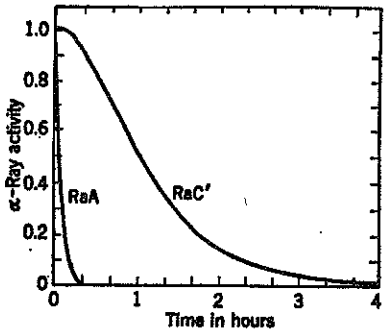

Fig. 8.2 Activity of the α-ray-emitting decay products of Rn, as they decay after having been in transient equilibrium at $t = 0$ with a Rn source having unit activity.

Eq. (8.1) is always the governing basic principle in all radioactive disintegrations. The decay of the series of products accumulated in Fig. 8.1, when the parent Rn is removed, is shown in Fig. 8.2.

Problems

1. In the production of a radioactive substance B by nuclear bombardment, as in a cyclotron or reactor, according to the scheme $A \xrightarrow[\lambda_A]{} B \xrightarrow[\lambda_B]{} C \xrightarrow[\lambda_C]{}$, show that a continuous and uniform bombardment of duration t produces an activity of B and C equal to

$$I_B = \lambda_B B = I_A(1 - e^{-\lambda_B t})$$

$$I_C = \lambda_C C = I_A\left(1 + \frac{\lambda_C}{\lambda_B - \lambda_C}e^{-\lambda_B t} - \frac{\lambda_B}{\lambda_B - \lambda_C}e^{-\lambda_C t}\right)$$

where $I_A \equiv A\lambda_A$ is the constant rate of production of B by the nuclear bombardment. Show that for relatively short bombardments, where $\lambda_B t$ and $\lambda_C t$ may

be neglected in comparison with unity, these expressions reduce after series expansion to

$$I_B = I_A(\lambda_B t)$$

$$I_C = \frac{I_A}{2}(\lambda_B t)(\lambda_C t)$$

2. After a bombardment of duration x, producing radioactive substance B, which decays into the radioactive substance C, the target is allowed to stand for a time t. Show that the activities of B and C are then

$$I_B = \lambda_B B = I_A(1 - e^{-\lambda_B x})e^{-\lambda_B t}$$

$$I_C = \lambda_C C = I_A\frac{\lambda_C}{\lambda_C - \lambda_B}\left[e^{-\lambda_B t}(1 - e^{-\lambda_B x}) - \frac{\lambda_B}{\lambda_C}e^{-\lambda_C t}(1 - e^{-\lambda_C x})\right]$$

3. Show that the maximum activity of C in the undisturbed target of the previous problem will occur at a time ϑ after the bombardment of duration x, where

$$\vartheta = \frac{1}{\lambda_C - \lambda_B}\ln\frac{(1 - e^{-\lambda_C x})}{(1 - e^{-\lambda_B x})}$$

and the maximum activity has the value

$$I_C = I_A e^{-\lambda_B \vartheta}(1 - e^{-\lambda_B x})$$

$$= I_A\frac{(1 - e^{-\lambda_B x})^{\lambda_C/(\lambda_C - \lambda_B)}}{(1 - e^{-\lambda_C x})^{\lambda_B/(\lambda_C - \lambda_B)}}$$

4. If the bombardment in Prob. 2 was long enough to produce equilibrium activities in $B\lambda_B$ and $C\lambda_C$,

(*a*) Show that at any time t after cessation of the bombardment the activity of C is

$$C\lambda_C = A\lambda_A\frac{\lambda_C}{\lambda_C - \lambda_B}\left(e^{-\lambda_B t} - \frac{\lambda_B}{\lambda_C}e^{-\lambda_C t}\right)$$

(*b*) On a basis of a careful examination of this expression and its time derivatives or its expansions for small t, construct a schematic graph of $C\lambda_C$ vs. t. Pay particular attention to the shape of this curve for the values of t which are very small and very large compared with the half-period of the substance B. Give approximate analytical expressions for the activity $C\lambda_C$ at these two extremes of time.

5. Actinon, from a 1-mc source of Ac which is in equilibrium with AcX, is passed through a collecting device in which the AcB produced by the decay of the An is accumulated. Assume that 27 per cent of the available AcB atoms are actually collected and that the accumulation time is x. Three separate accumulation experiments are then performed, with $x = 30$ sec, 36 min, and 24 hr. Calculate and plot the activity of AcC as a function of time for $t = 0$ to 3 hr after the end of the accumulation time, x, for the three values of x.

Ans.:

NOTE: The characteristic and markedly different shape of these three activity curves accounted for the discovery of AcB ($_{82}Pb^{211}$) by Brooks [*Phil. Mag.*, **8**: 373 (1904)] and Bronson [*Am. J. Sci.*, **19**: 185 (1905)]. The important general method of varying the accumulation or irradiation time, in order to disclose and evaluate an intermediate activity λ_B, is now standard procedure, especially for evaluating isomeric levels and for studying fission-product decay chains.

6. From the half-periods and atomic weights involved, determine the equilibrium *weight ratio* between radium and uranium, as in an ancient ore. *Ans.*: 0.34 μg Ra per gram U.

7. Calculate the ratio of the number of grams of protactinium to the number of grams of radium in an old uranium mineral. Use the nuclear constants given in Prob. 5, Chap. 15, Sec. 1. *Ans.*: 1.0 g Pa per gram Ra.

9. *Accumulation of Stable End Products*

The general theory of the accumulation of a radioactive product applies also to the accumulation of a stable end product. For any stable nuclide, $\lambda = 0$.

Then if A is radioactive and decays into B which is stable, we apply Eq. (2.7)

$$B = A_0 \frac{\lambda_A}{\lambda_B - \lambda_A} (e^{-\lambda_A t} - e^{-\lambda_B t})$$

which, with $\lambda_B = 0$, becomes

$$B = A_0(1 - e^{-\lambda_A t}) \tag{9.1}$$

$$B = A_0 - A \tag{9.2}$$

$$B = A(e^{\lambda_A t} - 1) \tag{9.3}$$

The first two equations for B express the obvious fact that $A_0 = A + B$, that is, the original A_0 atoms are at time t either still untransformed ($= A$) or have transformed into B. The third expression is useful where, for example, t is to be computed from measurements of the residual amount of A and of the amount of its decay product B which has accumulated. This is the principle of those *geological-age measurements* which are based on the accumulation of lead in ancient uranium or thorium minerals.

The accumulation of a stable granddaughter product C follows from Eq. (7.2), which with $\lambda_C = 0$ in Eqs. (7.3) becomes

$$C = A_0 \left(- \frac{\lambda_B}{\lambda_B - \lambda_A} e^{-\lambda_A t} - \frac{\lambda_A}{\lambda_A - \lambda_B} e^{-\lambda_B t} + 1 \right) \tag{9.4}$$

$$C = A_0 \left[1 - e^{-\lambda_A t} - \frac{\lambda_A}{\lambda_B - \lambda_A} (e^{-\lambda_A t} - e^{-\lambda_B t}) \right] \tag{9.5}$$

$$C = A_0 - A - B \tag{9.6}$$

Thus, at time t, the original A_0 atoms are divided between residual A, "holdup" as B, and stable end product C, as required by elementary conservation.

When the supply of active material is from a nuclear reaction, e.g., from

$$Na^{23} \xrightarrow[\lambda_A]{(d,p)} Na^{24} \xrightarrow[\lambda_B]{\beta^-} Mg^{24} \xrightarrow[\lambda_C = 0]{\text{stable}}$$

then we want an expression for C in terms of the target activity $A_0\lambda_A$. In dealing with λ_C ($= 0$), and with λ_A ($\to 0$), mathematical caution is required! It must be recognized that $e^{-\lambda_A t}$ is not *exactly* equal to unity, because λ_A is not zero but only very small. The significant terms in the correct expression for C will arise as the difference between two very large terms. In either Eq. (9.4) or (9.5), the substitution

$$e^{-\lambda_A t} = 1 - \lambda_A t$$

is justified because λ_A is *nearly* zero. After collecting terms and neglecting λ_A in comparison with λ_B, we obtain the result

$$C = A_0\lambda_A \left[t - \frac{1}{\lambda_B} (1 - e^{-\lambda_B t}) \right] \tag{9.7}$$

On comparison with Eq. (5.8), for B, this is seen to be equal to

$$C = A_0\lambda_A t - B \tag{9.8}$$

Thus the steady production rate $A_0\lambda_A$, continued for a time t, produces B radioactive atoms and C stable atoms. If t is large, B may become negligible compared with $A_0\lambda_A t$.

In dealing with the accumulation of the stable end products of longer series, such as the fission chains, the same mathematical precautions are necessary. It is rigorously correct to set the decay constant λ of the final stable product equal to zero; however, the difference between unity and $e^{-\lambda_A t}$ must be preserved as $\lambda_A t$, even though λ_A is nearly zero.

Problems

1. In the series disintegration

$$A \xrightarrow[\lambda_A]{} B \xrightarrow[\lambda_B]{} C \xrightarrow[\lambda_C]{} D \text{ (stable)}$$

show that, if $A\lambda_A$ is the constant activity of a very long-lived source, the number of atoms of D collected in a time t is given by

$$\begin{aligned} D &= A\lambda_A \left[t - \frac{1}{\lambda_B} - \frac{1}{\lambda_C} - \frac{\lambda_C}{\lambda_B(\lambda_B - \lambda_C)} e^{-\lambda_B t} + \frac{\lambda_B}{\lambda_C(\lambda_B - \lambda_C)} e^{-\lambda_C t} \right] \\ &= A\lambda_A t - B - C \end{aligned}$$

2. Tellurium is bombarded by deuterons in a cyclotron, forming

$$_{52}Te^{130}(d,p)Te^{131} \xrightarrow[T = 30 \text{ hr}]{\beta^-} I^{131} \xrightarrow[T = 8.0 \text{ d}]{\beta^-} Xe^{131} \text{ (stable)}$$

The bombardment conditions are such that the (d,p) reaction is equivalent to a source strength of 2 mc (i.e., 74×10^6 disintegrations per second).

(a) What is the initial rate of production of I^{131}, in microcuries per hour?

(*b*) How many atoms of Xe^{131} would be produced *during* a single 6-hr bombardment?

(*c*) What would be the *total* number of atoms of Xe^{131} obtained eventually, if this target were allowed to stand undisturbed for several months following a single 6-hr bombardment?

Ans.: (*a*) zero; (*b*) 8×10^8 atoms; (*c*) 1.60×10^{12} atoms.

3. One gram of natural uranium is carefully purified from ionium and radium and then allowed to stand for about 1 to 10 yr.

(*a*) What will be the activity of radium, in curies, which will grow in the sample in t yr?

(*b*) How many cubic centimeters (normal temperature and pressure) of He will grow in the sample in t yr?

NOTE: As both answers are to be compared with experimental results, a precision of 1 or 2 per cent is entirely adequate for computing (*a*) and (*b*).

Ans.: (*a*) $6 \times 10^{-16} t^2$ curie Ra/(yr^2)(g U); (*b*) $3 \times 10^{-6} t$ cm^3 He/(yr)(g U).

4. The half-period of U^{235} was first determined accurately by mass-spectroscopic measurements of the relative isotopic abundance of Pb^{207} and Pb^{206} which are the end products of the decay of U^{235} and U^{238}, accumulated in ancient uranium minerals [A. O. Nier, *Phys. Rev.*, **55**: 153 (1939); **60**: 112 (1941)]. The age t was determined in the same minerals from measurements of U^{238} and Pb^{206}, and the ratio of $U^{238}/U^{235} = 139 \pm 1$ was found to be independent of t. Show that the ratio of the lead isotopes Pb^{207}/Pb^{206} depends on t and on the decay constants λ_A of U^{235}, and λ_U of U^{238}, in the following way

$$\frac{Pb^{207}}{Pb^{206}} = \frac{1}{139}\frac{(e^{\lambda_A t} - 1)}{(e^{\lambda_U t} - 1)}$$

where $\lambda_A = 139\, R\lambda_U$ and R is the activity ratio of U^{235}/U^{238} in natural uranium. Plot the Pb^{207}/Pb^{206} ratio expected in the radiogenic lead, if $R = 0.04$ and if $R = 0.05$, against an age scale from 0 to 2×10^9 yr, and compare with Nier's measurements. Determine the half-period of U^{235}, if the data fit an activity ratio $R = 0.046$. *Ans.*: 7.1×10^8 yr.

5. (*a*) If a certain mineral contains 1 g of potassium and is known to be 2.0×10^9 yr old, what is the maximum number of milliliters of argon (measured at 0°C, 760 mm Hg) which should have accumulated in the mineral? Why is your numerical result a maximum value? Use the radioactive constants of K^{40} given in Prob. 2 of Chap. 15, Sec. 1.

(*b*) Show that the existence of competing EC transitions of K^{40} to A^{40} influences the accumulation of Ca^{40} from the β decay of K^{40} in such a way that

$$Ca^{40} = K^{40}\left(1 + \frac{\lambda_{EC}}{\lambda_\beta}\right)^{-1}(e^{\lambda_\beta(1+\lambda_{EC}/\lambda_\beta)t} - 1)$$

(*c*) Calculate the ratio of the number of atoms of radiogenic Ca^{40} per atom of K^{40} expected in a potassium mica which is 2.0×10^9 yr old.

Ans.: (*a*) 0.0154 cm^3 A^{40} per gram K; (*b*) 2.1.

10. *Summation Rules*

In many practical problems much of the involvement of the brute-force mathematical application of the Bateman equations can be skipped, if physical principles and thought are used instead. We illustrate these fruitful physical approaches by explicit development of "summation rules." These unify the processes of accumulation and decay. They apply to any member of a radioactive decay series. They apply also to any other physical process in which successive steps are linked by exponential functions of time or space, as in the multiple scattering and absorption of γ rays, β rays, and neutrons.

a. Summation of Decay and Accumulation Curves. In Fig. 10.1, the accumulation of daughter activity $B\lambda_B$ from a long-lived parent activity $A_0\lambda_A$ follows the growth curve 1, which is

$$(B\lambda_B)_1 = A_0\lambda_A(1 - e^{-\lambda_B t}) \tag{10.1}$$

At any arbitrary time, $t = x$, after the beginning of the bombardment, the activity $B\lambda_B$ is

$$(B\lambda_B)_2 = A_0\lambda_A(1 - e^{-\lambda_B x}) \tag{10.2}$$

If we separate this activity out, its subsequent decay will follow curve 2, and the activity remaining at any later time, $t = x + y$, will be

$$(B\lambda_B)_2 = (B\lambda_B)_x e^{-\lambda_B y} = A_0\lambda_A e^{-\lambda_B y} - A_0\lambda_A e^{-\lambda_B(x+y)} \tag{10.3}$$

If, in addition to this, the parent source continues to operate, it will produce new daughter activity along the curve 3, and at time $t = x + y$ this activity will be

$$(B\lambda_B)_3 = A_0\lambda_A(1 - e^{-\lambda_B y}) \tag{10.4}$$

The total daughter activity at time $t = x + y$ is given by the sum of these two fractions (curves 2 and 3) and is equal to

$$(B\lambda_B)_2 + (B\lambda_B)_3 = A_0\lambda_A(1 - e^{-\lambda_B(x+y)}) = (B\lambda_B)_1 \tag{10.5}$$

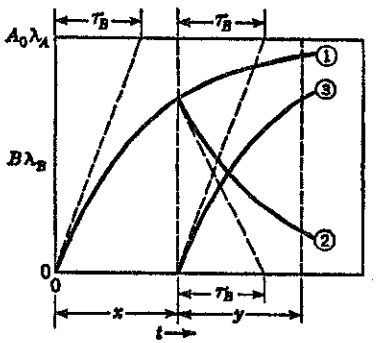

Fig. 10.1 The total accumulated activity, curve 1, is always the sum of a decay curve 2 and a new growth curve 3, where curves 2 and 3 begin at any arbitrary time $t = x$. See Eqs. (10.1) to (10.5). Also, (slope of curve 1) = (slope of curve 3) + (slope of curve 2) at any arbitrary time $t = x + y$.

which is simply the original uninterrupted growth curve. Physically, this is equivalent to noting that the mere act of separating the activity $(B\lambda_B)_x$ from the parent has no effect whatsoever on its subsequent decay. Once it is produced, *the subsequent behavior of each atom of B is entirely independent of its environment.*

It is also helpful to note that the slope of the accumulation curve 1 is always equal to the sum of the slopes of the decay and growth curves 2 and 3. This generalization can be visualized graphically for the particular time $t = x$. For any value of time t we have

$$\frac{dB}{dt} = A_0\lambda_A - B\lambda_B \tag{10.6}$$

Multiplying both sides by λ_B gives

$$\frac{d(B\lambda_B)}{dt} = A_0\lambda_A\lambda_B - B\lambda_B\lambda_B = \frac{A_0\lambda_A}{\tau_B} - \frac{B\lambda_B}{\tau_B} \tag{10.7}$$

The term $(A_0\lambda_A/\tau_B)$ is the "yield" or initial slope of the growth curve 3, while $(-B\lambda_B/\tau_B)$ is the initial slope of the decay curve 2. Both slopes are shown dotted on Fig. 10.1.

It can be shown that, under the most general conditions, any growth curve is always the sum of two curves like 2 and 3, one representing the decay of the product and the other representing the immediate growth of new activity. Figure 10.2 expresses this generalization graphically when λ_A is not neglected. Analogous relationships are also valid for all later generations, $C\lambda_C$, $D\lambda_D$, . . . , in a decay series and can be visualized by superimposing Fig. 8.2 on Fig. 8.1. Stated in words, the summation-rule generalization is

$$\begin{bmatrix}\text{Accumulation}\\ \text{at time } t\\ \text{(curve 3 growth)}\end{bmatrix} = \begin{bmatrix}\text{equilibrium amount}\\ \text{at time } t\\ \text{(curve 1 equilibrium)}\end{bmatrix} - \begin{bmatrix}\text{residue of a hypothetical initial equilibrium amount, which decays during the accumulation period}\\ \text{(curve 2 decay)}\end{bmatrix} \tag{10.8}$$

As an elementary illustration, consider the accumulation of $B\lambda_B$ from a decaying parent $A\lambda_A$, with $0 < \lambda_A < \lambda_B$. Then from Eq. (10.8) and Fig. 10.2 with $x = 0$,

$$\begin{aligned} B\lambda_B &\equiv \text{curve 3} = \text{curve 1} - \text{curve 2}\\ &= \left(A\lambda_A\frac{\lambda_B}{\lambda_B - \lambda_A}\right) - \left(A_0\lambda_A\frac{\lambda_B}{\lambda_B - \lambda_A}\right)e^{-\lambda_B t}\\ &= A_0\lambda_A\frac{\lambda_B}{\lambda_B - \lambda_A}(e^{-\lambda_A t} - e^{-\lambda_B t}) \end{aligned} \tag{10.9}$$

which is the conventional general expression, Eq. (2.8), for the growth of a daughter activity.

The broad significance of the summation rules is that any radioactive parent material (or any nuclear reaction producing a radioactive daughter product) can be considered *to be always in equilibrium with its daughter substance,* if we are willing to overlook consideration of the physical whereabouts of the daughter. Thus 1 g of radium always supports 1 curie of radon, whether or not the radon is confined in the vessel which contains the radium. A hospital which owns 1 g of radium will also always have responsibility for 1 curie of radon. It makes no difference whether the radon is left with the radium or is pumped off the source every 24 hr and distributed in therapeutic applicators throughout the hospital; there will always be a *total* of 1 curie of radon, somewhere in the universe, whose existence is dependent on that 1 g of radium.

b. Transposition of Time Axis. Suppose a neutron source is available which can produce a maximum of 100 mc of Na^{24} through the reaction

$Na^{23}(n,\gamma)Na^{24}$. It is operated for an accumulation time t_a, turned off for a decay time t_d, then operated again for a second accumulation time t_{aa}, as shown in Fig. 10.3. The final Na^{24} activity at time $t_a + t_d + t_{aa}$ can be obtained from a single conventional accumulation curve, by suitable transposition of the coordinates. We have seen that the slope of the accumulation curve is always the yield $(A\lambda_A/\tau_B)$ minus the decay slope $(B\lambda_B/\tau_B)$ and hence depends only on the activity present and not on how or where this activity was produced. At the end of the decay period t_d, call the residual activity $(B\lambda_B)_2$. The subsequent accumulation

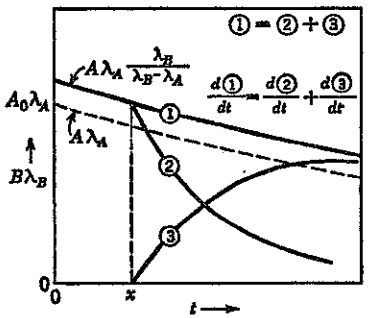

Fig. 10.2 Graphical representation of the summation rules for the activity $B\lambda_B$ of a daughter product, when $0 < \lambda_A < \lambda_B$, and for any x. The dotted curve is the decay of parent activity, $A\lambda_A = A_0\lambda_A e^{-\lambda_A t}$.

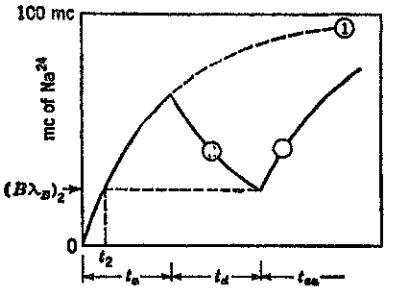

Fig. 10.3 Net accumulation from discontinuous bombardments, t_a and t_{aa}, can be read from a single conventional accumulation curve 1 by transposing the time axis.

curve 3 is identical with the original accumulation curve 1 except that it is transposed along the time axis by an amount $(t_a + t_d - t_2)$, where t_2 is the time at which the activity was $(B\lambda_B)_2$ on the original accumulation curve 1.

Problems

A little contemplation saves a lot of calculation.

1. A neutron source is available in your laboratory which produces at equilibrium 100 mc of P^{32} (T = 14 days) from $P^{31}(n,\gamma)P^{32}$. For a particular experiment, you need a maximum possible activity of P^{32}. Just as you begin your bombardment, a friend gives you 75 mc of P^{32}. How long should you run your own bombardment so that your total P^{32} on hand will be maximum? What is this maximum activity, in millicuries? What benefit, if any, do you get from the gift? Explain why this is so, using only the exponential growth curve of P^{32} for your neutron source.

2. Show that Eq. (10.5) is also valid for the general case in which the parent activity is not constant but decays as $A\lambda_A = A_0\lambda_A e^{-\lambda_A t}$.

3. In Fig. 10.1 show that, at *any* time $t = x + y$, the

$$\text{(slope of curve 1)} = \text{(slope of curve 2)} + \text{(slope of curve 3)}$$

4. (*a*) In any decay series $A \rightarrow B \rightarrow C \rightarrow$, show by comparison of growth

INTERNATIONAL SERIES IN PURE AND APPLIED PHYSICS

LEONARD I. SCHIFF, *Consulting Editor*

Allis and Herlin Thermodynamics and Statistical Mechanics
Becker Introduction to Theoretical Mechanics
Clark Applied X-rays
Evans The Atomic Nucleus
Finkelnburg Atomic Physics
Ginston Microwave Measurements
Green Nuclear Physics
Gurney Introduction to Statistical Mechanics
Hall Introduction to Electron Microscopy
Hardy and Perrin The Principles of Optics
Harnwell Electricity and Electromagnetism
Harnwell and Livingood Experimental Atomic Physics
Harnwell and Stephens Atomic Physics
Houston Principles of Mathematical Physics
Houston Principles of Quantum Mechanics
Hund High-frequency Measurements
Kennard Kinetic Theory of Gases
Marshak Meson Physics
Morse Vibration and Sound
Morse and Feshbach Methods of Theoretical Physics
Muskat Physical Principles of Oil Production
Read Dislocations in Crystals
Richtmyer, Kennard, and Lauritsen Introduction to Modern Physics
Schiff Quantum Mechanics
Seitz The Modern Theory of Solids
Slater Introduction to Chemical Physics
Slater Microwave Transmission
Slater Quantum Theory of Matter
Slater and Frank Electromagnetism
Slater and Frank Introduction to Theoretical Physics
Slater and Frank Mechanics
Smythe Static and Dynamic Electricity
Stratton Electromagnetic Theory
Thorndike Mesons: A Summary of Experimental Facts
Townes and Schawlow Microwave Spectroscopy
White Introduction to Atomic Spectra

The late F. K. Richtmyer was Consulting Editor of the series from its inception in 1929 to his death in 1939. Lee A. DuBridge was Consulting Editor from 1939 to 1946; and G. P. Harnwell 1947 to 1954.

THE ATOMIC NUCLEUS

Robley D. Evans, Ph.D.

PROFESSOR OF PHYSICS
MASSACHUSETTS INSTITUTE OF TECHNOLOGY

New York Toronto London
McGRAW-HILL BOOK COMPANY, INC.
1955

ORTEC
INCORPORATED
100 MIDLAND ROAD · OAK RIDGE · TENNESSEE 37830
AN EG&G COMPANY
TELEPHONE (615) 482-4411
TELEX 55-7450

QUALITY ASSURANCE DATA
Semiconductor Radiation Detectors

WARRANTY BASIS

Shipment Date 10-11-76 Serial No. 16-1790

Model No. BA-024-300-500

Active Area (nominal) 300 mm²

Alpha Resolution 24 Kev FWHM(a)

Noise width 19 Kev FWHM(b)

Sensitive Depth (minimum) 500 microns

Operating Bias 300 volts

Pos ☒ Neg ☐

ACTUAL MEASUREMENTS

Alpha Resolution 20.3 Kev FWHM(a)

Noise width 16.0 Kev FWHM(b)

Reverse Current 0.95 μamps @ 250 volts

Temperature 23 °C

Sensitive Thickness ≥ 500 microns

Nominal Resistivity 6500 Ωcm.

Electrode Thickness: Au 40.3 μgm/cm²

Al 40.0 μgm/cm²

NOTES:

WARRANTY TERMS

Detectors are guaranteed to meet the minimum specifications of the warranty basis data above for a period of 12MO from the date of shipment if used in careful laboratory conditions as outlined in the ORTEC Detector Instruction Manual. During the term of the original warranty period the detector will be repaired or replaced at ORTEC option, at no charge to the user with service credit extended for unused portion of warranty period from date of notification of failure.

ORTEC makes no other warranties, express or implied, and specifically NO WARRANTY OF MERCHANTIBILITY OR FITNESS FOR A PARTICULAR PURPOSE.

ORTEC's exclusive liability is limited to repairing or replacing, at ORTEC's option, items found by ORTEC to be defective in workmanship or materials within one year from the date of delivery. ORTEC's liability on any claim of any kind, including negligence, loss or damages arising out of, connected with, or from the performance or breach thereof, or from the manufacture, sale, delivery, resale, repair, or use of any item or services covered by this agreement or purchase order, shall in no case exceed the price allocable to the item or service furnished or any part thereof that gives rise to the claim. In no event shall ORTEC be liable for special or consequential damages.

GENERAL SPECIFICATIONS

1. All detectors are operated in excess of 12 hours in vacuum of 10^{-6} mm of Hg before taking data shown.

2. Surface barrier type detectors have a front surface dead layer no greater than that corresponding to 20 Kev energy loss from a 5.5 Mev alpha.

a. Alpha resolution is the full-width at half-maximum (FWHM) of a 5.5 Mev thin Am^{241} alpha source spectrum line, measured with detector and source in vacuum, with stated high voltage, and includes the noise contribution of an ORTEC Amplifier System.

b. Noise Width is the FWHM of an ORTEC precision pulse generator line spectrum with detector connected as a noise source to input of an ORTEC Amplifier System, and at stated bias voltage. Noise width is generally somewhat less than alpha resolution, and is very nearly equal to beta or proton resolution for totally absorbed particles.

Data Certified by Reba E Hiatt

Special Test Data

Printed in U.S.A.

2332 05K 0976

Be thoroughly familiar with the information that is furnished in this manual, and follow the operating instructions carefully. Know the symptoms of trouble so that the detector can be removed from danger before its usefulness is degraded or destroyed, and your EG&G ORTEC Charged Particle Detector will continue to provide excellent service over a very long period of time.

DAMAGE IN TRANSIT

Unpack your detector with care. DO NOT allow anything to touch the sensitive (gold) surface. In the event of loss or damage in transit, notify the transportation company immediately. Retain all containers and packing materials for their inspection. Please advise EG&G ORTEC within 10 days of any such loss or damage, and request instructions before making a return shipment.

RETURNS

If a detector should malfunction, please contact EG&G ORTEC Detector Marketing Department for information on possible causes and remedies. Should the device prove defective, this procedure will help us to repair or replace your device more quickly. If it is necessary to return your detector because of malfunction, please enclose as much information as possible concerning the symptoms and past history of the detector. This information will help make it possible for us to furnish you with detectors of even higher quality and greater reliability in the future. When packing the detector for return shipment to EG&G ORTEC, please replace the white protective cap that was furnished with the detector. Address the shipment to EG&G ORTEC, Attn.: Silicon Charged Particle Quality Control, 100 Midland Road, Oak Ridge, Tennessee 37830.

EG&G ORTEC will not accept for repair detectors which show signs of radiation contamination at levels which, in our opinion, might endanger our employees or impair our ability to manufacture low-background radiation detectors.

Silicon Charged Particle Radiation Detectors Instruction Manual

Printed in U.S.A.

3077 05K 0379

WARRANTY

EG&G ORTEC Charged Particle Detectors are warranted to be free from defects in material or workmanship.

Performance specifications for the A-Series, B-Series, C-Series, I-Series, P-Series, and R-Series detectors are warranted for a period of one year from date of purchase. The F-Series are warranted for three months.

Premium specifications for E-Series detectors are warranted for three months after purchase. For the succeeding nine months, E-Series detectors are warranted to operate within the specifications of comparable best category A-Series detectors.

The warranty period for all X-Series and for those D-Series detectors that are <26 microns thick is three months from purchase date, while those D-Series detectors that are ≥26 microns thick carry a one year warranty against performance degradation. These detectors are extremely fragile and are not warranted against breakage.

Detectors that have been subjected to **mishandling** or **radiation damage** are not covered under this warranty. Failure to adhere to the **Use** and **Handling Precautions** as prescribed in **Section 2** of this manual will constitute **mishandling**, as will obvious **physical damage** to the detector. **Radiation damage** can be determined by standard tests performed at EG&G ORTEC laboratories.

EG&G ORTEC makes no other warranties, express or implied, and specifically NO WARRANTY OF MERCHANTABILITY OR FITNESS FOR A PARTICULAR PURPOSE.

EG&G ORTEC's exclusive liability is limited to repairing or replacing, at EG&G ORTEC's option, items found by EG&G ORTEC to be defective in workmanship or materials within one year from the date of delivery. EG&G ORTEC's liability on any claim of any kind, including negligence, loss or damages arising out of, connected with, or from the performance or breach thereof, or from the manufacture, sale, delivery, resale, repair, or use of any item or services covered by this agreement or purchase order shall in no case exceed the price allocable to the item or service furnished or any part thereof that gives rise to the claim. In no event shall EG&G ORTEC be liable for special or consequential damages.

CONTENTS

ILLUSTRATIONS

1. MECHANICAL FEATURES OF STANDARD EG&G ORTEC CHARGED PARTICLE DETECTORS

The three basic EG&G ORTEC silicon charged particle detector configurations are shown in Fig. 1.1.* In each section of this figure, D is the effective diameter corresponding to the active area of the device, W is the depth of the sensitive (depletion) region, L is the total thickness of the silicon wafer, and L minus W is the thickness of the undepleted region. The region W corresponds to the silicon that contains an electric field resulting from the externally applied reverse bias (V_b) on the diode. Free charge carriers created in this region by the ionizing radiation are separated by the electric field. Integration of the current induced on the detector's contacts yields a charge proportional to the energy of the ionizing radiation.**

Information of the thickness of the electrodes in the different configurations is contained in the EG&G ORTEC Charged Particle Detectors Data Summary Chart (Table 7.3).

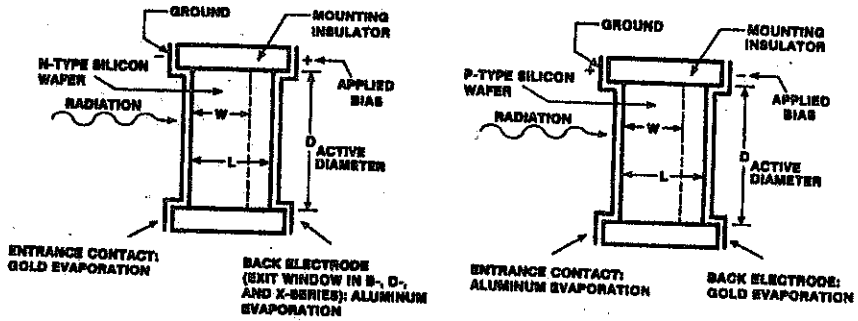

(a) A-, B-, C-, D-, E-, F-, and X-Series Detectors.

(b) R-Series (Ruggedized) Detectors.

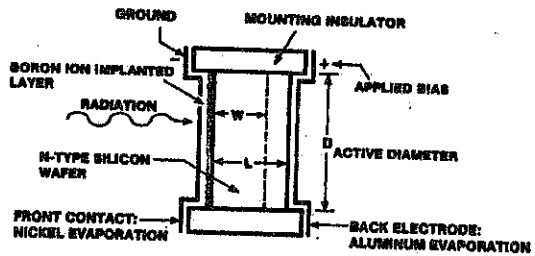

(c) I-Series (Ion Implanted) Detectors.

Fig. 1.1. Design of Typical EG&G ORTEC Charged Particle Detectors.

*The G-Series (HP Ge Ion Implanted) and P-Series (Position Sensitive) charged particle detectors are covered in separate manuals.

**For a more complete discussion of semiconductor detector physics see References 11, 15, and 16 (listed in Section 7 of this manual).

Figure 1.2 shows a cross section of a standard A-Series Charged Particle Detector. The sensitive surface (H) is evaporated with a thin layer of gold which must NEVER be touched or otherwise mechanically damaged. The circular silicon wafer (S) is mounted in an insulating ring (I) whose back and front surfaces are metallized. The front surface of this ring is grounded to the metal case (C), and thereby to the shield side of a standard Microdot or BNC connector (M). The back surface of the insulating ring is connected to the center electrode of the connector which serves as the signal output and bias voltage connection.

In the A-, B-, C-, D-, E-, F-, and X-Series detectors, the center electrode of the connector is supplied with positive bias potential and provides a negative output signal. In contrast, the EG&G ORTEC R-Series (Ruggedized) Charged Particle Detectors operate with these polarities reversed.

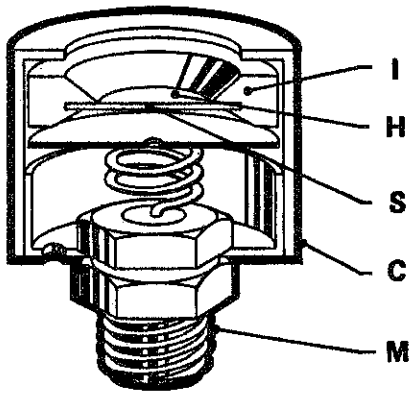

Fig. 1.2. Cross Section of an A-Series Charged Particle Detector in a B Mount.

2. HANDLING PRECAUTIONS FOR EG&G ORTEC CHARGED PARTICLE DETECTORS

NOTICE:

Read the Following Handling Precautions Carefully.

> FAILURE TO ADHERE TO THESE INSTRUCTIONS WILL USUALLY RESULT IN AN UNWORKABLE DETECTOR AND WILL NULLIFY YOUR WARRANTY.

2.1. A-, B-, C-, E-, AND F-SERIES*

1. Avoid mechanical shock. Silicon fractures easily. Damage to the epoxy-silicon interface will destroy the contact structure of the silicon diode.

2. Never touch the gold electrode on the sensitive surface. Damage to this surface will destroy the diode characteristics of your silicon detector. Keep the protective cap in place when the detector is not in use. A gentle air stream from a clean rubber syringe may be used to remove dust or lint.

3. Do not expose the detector to reducing atmospheres, such as hydrogen gas.

Avoid ambients where chemical contamination is present; e.g., mercury vapor, pump oil vapor, organic solvents, ionic salts, acetylene vapors, certain caustic or acid fumes (especially those of a reducing nature), soldering flux flames, large quantities of water vapor, etc. If the test chamber is cleaned with a solvent such as acetone or alcohol, evacuate the chamber thoroughly several times before installing the detector. If the detector is accidentally exposed to volatile contaminants, thoroughly evacuate the chamber several times with the detector installed before applying the bias voltage. Where ultimate performance and long term stability are required, it is preferable to use a cold-trapped vacuum system.

4. Apply bias only through a large ($\geq$1 megohm minimum) series resistance. **Do not apply bias in excess of the rated operating voltage.** Do not apply excessive bias to the detector, nor allow it to operate under breakdown conditions. Unless you are adept at recognizing the onset of microplasma and are willing to risk destroying the diode, do not apply bias in excess of the rated operating voltage. If you require a detector which will operate at higher bias voltage, you will probably find it more satisfactory to allow us to select one for you.

Follow these steps when applying bias to a detector:

1. Apply 10 to 20 volts to the detector. The noise, as observed on an oscilloscope or noise meter, should decrease (assuming a low noise charge sensitive amplifier configuration is used).

2. Continue to increase the voltage in small steps, allowing the noise meter to recover from transients to a reasonably steady reading before making further increases in voltage. Frequently, the noise will continue to decrease slowly for a period of several minutes to several hours; this is normal, particularly for detectors which have not been used recently.

3. Sudden momentary increases in the noise pulses are an indication of incipient microplasma. If this phenomenon occurs, proceed very slowly, and if the frequency and/or intensity of noise pulses increase, reduce the bias by approximately 30 percent and allow the detector to "age" (for a time sufficient to permit increases in the bias level without the strong pulsing noise effect) before proceeding.

4. A sudden, very large increase in noise, usually accompanied by an increase and/or fluctuations in the reverse current, is an indication of com-

*These series will be referred to as the "Gold Surface Barrier Series."

plete microplasma breakdown. Remove the bias voltage immediately in order to minimize irreversible damage to the detector.

5. After the desired bias voltage is attained, observe the noise level for a short time, in order to determine that it is not increasing and that there is no incipient microplasma breakdown.

Do not change the pressure around the diode suddenly while high bias voltage is applied. The preferred procedure is to pump down or let up, slowly, with no bias voltage applied to the detector. If the detector is stored for extended time in vacuum, it is best to leave a small nominal bias applied even when not in use.

The pressure region from 10 μm to several millimeters of Hg is a particularly serious one for surface breakdown. Neither the connector nor the diode is warranted for high voltage operation in this pressure region.

6. If the detector is cooled below room temperature, it is essential that it be operated in a very clean vacuum system; otherwise, condensation of water or organic vapors may initiate breakdown and excessive current leakage on the insulator and the diode. Adequately "clean" vacuum is best obtained with liquid nitrogen traps in close proximity to the space containing the detector, and between the detector and sources of contamination such as diffusion pumps. The performance of standard EG&G ORTEC detectors is not guaranteed below –30°C or above 25°C. If a cryogenic detector is required, it can be supplied on special order.

Artificial high humidity problems may be created when detector and preamp assemblies are operated at reduced temperatures. Here connections or input components may be cooled well below ambient air temperature with resultant condensation of moisture.

The use of careful design to prevent overloading of exposed components, baffles to properly divert cold gases, and attention to cleanliness of feedthrough connections are suggested.

7. When using radioactive sources, avoid unnecessary radiation damage or contamination by closing a shutter in front of the detector when it is not in use. Do not allow high-intensity beams, such as the main beam in an accelerator, to fall directly on the detector.

Always shield both the detector and all signal leads when using the detector in the vicinity of a charged particle accelerator beam; such a beam produces copious quantities of secondary low-energy electrons and ions from the target and residual background gas. Ion or electron currents to unshielded detector leads can cause excessive amplifier noise. Also, bombardment of the high purity silicon crystal can produce severe radiation damage in only a few hours of operation.

In addition to all precautions enumerated for the above-mentioned series, the Deep Series (nominally >2000 microns) require very high bias voltages. It is very important that precautions against humidity and unclean conditions be taken to prevent breakdown of feedthroughs and connectors used with these high voltage devices. An air conditioned laboratory is highly recommended. In any case, be sure that all electronic components associated with your high voltage detector system are clean and dry.

2.2. THIN D- AND X-SERIES

All above comments for the proper handling of the gold surface barrier series also apply to the thin D- and X-Series detectors. The following additional comments are especially important when handling these very fragile devices.

1. Do not overbias the detector. Very thin ΔE detectors require only a very modest bias voltage to produce adequate electric field strengths and small amounts of overbias can produce excessive electric field strengths.

REMEMBER: For a 10-μm thick detector, each 10 volts of overbias corresponds approximately to an additional field strength of 10,000 volts/cm.

2. In order to preserve the high spectroscopic quality of your D- or X-Series detector, **always operate it in a clean, well-trapped vacuum.**

3. When mounting your thin D- or X-Series detector, be careful not to exert strain on the mounting assembly. Distortion of the assembly ring can fracture this paper-thin silicon crystal!

4. **Do not cool your thin D- or X-Series detector,** nor expose it to temperature conditions above 25°C.

The capacitance of these detectors is their most significant contribution to total system noise. Cooling, therefore, is not expected to significantly contribute to the detector's performance, and since the expansion coefficient of the epoxy encapsulant is not an absolute match to that of the silicon, there is a danger of fracturing the silicon during extreme temperature change.

For very thin detectors which require only small operating voltages, ambient temperature fluctuations can cause significant changes in the detector bias voltage.

2.3. RUGGEDIZED R-SERIES

In contrast to the ultra sensitive gold surface on the gold surface barrier detector, the Ruggedized Series detector has a thin layer (1850 Å) of evaporated aluminum on its front surface. Since aluminum is more adherent to an etched silicon surface than gold, the front surface of the Ruggedized detector is relatively more rugged than is that of the gold series. However, all reasonable precautions should still be enforced with this state-of-the-art scientific instrument.

Destruction of its aluminum surface is less likely than would be if it were a gold surface barrier, but sharp instruments can scratch it and possibly increase its noise and resolution characteristics.

If contaminated, the aluminum surface may be cleaned gently with methanol and a cotton swab. The detector should be dried thoroughly before use. If moisture is absorbed into the lavite rings, it may be necessary to allow the device to remain in vacuum for several hours before operating. Detailed cleaning instructions are included with each shipment of Ruggedized detectors.

All other precautionary steps for the gold surface barrier detector series apply to the Ruggedized Series.

2.4. ION IMPLANTED I-SERIES

For those applications where the ultimate in reliability and ruggedness is required, the I-Series ion implanted detectors should be chosen.

The contact is "buried in" under the silicon surface and the metallization shown in Fig. 1.1 is applied only for the purpose of reducing the electrical resistivity of the contact. As a consequence, the front contact of an I-Series detector is extremely robust and easily cleanable. Moreover as the junction is not established by a Schottky barrier, but rather by an ion implanted junction, the I-Series detectors are expected to be less sensitive to environmental conditions than any other EG&G ORTEC charged particle detector.

3. OPERATING INSTRUCTIONS FOR EG&G ORTEC CHARGED PARTICLE DETECTORS

3.1. APPLICATION OF BIAS

3.1.a. Gold Surface Barrier and I-Series Detectors

In these detectors, the center electrode of the connector is supplied with positive bias potential and provides a negative output signal.

The recommended operating bias voltage for your detector is recorded on your Detector Data Sheet. This is the bias voltage required to produce the specified alpha particle resolution and noise characteristics, and is a function of the resistivity of the silicon used in the manufacture of the detector and its associated depletion depth. The resistivity of the silicon used in the fabrication of EG&G ORTEC silicon detectors is carefully selected to achieve optimum field strength for best charge collection characteristics at a specific depletion depth and reverse bias voltage.

Do not operate your detector at a bias greater than specified. It is specified to operate at its optimum overbias. Increasing the bias may result in microplasma breakdown which will result in irrepairable damage and will nullify your warranty. Bias is best applied slowly and in increments of 1/10th full operating bias. Be alert to signs of trouble, as indicated in Sections 2 and 4 of this manual.

A special word of caution is needed for detectors with a depletion layer greater than 2000 microns. These detectors often require operating voltages in excess of 3000 volts, so it is very important to assure that all connectors are very clean and dry.

Noise spikes and other signs of breakdown are very apt to be due to the connector or the preamp. EG&G ORTEC supplies a specially designed high voltage preamp for this detector series. Ask about the proper preamplifier when purchasing high voltage charged particle detectors.

3.1.b. Thin D- and X-Series Detectors

The recommended operating bias voltage for your detector is recorded in the WARRANTY BIAS section of your copy of the detector test data sheet. For detectors $\geq$26 μm thick, this is the bias voltage required to produce the specified alpha particle resolution with the alphas incident through the back (low field strength) contact. For detectors $<$26 μm thick, this is the bias required to provide an electric field strength sufficient to efficiently collect charge produced by an alpha particle adjacent to the rear (low field strength) contact.

The preamplifiers for these devices have an ~100 MΩ (or greater) bias resistor; thus the voltage drop in the bias resistor can easily exceed the detector bias. In this case, it is necessary to make a careful measurement of the detector reverse leakage current so that the resulting voltage drop across the bias resistor can be calculated. The effective resistance of the bias resistor can be measured readily by shorting the preamplifier with a 50Ω or 100Ω terminator and then measuring the resulting I-V characteristics.

3.1.c. Ruggedized Series Detectors

In contrast to other charged particle detectors, the Ruggedized Series requires that a negative bias potential be supplied to the center electrode of the connector. The output signal will then be positive. (Ruggedized detectors that will accept positive bias are available on special order.)

In addition to reversed polarity, all standard precautions for application of bias are also applicable to the Ruggedized Series.

3.2. CONTROL OF RADIATION DAMAGE

EG&G ORTEC detectors owe many of their most useful properties to the fact that they are made from extremely pure (impurities of the order of parts per billion), perfect, single crystals of silicon. This high degree of crystal perfection makes semiconductor detectors sensitive to radiation damage, since irradiation-produced defects may affect the electrical behavior of the device as effectively as impurities.

Permanent radiation damage effects in silicon result primarily from dislocations within the crystal lattice. Incident radiation of sufficient energy can displace a silicon atom from its equilibrium site to an interstitial position, the energy level necessary for the displacement depends on the type of incident radiation. The resulting vacancy-interstitial pair, or Frenkel defect, acts as a charge carrier trapping site. These sites contribute to resolution broadening by reducing the charge collection efficiency. In addition, they contribute to the device noise and current by acting as charge carrier generation-recombination centers. Poor charge collection from trapping effects can be improved by increasing the bias voltage (average electric field).

Totally depleted detectors, which usually have larger average electric fields as well as constant depletion depth, are considerably more radiation-damage resistant than partially depleted devices.

The causes and effects of radiation damage in surface barrier radiation detectors are enumerated in Table 7.2.

3.3. ALPHA PARTICLE RESOLUTION MEASUREMENTS

Measurements of alpha particle resolution must be performed in vacuum, and the alpha particle source must be very thin and uniform so that it does not affect the resolution. This resolution varies with source-to-detector spacing at very close spacings. Unless otherwise noted, the original alpha particle resolution measurement on your EG&G ORTEC detector was performed with source-to-detector spacing equal to 1-1/2 times the active diameter of the detector.

All alpha resolutions and noise measurements are made with EG&G ORTEC preamplifiers and amplifiers. No specific model numbers are reported here for these instruments because EG&G ORTEC updates preamplifiers and amplifiers with advancement of the state-of-the-art, and the best available instruments are used for the measurements. Your nearest EG&G ORTEC representative will be glad to bring you up to date on the best electronics to use with your detector.

Although the alpha resolution and noise measurements are standardized on 0.5 μs differential and integral time constants in the shaping amplifier, it is possible for certain detector models to provide a better performance when using different values for the differential and integral time constants. In particular, larger time constants may result in better alpha resolution and/or noise characteristics for detectors with very large capacitance values (several hundred pF).

3.4. THICKNESS OF ACTIVE AREA AND FIELD STRENGTH REQUIREMENTS

The active thickness of a charged particle detector is a function of the bulk resistivity of the silicon wafer and the operating voltage. Figure 7.4 is a nomogram that shows these relationships.

EG&G ORTEC charged particle detectors are fabricated from ultra pure silicon with resistivities specifically selected, so as to give optimum field strength for good resolution for charged particles at the specified thickness and operating voltage.

EG&G ORTEC totally depleted charged particle detectors are required to operate at sufficient overbias to allow good charge collection for alpha particles at the rear contact.

Figure 7.13 graphs maximum field strength as a function of silicon resistivity and operating voltage.

The maximum field strength of first category EG&G ORTEC charged particle detectors averages about 5000 V/cm.

4. TYPICAL OPERATIONAL PROBLEMS

4.1. DIRTY 110-VOLT POWER LINE

If extraneous "hash" or noise which is synchronized with 60 cps appears in the scope at the output of the amplifier, be suspicious of noise on the power line or a ground loop problem. This problem can sometimes be helped by using a low harmonic distortion, constant voltage transformer with a floating secondary, noise filters, or by an isolation transformer, but is most effectively reduced by elimination of ground loops and use of high quality amplifying equipment.

4.2. PICKUP NOISE

The signal level at the input to the preamplifier is ordinarily in the millivolt region, and the normal noise level in a high resolution detector-amplifier arrangement is of the order of microvolts. Therefore, all signal leads and the detector must be well shielded from pickup. It is primarily for this reason that EG&G ORTEC has adopted the convention of operating the detector with the sensitive face at ground potential. These detectors are supplied with a shielded can, with the front face at ground potential.

4.3. GROUND LOOPS

Like all noise level instruments, semiconductor detector-amplifier combinations are subject to ground loop problems if the equipment is not properly installed. These problems are particularly bothersome in complicated instrument arrangements, arrangements with long interconnecting cables, or when interconnecting equipment from different manufacturers. In making noise level measurements with the detector replaced with an equivalent capacitance, the capacitor should be grounded to exactly the same point as the detector, in order to show equivalent ground loop noise.

5. TROUBLE SYMPTOMS AND DETERMINATION OF THEIR PROBABLE CAUSES

5.1. NOISE LEVEL DOES NOT DECREASE WHEN BIAS IS APPLIED TO THE DETECTOR

1. Make sure the pulser is turned off and all radiation sources are removed.
2. If the noise level corresponds to zero external input capacitance, check for an open circuit between the amplifier and detector.
3. Reduce detector bias voltage to zero and remove the cable to the detector at the preamplifier. The noise should decrease, the amount of decrease depending on the amount of capacitance removed from the input. If the noise level does not decrease, the trouble is in the amplifier system.
4. Check the noise level from the amplifier.
5. Check for ground loop noise.

6. Considerable diagnostic information can be obtained by examining the character of the noise with an oscilloscope attached to the amplifier output.

5.2. UNUSUALLY HIGH NOISE AT ZERO BIAS OR AT VERY LOW BIAS

1. High resistance in signal lead, connectors, etc., between preamplifier and detector.
2. Partial or intermittent short circuit from signal lead to ground.

5.3. NOISE SPIKES OR EXTRANEOUS COUNTS

1. Dirty power line, pickup noise, or ground loop noise.
2. Intermittent microplasma breakdown in the detector. Replace detector with equivalent capacitance grounded in same place as detector.
3. Unknown source of background radiation.

5.4. DETECTOR REVERSE LEAKAGE CURRENT ABNORMALLY HIGH

1. Leakage currents in vacuum feedthrough or other components in the system.
2. High ambient temperature at detector.
3. Breakdown in the detector (will be accompanied by excessive noise).
4. Radiation damaged detector.
5. Moisture or organic vapor condensation problems.

5.5. DRIFTS IN PULSE HEIGHT OUTPUT FROM MONOENERGETIC SOURCE

The drifts are probably in the amplifier or in the multichannel analyzer. See if pulser peak is also drifting while detector is exposed to radiation source.

5.6. DISTORTED PEAK SHAPES IN ENERGY SPECTRUM

1. The counting rate exceeds the capabilities of the amplifier system. Check the shape of the pulser spectrum peak while the detector is exposed to the source.
2. Gain shifts or drifts in the amplifier system or multichannel analyzer. Check shape and width of pulser peak.
3. The range of the ionizing particles exceeds the sensitive depth of the detector. This will produce an extra density of counts per channel on the high energy side of the spectrum.
4. High rate – low energy background radiation extraneous to the main spectrum which exceeds count rate capabilities of system.
5. Insufficient bias voltage on detector.
6. Radiation damaged detector.

5.7. ENERGY RESOLUTION DETERIORATES WITH TIME

1. Gain drifts or biased amplifier drift. Check pulser peak width with time.
2. System noise increasing with time.
3. Radiation damage.
4. Detector noise increasing with time.

5.8. DETECTOR CURRENT INCREASES OR BREAKDOWN VOLTAGE DECREASES WITH EXTENDED EXPOSURE TO HIGH VACUUM

1. Moisture or organic vapor condensation problems.
2. Detector breakdown occurs occasionally, even with carefully manufactured and inspected detectors, and for this reason, your EG&G ORTEC detector was checked out in a high vacuum ($\approx 10^{-6}$ Torr) at rated bias voltage for at least 16 hours before shipment to you. The problem is thought to be caused by pumping away adsorbed oxygen which is passivating an area on the detector where undesirable surface impurities are present, or where the very thin oxide film responsible for the p-type nature of the surface has a flaw. If the microplasma breakdown in this region has not been too extensive or prolonged, the detector will frequently recover after several days or weeks of exposure to room air. The probability of this problem is significantly reduced by keeping a small nominal bias on the detector while it is in vacuum.

5.9. DETECTOR FAILS TO MEET SPECIFIED RESOLUTION PERFORMANCE

1. Check amplifier system noise level and stability with detector replaced by equivalent capacitance.
2. Make sure peak broadening is not caused by poor source, kinematic source broadening, or unreasonable source-detector geometry.

5.10. DETECTOR WILL NOT WITHSTAND RATED BIAS VOLTAGE

1. Check to make sure breakdown is not in cables, connectors, feedthroughs, etc.
2. Check to make sure vacuum system is at proper pressure and is free from contaminating atmosphere.

6. SOME TYPICAL APPLICATIONS OF SILICON DETECTORS

6.1. CHARGED PARTICLE COUNTING

Silicon detectors make excellent beta-ray counters. For low energy betas, they are superior to sealed end-window gas counters since their dead layer

(window thickness) is smaller, the detector is more compact, the background is usually smaller, and the problem of gas stability with time is absent. Their compactness, time stability, freedom from need for a continuous gas supply, and lower background with less shielding, also make them preferable to gas flow counters for many applications.

The efficiency of silicon detectors for charged particles is essentially 100% for any case where the energy lost in the sensitive region is much larger than the noise level. Consequently, these devices make excellent counters for natural alpha particles, fission fragments, protons, etc. For such simple counting applications, the detector's sensitive depth need only be large enough that the particle energy loss is sufficient to trigger the discriminator. The range-energy curves and energy loss curves in Figs. 7.7 and 7.8 can be used to estimate the required sensitive depth for any particular application.

If the capacitance of a device is too high to permit efficient counting with acceptable electronic background, a deeper depletion device will increase the energy deposited for particles that exceed the depletion depth and also reduce the capacitance, thereby reducing the noise and allowable discriminator level.

EG&G ORTEC offers an instrument that has been designed specifically for alpha counting. It is the 576 Alpha Spectrometer. This instrument is furnished in a standard double-width NIM module, and it contains two independent vacuum chambers, two R-Series detectors, and all of the front-end electronics (up to the scalers) necessary for low-level alpha counting. Contact your nearest EG&G ORTEC representative for further information.

6.2. FISSION FRAGMENT SPECTROSCOPY

The EG&G ORTEC F-Series heavy ion detectors may be utilized for determination of heavy ion and fission fragment mass and energy distributions. Devices of this design have performed satisfactorily for energy measurements and spectrum analysis when operated in the high field "saturation" region; i.e., that region where the pulse height ceases to increase in bias voltage. This region of operation provides sufficient electric field strength for complete charge collection or total sweep out of the high density of charge carriers generated by the incoming, highly ionizing, heavy ion. Operation below this region results in poor charge collection and poor resolution.

An upper limit to the useful operating region is established by the problems of internal avalanche multiplication at excessively high field strengths, and by microplasma breakdown and surface multiplication at excessively high bias voltages. The raw material properties and design criteria for EG&G ORTEC heavy ion detectors are carefully chosen to give the widest possible saturation region without detectable spectrum distortion. Surface multiplication via tunneling injection is prevented by proven surface treatments.

For optimum performance of these detectors for fission fragment analysis, careful attention must be given to the elimination of low-energy tailing and other spectral distortion problems. Low-energy tailing may be the result of source nonuniformity, excessive source thickness, or improper collimation

of the source and detector. Spectrum distortion and dispersion can result from an inadequate collimation of the reaction-inducing beam or from pulse shape distortion in the amplifier system. Consequently, the performance of these spectrometers will be enhanced by proper consideration for the problems associated with the source, collimation, and selection of an appropriate electronics system.

6.3. RUGGEDIZED DETECTORS

The Ruggedized Detector is an excellent choice for tutorial situations that involve handling by students or other inexperienced persons. The devices are comparable to standard gold surface barriers in resolution and noise specifications, but are much less prone to damage due to a careless thumb print on the front entrance window.

The 1850 Å thick aluminum entrance window is essentially light tight, and can consequently be operated as an environmental monitoring device in ordinary room light.

6.4. CHARGED PARTICLE SPECTROMETRY (see Bibliography reference 11) AND TIME RESOLUTION

The ultra thin entrance window, high field strength, and excellent noise and resolution characteristics of EG&G ORTEC Charged Particle Detectors make them especially useful for charged particle spectrometry. Their linearity over a wide energy range and their fast response time give these silicon detectors a decided advantage over other types of counters.

Another property of charged particle detectors, which is essential to charged particle spectroscopy, includes their availability in depletion depths suited for different experimental situations. Moreover, the combination of one total absorption detector with one or more dE/dx detectors can be used in particle discrimination.

In addition, the charged particle detector is not affected by magnetic fields, so it can be used in a magnetic spectrograph, where its characteristic low background counting is essential. The low background level also suggests a charged particle detector as the ultimate choice for polarization experiments using charged particles.

The fast response time of a charged particle detector makes it especially useful in coincidence experiments involving measurement of nuclear decay schemes with background reduction by suppression of parasitic reactions. For extremely low noise levels in these experiments, the charged particle detector can be operated at low temperatures.

Because of the compact size of EG&G ORTEC Charged Particle Detectors, large numbers of them can be placed into scattering chambers for angular distribution studies of nuclear reactions. Such simultaneous recording of events at different angles reduces costly accelerator time.

Angular correlation measurements with a simplified analysis can be done by placing one detector 180° with respect to the beam. For this experiment, a C-Series annular EG&G ORTEC Charged Particle Detector can be used in a position that allows the beam to pass through its annulus.

7. INFORMATIVE GRAPHS AND CHARTS

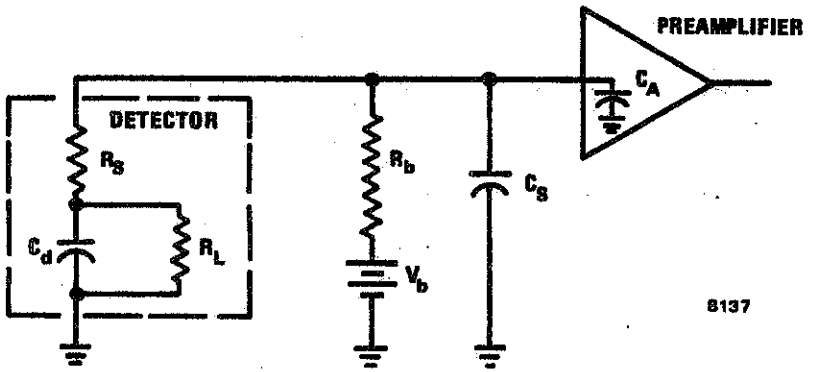

Fig. 7.1. Equivalent Circuit for Charged Particle Detector and First Preamplifier Stage.

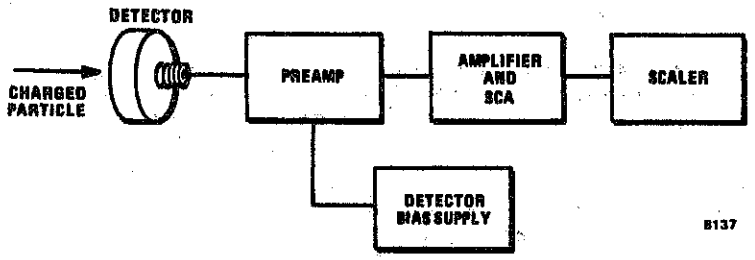

Fig. 7.2. Simple Charged Particle Counting System.

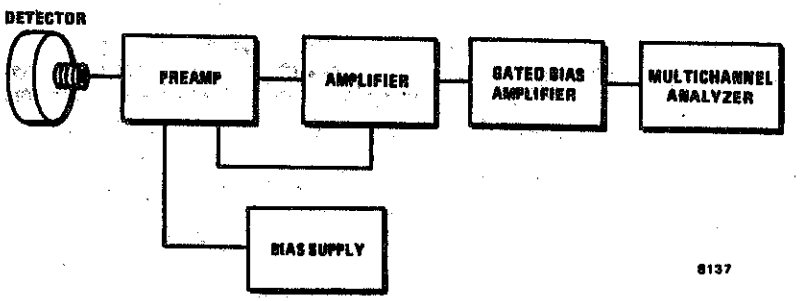

Fig. 7.3. Typical System for Charged Particle Spectroscopy.

Table 7.1. Selected Physical Properties of Silicon.

Atomic Density	5.0×10^{22} atoms $-$ cm^{-3}
Density	2.33 gm $-$ cm^{-3}
Dielectric Coefficient	12
Energy Gap	1.1 eV
Energy per Electron-Hole Pair	3.6 eV $-$ pair
Mobility	
Electron	1350 cm^2 $-$ volt^{-1} $-$ sec^{-1} (2.1×10^9 T$^{-2.5}$ cm^2 $-$ volt^{-1} $-$sec^{-1})
Hole	480 cm^2 $-$ volt^{-1} $-$ sec^{-1} (2.3×10^9 T$^{-2.7}$ cm^2 $-$ volt^{-1} $-$ sec^{-1})
Thermal Expansion, linear	4.2×10^{-6} (°C)$^{-1}$

Unless otherwise indicated, above quantities correspond to 25°C.

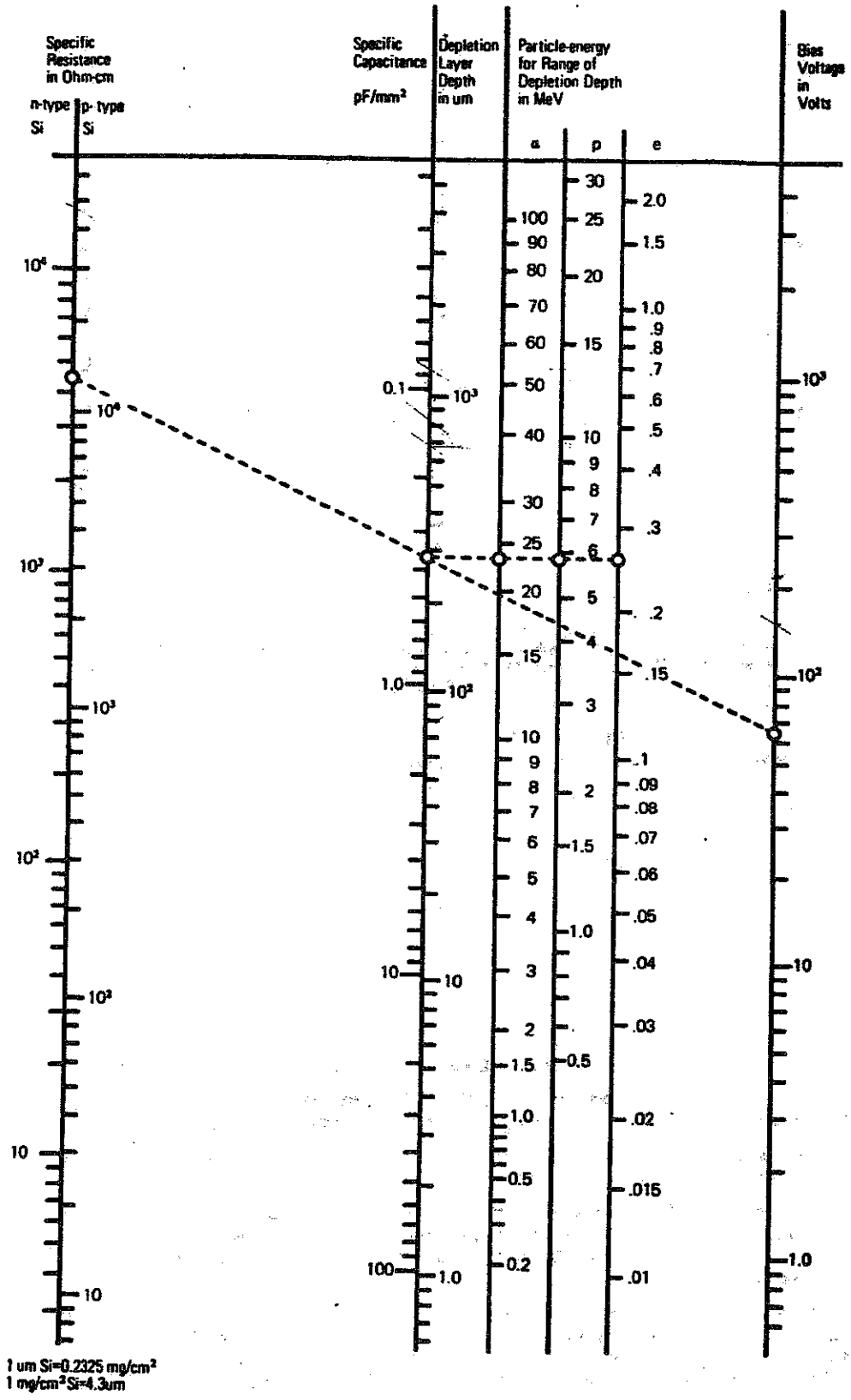

A straight edge intersecting the center vertical line at the required depletion depth will give combinations of resistivity and detector bias that may be used to achieve that depth. (Shown, for example, is the voltage that must be applied to a 13,000 ohm-cm p-type or 4500 ohm-cm n-type silicon detector to stop a 23-MeV alpha, a 6-MeV proton, or a 250-keV electron within the depletion depth.)

Fig. 7.4. Silicon Detector Parameters Nomogram.
[Similar to Nomogram reported by J. L. Blankenship, *IREE Trans.* NS-7(2-3):190 – 195 (1960).]

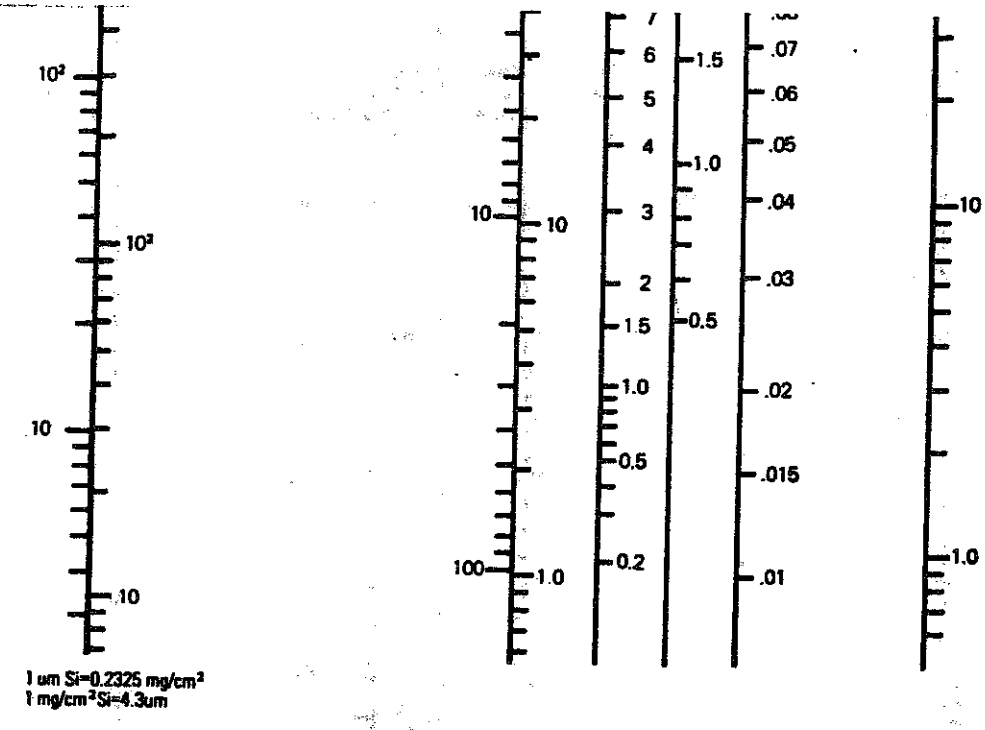

A straight edge intersecting the center vertical line at the required depletion depth will give combinations of resistivity and detector bias that may be used to achieve that depth. (Shown, for example, is the voltage that must be applied to a 13,000 ohm-cm p-type or 4500 ohm-cm n-type silicon detector to stop a 23-MeV alpha, a 6-MeV proton, or a 250-keV electron within the depletion depth.)

Fig. 7.4. Silicon Detector Parameters Nomogram.
[Similar to Nomogram reported by J. L. Blankenship, *IREE Trans.* NS-7(2-3):190 - 195 (1960).]

Silicon Detector Nomogram

This nomogram was obtained directly from the Schottky theory for an abrupt junction. In conjunction with the use of this nomogram, the following facts should be pointed out:

1. The fundamental derivation upon which the calculations are based ceases to be valid once the sensitive region extends completely through the wafer (dE/dx devices).

2. For detector configurations where the sensitive surface does not extend completely to the edge of the wafer (e.g., Schottky Barrier models), fringing field effects at the edge will cause a small departure from the capacitance relationships by changing the effective area as a function of applied bias.

3. The effective sensitive depth will be somewhat larger (from a few to 20 microns, depending on such factors as amplifier time constants) than the indicated barrier depth because of charge diffusion into the sensitive region. For betas (electrons), pronounced diffusion collection from depths as great as 500 μm has been frequently observed in surface barrier detectors.

4. In cryogenic applications where the resistivity of the silicon becomes very large, the Schottky Barrier model no longer gives a valid approximation of the internal field distribution.

5. The depletion depth and resultant capacitance are fundamentally related to the uncompensated impurity density N. Since for a fixed temperature (fixed mobility) the resistivity of the material is related to N through the mobility, it is possible to also add a scale relating to the sensitive depth to the **room temperature resistivity**. At other temperatures, the resistivity scale is not valid since the carrier mobilities are temperature dependent.

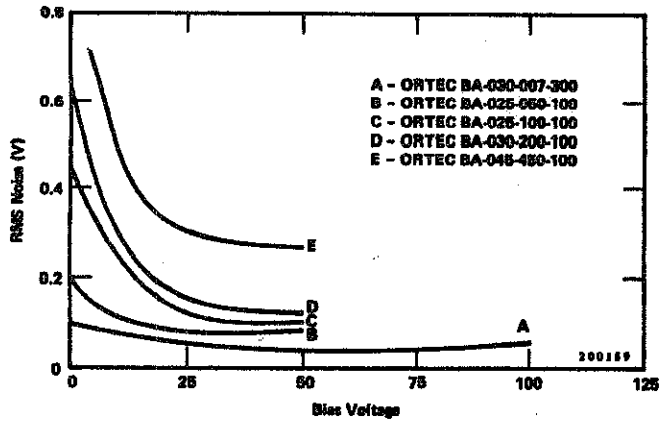

Fig. 7.5. Noise as a Function of Bias Voltage.

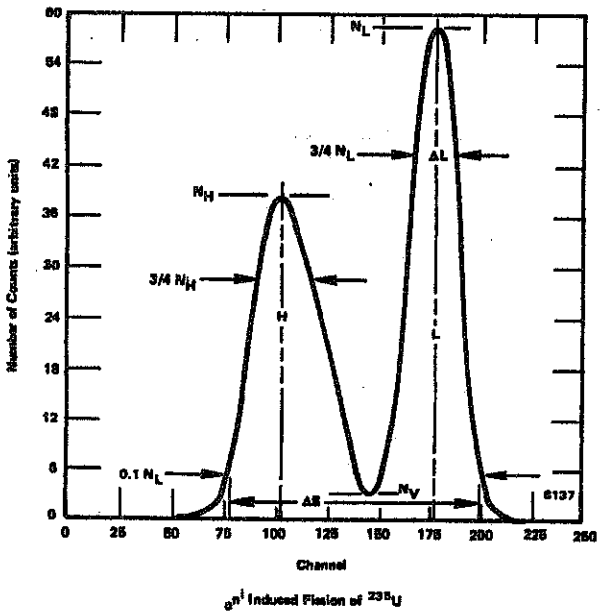

Fig. 7.6. Typical Energy Distribution Spectrum for ^{235}U.

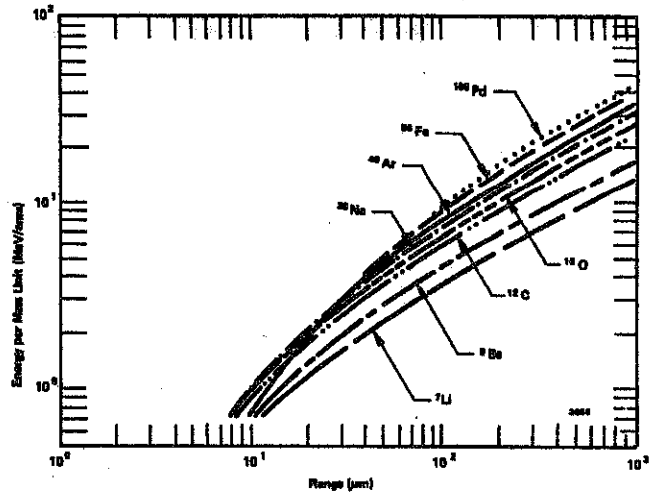

Fig. 7.7. Range-Energy Curves for Several Types of Heavy Ions in Silicon.
[Data taken from Northcliffe and Schilling (1970).]

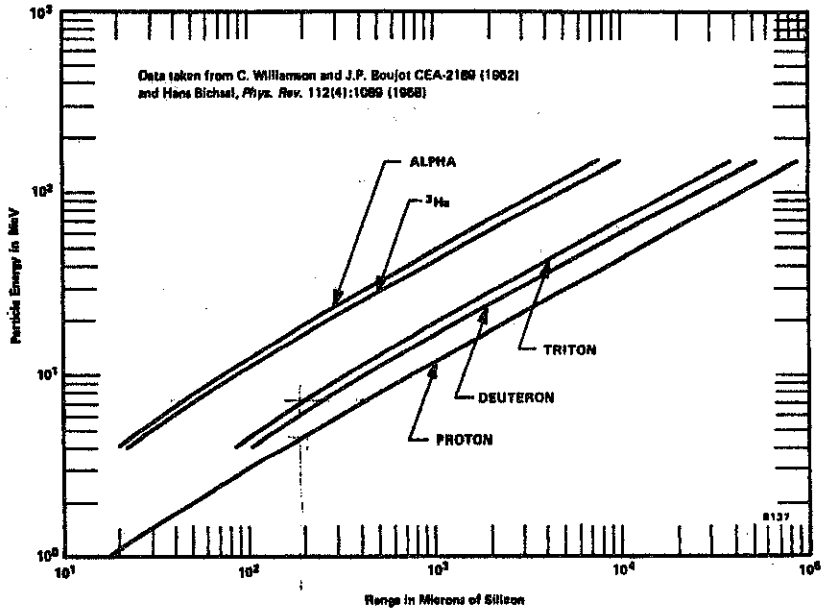

Fig. 7.8. Range-Energy Curves for Charged Particles in Silicon.
NOTE: Channeling of ions between crystal planes can result in significant variations from the data shown here.

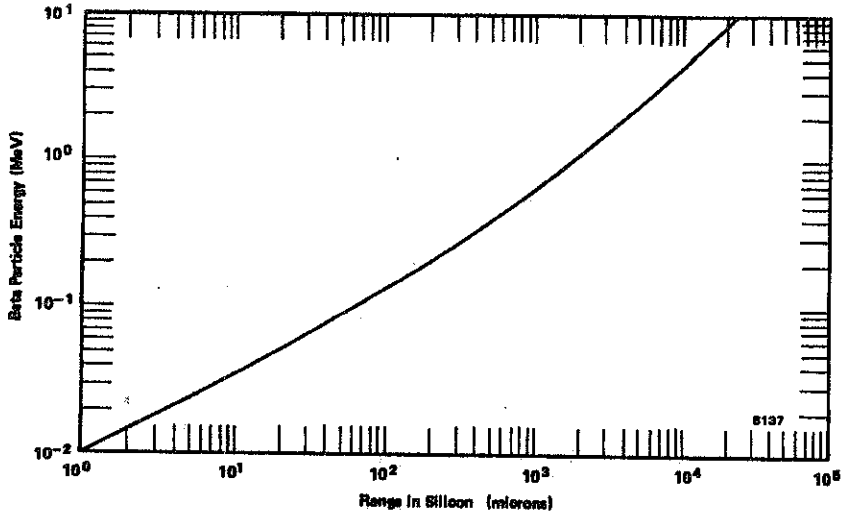

Fig. 7.9. Beta-Ray Range-Energy Curve in Silicon.
NOTE: Channeling of ions between crystal planes can result in significant variations from the data shown here.

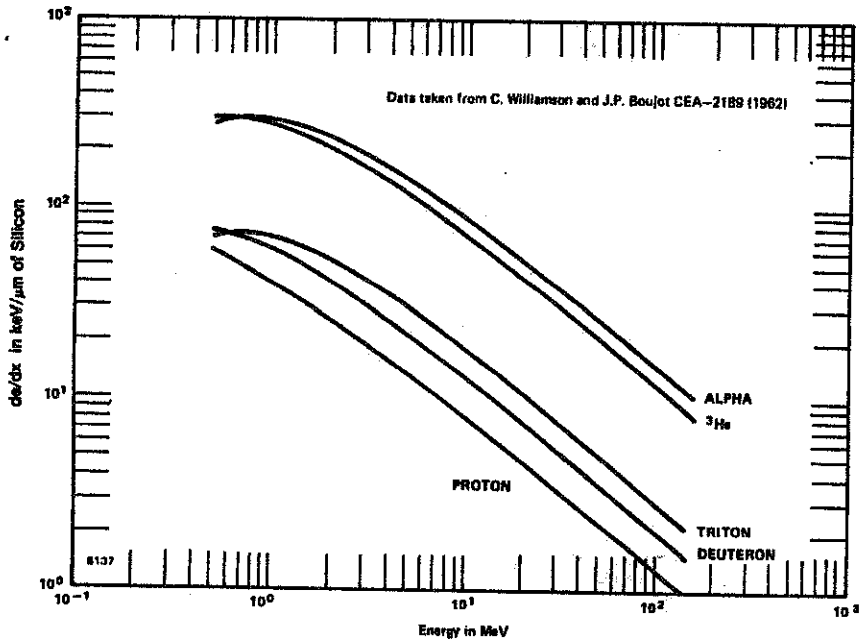

Fig. 7.10. Specific Energy Loss for Charged Particles in Silicon.
NOTE: Channeling of ions between crystal planes can result in significant variations from the data shown here.

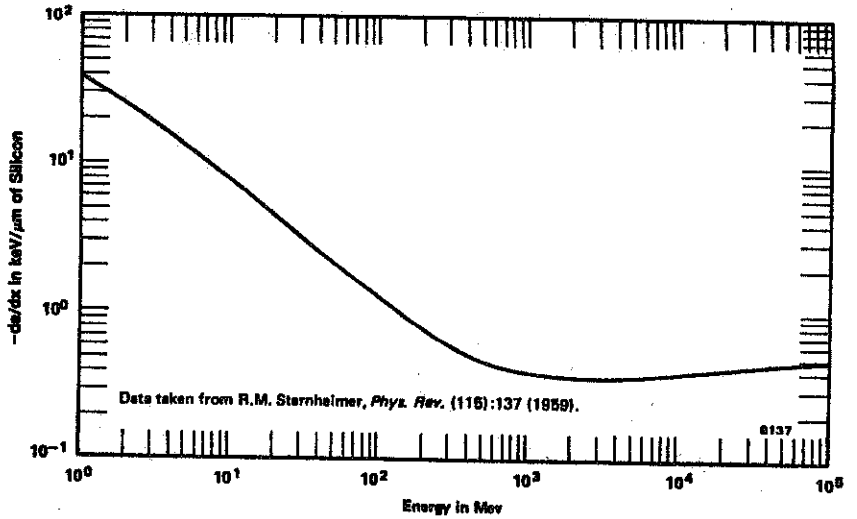

Fig. 7.11. Specific Energy Loss for Protons in Silicon.
NOTE: Channeling of ions between crystal planes can result in significant variations from the data shown here.

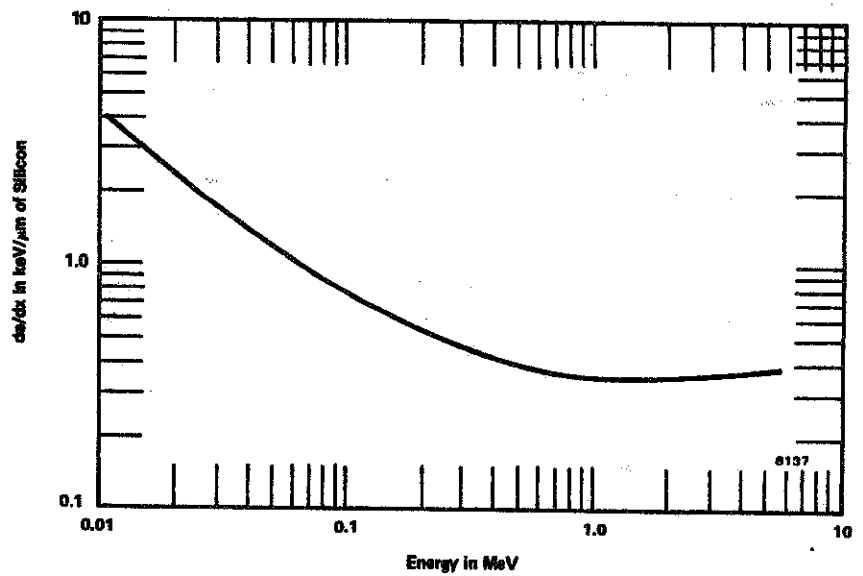

Fig. 7.12. Specific Energy Loss for Electrons in Silicon.
NOTE: Channeling of ions between crystal planes can result in significant variations from the data shown here.

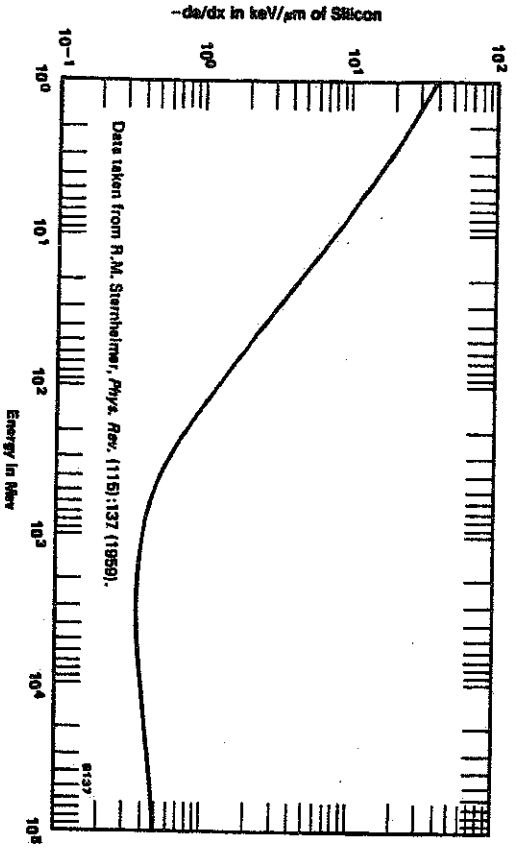

Fig. 7.11. Specific Energy Loss for Protons in Silicon.
NOTE: Channeling of ions between crystal planes can result in significant variations from the data shown here.

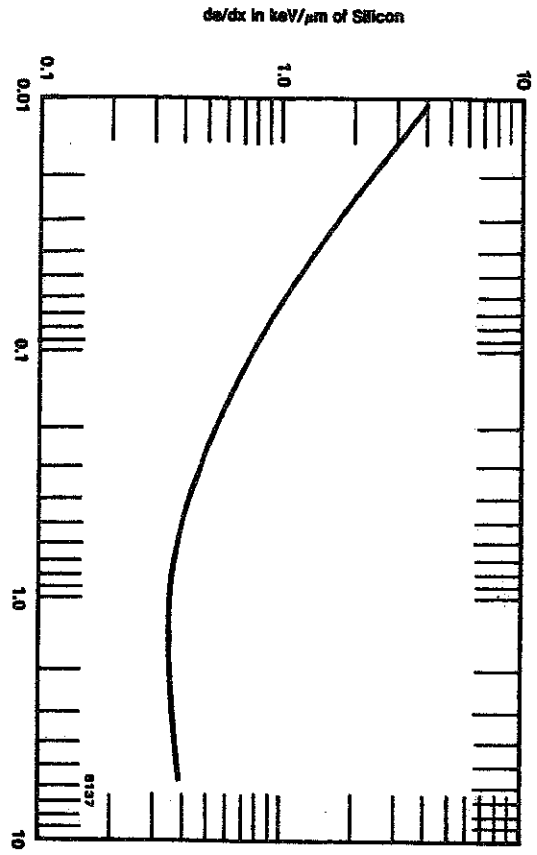

Fig. 7.12. Specific Energy Loss for Electrons in Silicon.
NOTE: Channeling of ions between crystal planes can result in significant variations from the data shown here.

Table 7.2. Radiation Damage for Charged Particle Detectors.

Detector Type	Incident Radiation	Energy	Total Dose in Ref. Experiment	Significant Deterioration	Device Failure	Type of Failure	Ref.
Surface Barrier	Electrons	2 MeV	2.3×10^{16} electrons/cm²	No data	No data	Multiple peaking; some noise increase. Multiple peaking removed by increasing bias voltage.	1
Surface Barrier	^{252}Cf fission fragments	104 MeV & 79 MeV	2.5×10^{9} fragments/cm²	~1.5×10^{8} fragments/cm²	~2×10^{9} fragments/cm²	Noise and reverse current increased; pulse height defect increased. Current damage partially annealed at room temperature.	9
Surface Barrier	Fast Neutrons	Fission Spectrum	10^{12} n/cm²	3.5×10^{11} n/cm²	2×10^{12} n/cm²	Resolution broadening; multiple peaking after 3.5×10^{11} n/cm²; no single peak response after 2×10^{12} n/cm².	4
Surface Barrier	Alphas	5.5 MeV	10^{11} α /cm²	$10^{8} - 10^{9}$/cm²	10^{11} α /cm²	Increased reverse current and noise; resolution broadening; multiple peaking between 10^{9} and 10^{10} α/cm².	5, 6
Surface Barrier	^{252}Cf fission fragments	104 MeV & 79 MeV	3.3×10^{9}/cm²	10^{9}/cm²	No data	Timing degradation.	12
Surface Barrier	Protons	0.6 – 5.0 MeV	10^{17}/cm²	10^{12}/cm²	5×10^{14}/cm²	Spectrum degradation.	14

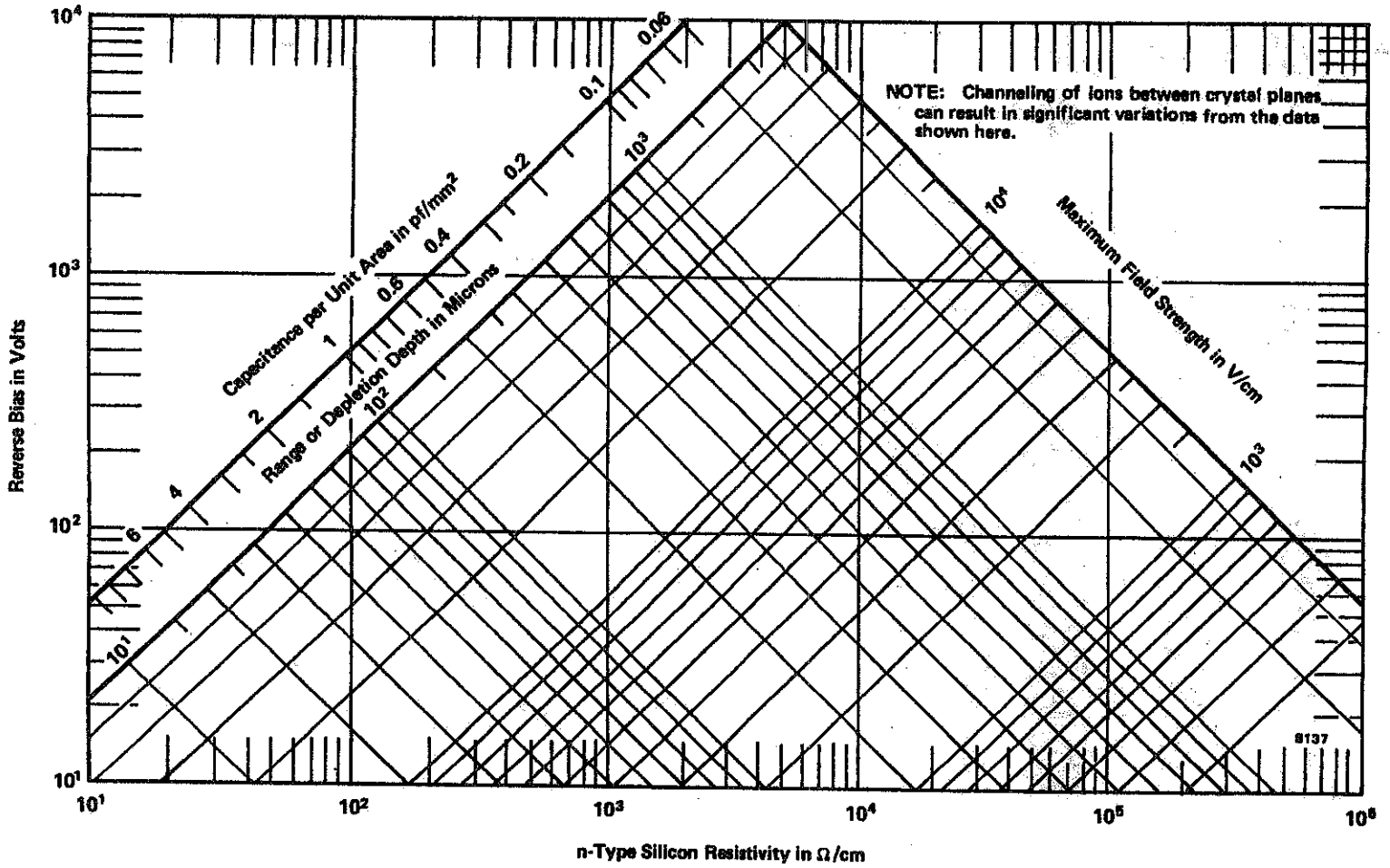

MAXIMUM FIELD STRENGTH—$E_g = 4.2 \times 10^4 (V_b/\rho_n)^{1/2}$ V/cm

CAPACITANCE PER UNIT AREA—$C_D/A_D = 212/(V_b\rho_n)^{1/2}$ pF/mm²

DEPLETION DEPTH—$D = 0.5 (V_b\rho_n)^{1/2}$ μ

EXAMPLE: If resistivity is 3400 Ω-cm and the bias voltage is 190 V, the detector parameters are determined by first locating the point of interception of 3400 Ω-cm and 190 V. This point falls on: (1) 1×10^4 V/cm maximum field strength line; (2) 400 μm depletion depth line; (3) 0.26 pF capacitance per unit area line. The intercept of the depletion depth line and the α, He^3, t, d, and p curves referred to the particle-energy scale give the maximum energy of the particle that will be stopped within the sensitive volume of the detector. It can be seen that the 400 μm depletion depth line intercepts the range curves as follows: He^3 = 25 MeV, α = 28 MeV, t = 11 MeV, d = 9 MeV, and p = 7 MeV.

NOTE: All curves are for n-type silicon.

Highly ionizing particles such as fission fragments produce avalanche multiplication fields in excess of ~6×10^4 V/cm.*

Range data were taken from Williamson and Boujot (CEA-2189, 1962).

*Chynoweth, A. G., "Multiplication Processes in p-n Junctions," National Academy of Sciences – National Research Publication 871:171 (1961).

Fig. 7.13. Field Strength Relationships in Silicon.

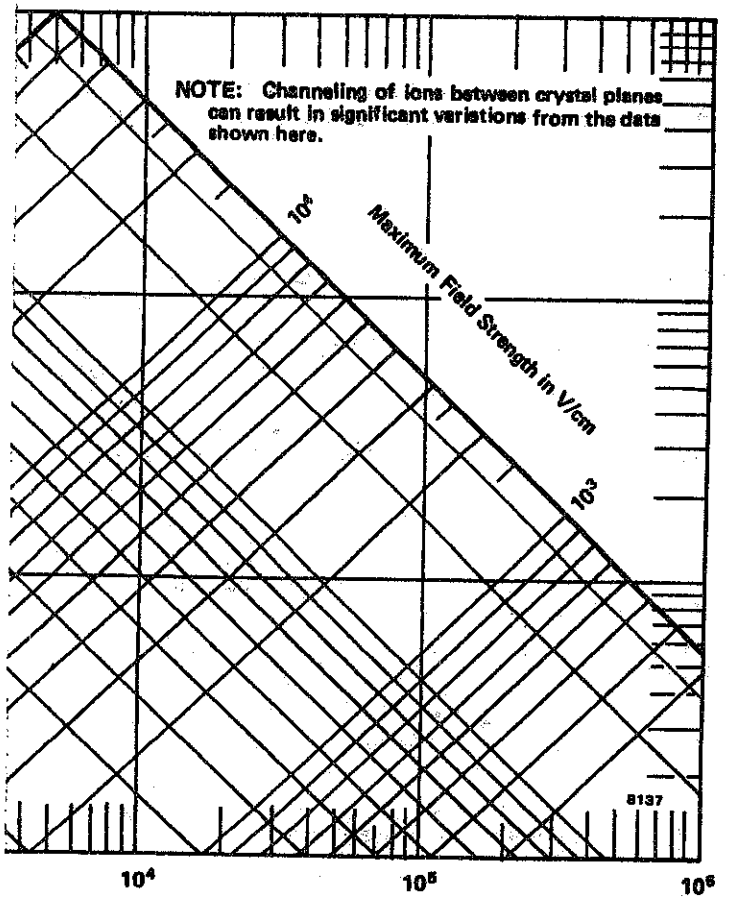

tivity in Ω/cm

CAPACITANCE PER UNIT AREA—$C_D/A_D = 212/(V_b\rho_n)^{1/2}$ pF/mm^2

0.5 $(V_b\rho_n)^{1/2}$ μ

NOTE: All curves are for n-type silicon.

Highly ionizing particles such as fission fragments produce avalanche multiplication fields in excess of ≈6 x 10^4 V/cm.*

Range data were taken from Williamson and Boujot (CEA-2189, 1962).

*Chynoweth, A. G., "Multiplication Processes in p-n Junctions," National Academy of Sciences – National Research Publication 871:171 (1961).

ationships in Silicon.

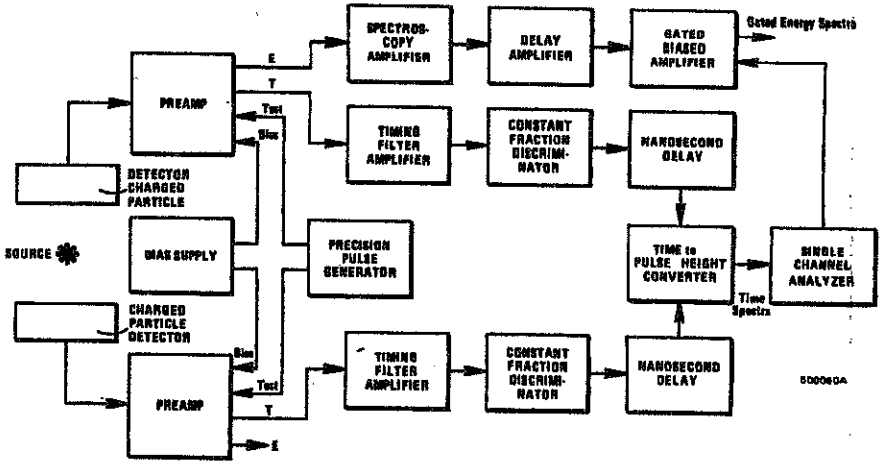

Fig. 7.14. Timing Spectra Permitting Energy Spectra to be Gated with Coincidence Events.

Bibliography references 7 through 10 provide additional information for Figs. 7.7 through 7.13.

BIBLIOGRAPHY

1. J. A. Coleman and J. W. Rodgers, "Radiation Damage in Lithium-Drifted p-i-n Junctions," *IEEE Trans. Nucl. Sci.* **NS-11**(3):213 (June 1964).

2. G. Dearnaley, "Radiation Damage by Charged Particles in Silicon Junction Detectors," *IEEE Trans. Nucl. Sci.* **NS-10**(1):106 (Jan. 1963).

3. A. R. Jones, "Measurements of Gamma Radiation Damage to p-n Junction Gamma Detectors," CRRD-1102 (Sept. 1962).

4. G. Dearnaley and A. B. Whitehead, "The Semiconductor Surface Barrier for Nuclear Particle Detection," *Nucl. Instrum. Methods* **12**:205 (1961).

5. F. J. Walter and R. R. Boshart, "Low Background Counting of Betas and Alphas with Silicon Detectors," *Nucl. Instrum. Methods* **42**(1):1 (June 1966).

6. R. V. Babcock, "Fast Neutron Damage to Silicon Junction Particle Detectors," *IRE Trans. Nucl. Sci.* **NS-8**(1):98 (Jan. 1961).

7. A. R. Sattler and G. Dearnaley, "Anomalous Energy Losses of Protons Channeled in Single-Crystal Germanium," *Phys. Rev. Letters* **15**:59 -62 (July 1965).

8. Harold L. Davis, "Energy Loss in Semiconductors Seen Causing Significant Problems," *Nucleonics* **23**(1):72 - 3 (Jan. 1965).

9. C. Erginsoy, H. E. Wegner, and W. M. Gibson, "Anisotropic Energy Loss of Light Particles of MeV Energies in Thin Silicon Single Crystals," *Phys. Rev. Letters* **13**:530 - 4 (Oct. 1974).

10. G. Dearnaley, "The Channeling of Ions through Silicon Detectors," *IEEE Trans. Nucl. Sci.* **NS-11**(3):249 - 53 (June 1964).

11. G. Bertolini and A. Coche, Editors, *Semiconductor Detectors*, American Elsevier Publishing Co., Inc. (1968).

12. P. Muldst and E. I. Haines, "Degradation of the Time Characteristics of Surface Barrier Detectors with Fission Fragment Dose," *Rev. Sci. Instrum.* **40**:507 (1969).

13. Y. M. Liu and J. A. Coleman, "Electron Radiation Damage Effects in Silicon Surface Barrier Detectors," *IEEE Trans. Nucl. Sci.* **NS-18**(1):192 (1971).

14. J. A. Coleman, D. P. Love, J. H. Trainor, and D. J. Williams, "Effects of Damage by 0.8 MeV - 5.0 MeV Protons in Silicon Surface Barrier Detectors," *IEEE Trans. Nucl. Sci.* **NS-15**(3):363 (1968).

15. "Heavy-Ion Spectroscopy with Silicon Surface Barrier Detectors," *EG&G ORTEC Application Note AN-40.*

16. F. S. Goulding and R. H. Pehl, "Semiconductor Detectors," Section IIIA in *Nuclear Spectroscopy and Reactions*, J. Cerny, Ed. Academic Press (1974).

ALPHA DECAY

Reference: Introd. Nuclear Physics, K.S. Krane
John Wiley & Sons 1987

Alpha particles were first identified as the least penetrating of the radiations emitted by naturally occurring materials. In 1903, Rutherford measured their charge-to-mass ratio by deflecting α particles from the decay of radium in electric and magnetic fields. Despite the difficulty of these early experiments, Rutherford's result was only about 25% higher than the presently accepted value. In 1909 Rutherford showed that, as suspected, the α particles were in fact helium nuclei; in his experiments the particles entered an evacuated thin-walled chamber by penetrating its walls, and after several days of collecting, atomic spectroscopy revealed the presence of helium gas inside the chamber.

Many heavy nuclei, especially those of the naturally occurring radioactive series, decay though α emission. Only exceedingly rarely does any other spontaneous radioactive process result in the emission of nucleons; we do not, for example, observe deuteron emission as a natural decay process. There must therefore be a special reason that nuclei choose α emission over other possible decay modes. In this chapter we examine this question and study the α decay process in detail. We also show how α spectroscopy can help us to understand nuclear structure.

8.1 WHY α DECAY OCCURS

Alpha emission is a Coulomb repulsion effect. It becomes increasingly important for heavy nuclei because the disruptive Coulomb force increases with size at a faster rate (namely, as Z^2) than does the specific nuclear binding force, which increases approximately as A.

Why is the α particle chosen as the agent for the spontaneous carrying away of positive charge? When we call a process *spontaneous* we mean that some kinetic energy has suddenly appeared in the system for no apparent cause; this energy must come from a decrease in the mass of the system. The α particle, because it is a very stable and tightly bound structure, has a relatively small mass compared with the mass of its separate constituents. It is particularly favored as an emitted particle if we hope to have the disintegration products as light as possible and thus get the largest possible release of kinetic energy.

Table 8.1 Energy Release (Q value) for Various Modes of D[illegible] of $^{232}U^a$

Emitted Particle	Energy Release (MeV)	Emitted Particle	Energy Release (MeV)
n	−7.26	^{4}He	+5.4
^{1}H	−6.12	^{5}He	−2.9
^{2}H	−10.70	^{6}He	−6.1
^{3}H	−10.24	^{6}Li	−3.7
^{3}He	−9.92	^{7}Li	−1.9

[a]Computed from known masses.

For a typical α emitter ^{232}U (72 y) we can compute, from the known masse the energy release for various emitted particles. Table 8.1 summarizes the result Of the particles considered, spontaneous decay is energetically possible *only* fc the α particle. A positive disintegration energy results for some slightly heavie particles than those listed, ^{8}Be or ^{12}C, for example. We will show, howeve (Section 8.4), that the partial disintegration constant for emission of such heav particles is normally vanishingly small compared with that for α emission. Suc decays would be so rare that in practice they would almost never be noticed. Thi suggests that if a nucleus is to be recognized as an alpha emitter it is not enoug for α decay to be energetically possible. The disintegration constant must als not be too small or else α emission will occur so rarely that it may not b detected. With present techniques this means that the half-life must be less tha about 10^{16} y. Also, β decay, if it has a much higher partial disintegratio constant, can mask the α decay. Most nuclei with $A > 190$ (and many wit $150 < A < 190$) are energetically unstable against α emission but only abou one-half of them can meet these other requirements.

8.2 BASIC α DECAY PROCESSES

The spontaneous emission of an α particle can be represented by the followin process:

$$^A_Z X_N \rightarrow ^{A-4}_{Z-2} X'_{N-2} + \alpha$$

The α particle, as was shown by Rutherford, is a nucleus of ^{4}He, consisting o two neutrons and two protons. To understand the decay process, we must stud the conservation of energy, linear momentum, and angular momentum.

Let's first consider the conservation of energy in the α decay process. We assume the initial decaying nucleus X to be at rest. Then the energy of the initial system is just the rest energy of X, $m_X c^2$. The final state consists of X′ and α, each of which will be in motion (to conserve linear momentum). Thus the final total energy is $m_{X'}c^2 + T_{X'} + m_\alpha c^2 + T_\alpha$, where T represents the kinetic energy of the final particles. Thus conservation of energy gives

$$m_X c^2 = m_{X'} c^2 + T_{X'} + m_\alpha c^2 + T_\alpha \qquad (8.1)$$

or

$$(m_X - m_{X'} - m_\alpha)c^2 = T_{X'} + T_\alpha \qquad (8.2)$$

quantity on the left side of Equation 8.2 is the net energy released in the decay, called the Q value:

$$Q = (m_X - m_{X'} - m_\alpha)c^2 \tag{8.3}$$

and the decay will occur spontaneously only if $Q > 0$. (The decay Q values for ^{232}U were listed in Table 8.1.) Q values can be calculated from *atomic* mass tables because even though Equation 8.3 represents a *nuclear* process, the electron masses will cancel in the subtraction. When the masses are in atomic mass units (u), expressing c^2 as 931.502 MeV/u gives Q values directly in MeV.

The Q value is also equal to the total kinetic energy given to the decay fragments:

$$Q = T_{X'} + T_\alpha \tag{8.4}$$

If the original nucleus X is at rest, then its linear momentum is zero, and conservation of linear momentum then requires that X′ and α move with equal and opposite momenta in order that the final momentum also be zero:

$$p_\alpha = p_{X'} \tag{8.5}$$

α decays typically release about 5 MeV of energy. Thus for both X′ and α, $T \ll mc^2$ and we may safely use nonrelativistic kinematics. Writing $T = p^2/2m$ and using Equations 8.4 and 8.5 gives the kinetic energy of the α particle in terms of the Q value:

$$T_\alpha = \frac{Q}{(1 + m_\alpha/m_{X'})} \tag{8.6}$$

Because the mass ratio is small compared with 1 (recall that X′ represents a heavy nucleus), it is usually sufficiently accurate to express this ratio simply as $4/(A - 4)$, which gives, with $A \gg 4$,

$$T_\alpha = Q(1 - 4/A) \tag{8.7}$$

Typically, the α particle carries about 98% of the Q value, with the much heavier nuclear fragment X′ carrying only about 2%. (This *recoil* energy of the heavy fragment is not entirely negligible. For a typical Q value of 5 MeV, the recoiling nucleus has an energy of the order of 100 keV. This energy is far in excess of that which binds atoms in solids, and thus the recoiling nucleus, if it is near the surface of the radioactive source, escapes from the source and can spread to the surroundings. If the α decay is part of a decay chain, then the recoiling daughter nucleus may itself be radioactive, and these recoils can result in the spread of radioactive material. Fortunately, the heavy recoil nuclei have an extremely short range in matter and their spread can be prevented by a thin coating, such as Mylar or lacquer, placed over the radioactive sample.)

The kinetic energy of an α particle can be measured directly with a magnetic spectrometer, and so the Q value of a decay can be determined. This gives us a way to determine atomic masses, such as in a case in which we might know the mass of long-lived X as a result of direct measurement but X′ is so short-lived that its mass cannot be determined by direct measurement.

8.3 α DECAY SYSTEMATICS

One feature of α decay is so striking that it was noticed as long ago as 1911, year that Rutherford "discovered" the nucleus. Geiger and Nuttall noticed th emitters with large disintegration energies had short half-lives and convers The variation is astonishingly rapid as we may see from the limiting case ^{232}Th (1.4×10^{10} y; $Q = 4.08$ MeV) and ^{218}Th (1.0×10^{-7} s; $Q = 9.85$ Me A factor of 2 in energy means a factor of 10^{24} in half-life! The theoret explanation of this Geiger-Nuttall rule in 1928 was one of the first triumph quantum mechanics.

A plot of log $t_{1/2}$ against Q in which all α emitters are included show considerable scatter about the general Geiger-Nuttall trend. Very smooth cur result, however, if we plot only α emitters with the same Z and if further select from this group only those with Z and N both even (Figure 8. Even-odd, odd-even, and odd-odd nuclei obey the general trend but do not p into quite such smooth curves; their periods are 2–1000 times longer than th for even-even types with the same Z and Q.

It is interesting that ^{235}U (even Z, odd N) is one of these "extra-long-li types. If its half-life were 1000 times shorter, this important nucleus would n occur in nature, and we probably would not have nuclear reactors today! We in Chapter 13 that the same feature that apparently accounts for the long l against α decay, namely the odd neutron, also makes ^{235}U very susceptible fission by thermal neutrons.

Figure 8.2 shows another important systematic relationship for α emitte Looking for the moment only at the data for $A > 212$, we see that addi neutrons to a nucleus reduces the disintegration energy, which, because of t

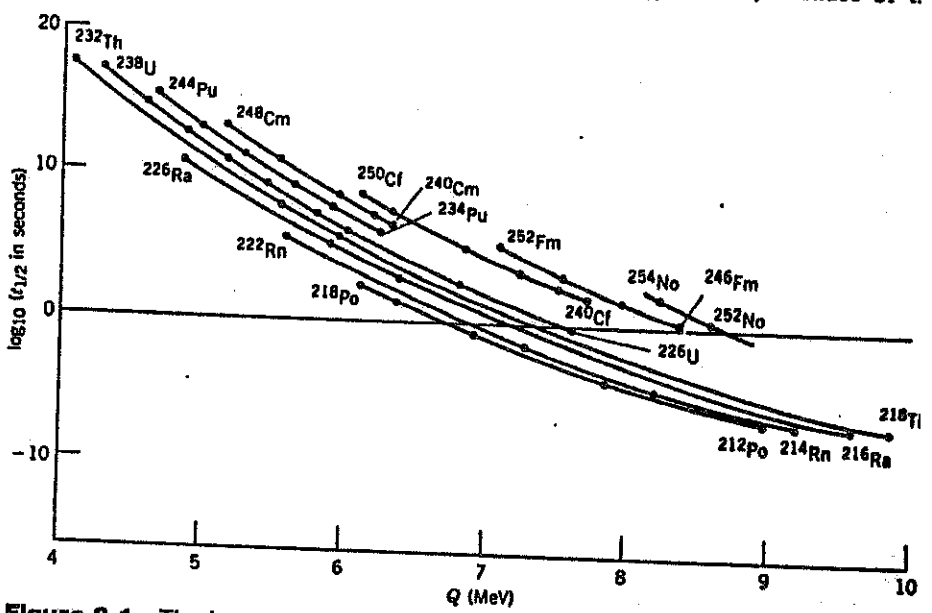

Figure 8.1 The inverse relationship between α-decay half-li d decay energy called the Geiger-Nuttall rule. Only even-Z, even-N nuclei hown. The solic lines connect the data points.

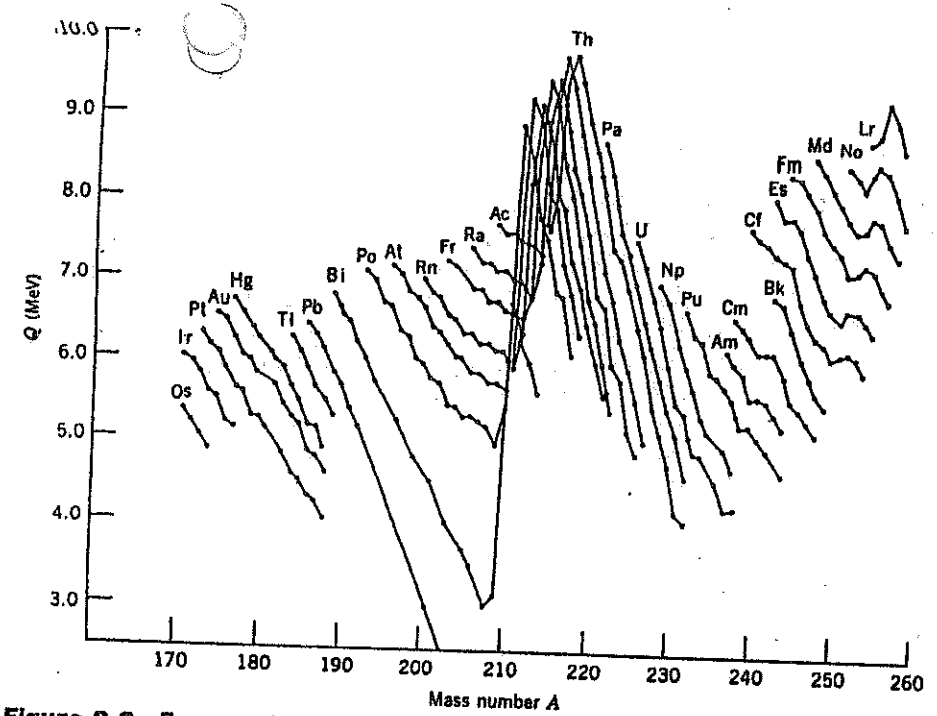

Figure 8.2 Energy released in α decay for various isotopic sequences of heavy nuclei. In contrast to Figure 8.1, both odd-A and even-A isotopes are shown, and a small amount of odd-even staggering can be seen. The effects of the shell closures at $N = 126$ (large dip in data) and $Z = 82$ (larger than average spacing between Po, Bi, and Pb sequences) are apparent.

Geiger-Nuttall rule, increases the half-life. The nucleus becomes more stable. A striking discontinuity near $A = 212$ occurs where $N = 126$ and is another example of nuclear shell structure.

We can compare the systematic dependence of Q on A with the prediction of the semiempirical mass formula, Equation 3.28.

$$Q = B(^4\text{He}) + B(Z-2, A-4) - B(Z, A) \tag{8.8}$$

$$\cong 28.3 - 4a_v + \tfrac{8}{3}a_s A^{-1/3} + 4a_c Z A^{-1/3}(1 - Z/3A) - 4a_{sym}(1 - 2Z/A)^2 + 3a_p A^{-7/4} \tag{8.9}$$

where the approximation in Equation 8.9 is $Z, A \gg 1$. For ^{226}Th, this formula gives $Q = 6.75$ MeV, not too far from the measured value of 6.45 MeV. What is perhaps more significant is that the general trend of Figure 8.2 is reproduced: for ^{232}Th, Equation 8.9 gives $Q = 5.71$ MeV (to be compared with $Q = 4.08$ MeV), while for ^{220}Th the formula gives $Q = 7.77$ MeV (compared with $Q = 8.95$ MeV). Keep in mind that the parameters of the semiempirical mass formula are chosen to give rough agreement with observed binding energies across the entire range of nuclei. It is important that the formula gives us rough agreement with the decay Q values and that it correctly gives $Q > 0$ for the heavy nuclei. It also

correctly predicts the decrease of Q with increasing A for a ...uence of isotop such as those of thorium, although it gives too small a change of Q with A (t formula gives $\Delta Q = -0.17$ MeV per unit change in A, while for Th the observ average change is $\Delta Q = -0.40$ MeV per unit change in A).

8.4 THEORY OF α EMISSION

The general features of Figure 8.1 can be accounted for by a quantum mechanic theory developed in 1928 almost simultaneously by Gamow and by Gurney a Condon. In this theory an α particle is assumed to move in a spherical regi determined by the *daughter* nucleus. The central feature of this *one-body model* that the α particle is preformed inside the parent nucleus. Actually there is n much reason to believe that α particles do exist separately within heavy nucl nevertheless, the theory works quite well, especially for even-even nuclei. Th success of the theory does not prove that α particles are preformed, but mere that they behave as if they were.

Figure 8.3 shows a plot, suitable for purposes of the theory, of the potenti energy between the α particle and the residual nucleus for various distanc between their centers. The horizontal line Q is the disintegration energy. No that the Coulomb potential is extended inward to a radius a and then arbitrari cut off. The radius a can be taken as the sum of the radius of the residual nucle and of the α particle. There are three regions of interest. In the spherical regio $r < a$ we are inside the nucleus and speak of a potential well of depth $-V$ where V_0 is taken as a positive number. Classically the α particle can move in th region, with a kinetic energy $Q + V_0$ but it cannot escape from it. The annula shell region $a < r < b$ forms a potential barrier because here the potential energ

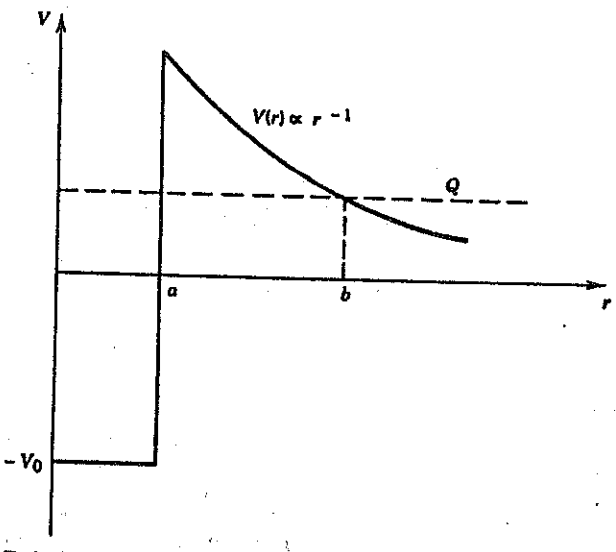

Figure 8.3 Relative potential energy of α-particle, daughter-nucleus system as a function of their separation. Inside the nuclear surface at $r = a$, the potential is represented as a square well; beyond the surface, only the Coulomb repulsion operates. The α particle tunnels through the Coulomb barrier from a to b.

is more than the total available energy Q. Classically the α particle cannot enter this region from either direction, just as a tennis ball dropped from a certain height cannot rebound higher; in each case the kinetic energy would have to be negative. The region $r > b$ is a classically permitted region outside the barrier.

From the classical point of view, an α particle in the spherical potential well would sharply reverse its motion every time it tried to pass beyond $r = a$. Quantum mechanically, however, there is a chance of "leakage" or "tunnelling" through such a barrier. This barrier accounts for the fact that α-unstable nuclei do not decay immediately. The α particle within the nucleus must present itself again and again at the barrier surface until it finally penetrates. In ^{238}U, for example, the leakage probability is so small that the α particle, on the average, must make $\sim 10^{38}$ tries before it escapes ($\sim 10^{21}$ per second for $\sim 10^{9}$ years)!

The barrier also operates in reverse, in the case of α-particle scattering by nuclei (see Sections 3.1 and 11.6). Alpha particles incident on the barrier from outside the nucleus usually scatter in the Coulomb field if the incident energy is well below the barrier height. Tunnelling through the barrier, so that the nuclear force between the particle and target can cause nuclear reactions, is a relatively improbable process at low energy. The theoretical analysis of nuclear reactions induced by charged particles uses a formalism similar to that of α decay to calculate the barrier penetration probability. Fusion reactions, such as those responsible for the energy released in stars, also are analyzed using the barrier penetration approach (see Section 14.2).

The disintegration constant of an α emitter is given in the one-body theory by

$$\lambda = fP \tag{8.10}$$

where f is the frequency with which the α particle presents itself at the barrier and P is the probability of transmission through the barrier.

Equation 8.10 suggests that our treatment is going to be semiclassical in that our discussion of the situation for $r < a$ is very "billiard-ballish." A rigorous wave-mechanical treatment, however, gives about the same results for this problem. The quantity f is roughly of the order of v/a where v is the relative velocity of the α particle as it rattles about inside the nucleus. We can find v from the kinetic energy of the α particle for $r < a$. Estimating $V_0 \approx 35$ MeV for a typical well depth gives $f \approx 6 \times 10^{21}$/s for $Q \approx 5$ MeV. We will see later that we do not need to know f very precisely to check the theory.

The barrier penetration probability P must be obtained from a quantum mechanical calculation similar to the one-dimensional problem discussed in Section 2.3. Let's first use the result of that calculation, Equation 2.39, to estimate the probability P. Of course, the calculation that led to Equation 2.39 was based on a one-dimensional rectangular barrier, which is not directly applicable to the $1/r$ Coulomb potential, but we can at least find a rough order-of-magnitude estimate. The result, Equation 2.39, depends on the width of the barrier and on its height (called V_0 for the rectangular barrier) above the energy E of the particle. The Coulomb barrier of Figure 8.3 has height B at $r = a$, where

$$B = \frac{1}{4\pi\epsilon_0}\frac{zZ'e^2}{a} \tag{8.11}$$

In this expression the α particle has charge ze and the daughter nucleus, which provides the Coulomb repulsion, has charge $Z'e = (Z - z)e$. The height of the barrier thus varies from $(B - Q)$ above the particle's energy at $r = a$ to zero at $r = b$, and we can take a representative average height to be $\frac{1}{2}(B - Q)$. We can similarly choose a representative average width to be $\frac{1}{2}(b - a)$. The factor k_2 in Equation 2.39 then becomes $\sqrt{(2m/\hbar^2) \cdot \frac{1}{2}(B - Q)}$. For a typical heavy nucleus ($Z = 90$, $a = 7.5$ fm), the barrier height B is about 34 MeV, so the factor k_2 is about 1.6 fm^{-1}. The radius b at which the α particle "leaves" the barrier is found from the equality of the particle's energy and the potential energy:

$$b = \frac{1}{4\pi\epsilon_0}\frac{zZ'e^2}{Q} \tag{8.1}$$

and for a typical case of a heavy nucleus with $Q \approx 6$ MeV, $b \approx 42$ fm. Then $k_2 \cdot \frac{1}{2}(b - a) \gg 1$ and we can approximate Equation 2.39 as

$$P \cong e^{-2k_2 \cdot (1/2)(b-a)} \tag{8.1}$$

since the factors in front of the exponential are of unit order of magnitude. For the case we are estimating here, $P \sim 2 \times 10^{-25}$ and thus $\lambda \sim 10^{-3}$/s and $t_{1/2} \sim 700$ s. A slight change of Q to 5 MeV changes P to 1×10^{-30} and $t_{1/2} \sim 10^{8}$ s. Even this very crude calculation is able to explain the many orders of magnitude change of $t_{1/2}$ between $Q = 5$ MeV and $Q = 6$ MeV, as illustrated in Figure 8.1.

The exact quantum mechanical calculation is very similar in spirit to the crude estimate above. We can think of the Coulomb barrier as made up of a sequence of infinitesimal rectangular barriers of height $V(r) = zZ'e^2/4\pi\epsilon_0 r$ and width dr. The probability to penetrate each infinitesimal barrier, which extends from r to $r + dr$, is

$$dP = \exp\left(-2\,dr\sqrt{(2m/\hbar^2)[V(r) - Q]}\right) \tag{8.1}$$

The probability to penetrate the complete barrier is

$$P = e^{-2G} \tag{8.1}$$

where the *Gamow factor* G is

$$G = \sqrt{\frac{2m}{\hbar^2}}\int_a^b [V(r) - Q]^{1/2}\,dr \tag{8.1}$$

which can be evaluated as

$$G = \sqrt{\frac{2m}{\hbar^2 Q}}\frac{zZ'e^2}{4\pi\epsilon_0}\left[\arccos\sqrt{x} - \sqrt{x(1-x)}\right] \tag{8.1}$$

where $x = a/b = Q/B$. The quantity in brackets in Equation 8.17 is approximately $\pi/2 - 2x^{1/2}$ when $x \ll 1$, as is the case for most decays of interest. Then the result of the quantum mechanical calculation for the half-life of α decay is

$$t_{1/2} = 0.693\frac{a}{c}\sqrt{\frac{mc^2}{2(V_0 + Q)}}\exp\left\{2\sqrt{\frac{2mc^2}{(\hbar c)^2 Q}}\frac{zZ'e^2}{4\pi\epsilon_0}\left(\frac{\pi}{2} - 2\sqrt{\frac{Q}{B}}\right)\right\} \tag{8.1}$$

Table 8.2 C[illegible]ed α-Decay Half-lives for Th Isotopes

A	Q (MeV)	$t_{1/2}$ (s)	
		Measured	Calculated
220	8.95	10^{-5}	3.3×10^{-7}
222	8.13	2.8×10^{-3}	6.3×10^{-5}
224	7.31	1.04	3.3×10^{-2}
226	6.45	1854	6.0×10^{1}
228	5.52	6.0×10^{7}	2.4×10^{6}
230	4.77	2.5×10^{12}	1.0×10^{11}
232	4.08	4.4×10^{17}	2.6×10^{16}

The results of this calculation for the even isotopes of Th are shown in Table 8.2. The agreement is not exact, but the calculation is able to reproduce the trend of the half-lives within 1–2 orders of magnitude over a range of more than 20 orders of magnitude. We have neglected several important details in the calculation: we did not consider the initial and final nuclear wave functions (Fermi's Golden Rule, Equation 2.79, must be used to evaluate the decay probability), we did not consider the angular momentum carried by the α particle, and we assumed the nucleus to be spherical with a mean radius of $1.25A^{1/3}$ fm. The latter approximation has a very substantial influence on the calculated half-lives. The nuclei with $A \gtrsim 230$ have strongly deformed shapes, and the calculated half-lives are extremely sensitive to small changes in the assumed mean radius. For instance, changing the mean radius to $1.20A^{1/3}$ (a 4% change in a) changes the half-lives by a factor of 5! In fact, because of this extreme sensitivity, the procedure is often reversed—the measured half-lives are used to deduce the nuclear radius; what actually comes out of the calculation is more like the sum of the radii of the nucleus X′ and the α particle, if we assume their charge distributions to have a sharp edge. This result can then be used to obtain an estimate of the nuclear radius; see, for example, L. Marquez, *J. Phys. Lett.* 42, 181 (1981).

Even though this oversimplified theory is not strictly correct, it gives us a good estimate of the decay half-lives. It also enables us to understand why other decays into light particles are not commonly seen, even though they may be allowed by the Q value. For example, the decay $^{220}\text{Th} \rightarrow {}^{12}\text{C} + {}^{208}\text{Po}$ would have a Q value of 32.1 MeV, and carrying through the calculation using Equation 8.18 gives $t_{1/2} = 2.3 \times 10^{6}$ s for the ^{220}Th decay into ^{12}C. This is a factor of 10^{13} longer than the α-decay half-life and thus the decay will not easily be observable.

Recently, just such a decay mode has in fact been observed, the first example of a spontaneous decay process involving emission of a particle heavier than an α. The decay of ^{223}Ra normally proceeds by α emission with a half-life of 11.2 d, but there has now been discovered the decay process $^{223}\text{Ra} \rightarrow {}^{14}\text{C} + {}^{209}\text{Pb}$. The probability for this process is very small, about 10^{-9} relative to the α decay. Figure 8.4 indicates the heroic efforts that are necessary to observe the process. To confirm that the emitted particle is ^{14}C requires the $\Delta E \cdot T$ technique discussed in Chapter 7. Figure 8.4 shows a portion of the high-energy end of the tail of the hyperbola expected for observation of carbon. From the mass tables,

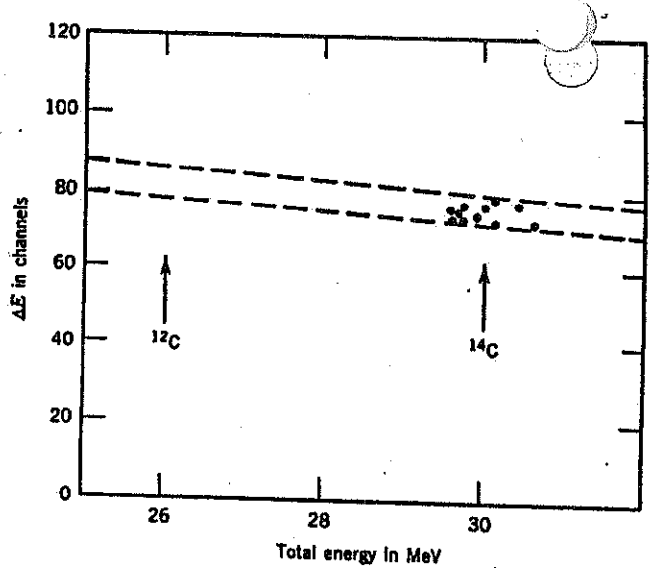

Figure 8.4 A portion of the tail of the $\Delta E \cdot T$ hyperbola showing the observ ^{14}C events from the decay of ^{223}Ra. The dashed lines show the limits expected carbon. The 11 ^{14}C events result from 6 months of counting. From H. J. Ro and G. A. Jones, *Nature* 307, 245 (1984). Reprinted by permission, copyright Macmillan Journals Limited.

the decay Q value is calculated to be 31.8 MeV, which (when corrected for t recoil) gives a ^{14}C kinetic energy of 29.8 MeV. By contrast, the calculated ener for ^{12}C emission would be about 26 MeV. The total of 11 events observ represents about *six months* of counting with a source of 3.3 μCi of ^{223}Ra secular equilibrium with 21-y ^{227}Ac, a member of the naturally occurring actiniu series beginning with ^{235}U.

Calculating the Gamow factor for ^{14}C emission gives a decay probability about 10^{-3} relative to α emission; the discrepancy between the calculated ar observed (10^{-9}) values results from the assumptions about the preformation the particle inside the nucleus. You will recall that our theory of α decay is base on the assumption that the α is preformed inside the nucleus. What tl experiment tells us is that the probability for forming ^{14}C clusters inside tl nucleus is about 10^{-6} relative to the probability to preform α's.

For a description of the experiment, see H. J. Rose and G. A. Jones, *Natu* 307, 245 (1984). Emission of ^{14}C from several other nuclei in this region has als been observed, and emission of heavier decay fragments, including ^{24}Ne, h been reported.

Going in the opposite direction, we can use Equation 8.18 with $z = 1$ evaluate the half-life for proton decay—that is, the spontaneous emission of proton by an unstable nucleus. In this case the Coulomb barrier will be only ha as high as it is for α decay, but these decays are inhibited for a stronger reaso the Q values for proton decay are generally negative and so the decays a absolutely forbidden by energy conservation. Such decays have recently bee observed for a few proton-rich unstable nuclei, which are formed in nuclea reactions by bombarding a target with $N \approx Z$ using a projectile having $N \approx$

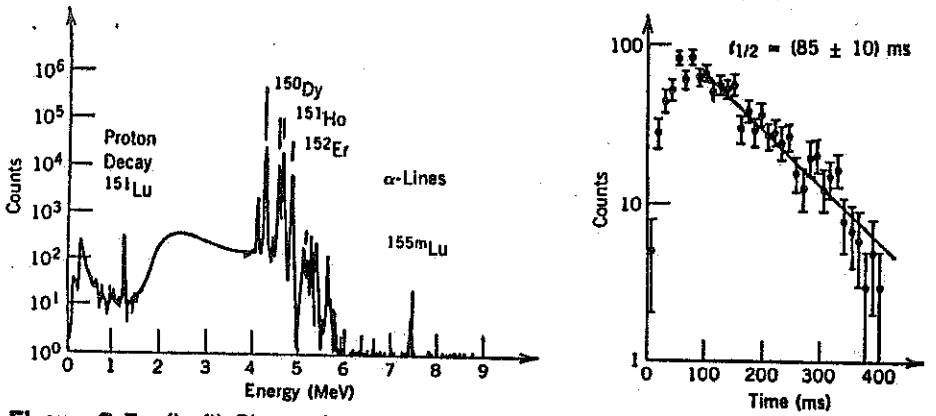

Figure 8.5 (Left) Charged-particle spectrum emitted in the radioactive decays of products of the reaction ^{96}Ru + ^{58}Ni. The peaks above 4 MeV represent α decays; the 1.2-MeV peak is from proton emission. (Right) The decay with time of the proton peak gives a half-life of 85 ms. From S. Hofmann et al., *Z. Phys. A* **305**, 111 (1982).

This creates a heavy nucleus with $N \approx Z$, a very unstable configuration, and proton emission may be energetically possible, as the nucleus tries to relieve itself of its proton excess. The Q value for proton decay can be found by a slight modification of Equation 8.3, which gives exactly the negative of the proton separation energy, Equation 3.27. Proton decay will be energetically possible when the Q value is positive and therefore when the separation energy is negative. A glance at the mass tabulations (see A. H. Wapstra and G. Audi, *Nucl. Phys. A* **432**, 1 (1985)) shows only a few very rare cases in which the proton separation energy is negative, and even these are not directly measured but instead obtained by extrapolations from more stable nuclei.

In an experiment reported by Hofmann *et al.*, *Z. Phys. A* **305**, 111 (1982), a target of ^{96}Ru was bombarded with ^{58}Ni projectiles. Figure 8.5 shows the spectrum of light particles emitted following the reaction. The more energetic peaks are identified as α decays from unstable nuclei in the neighborhood of $A = 150$ produced in the reaction. The peak at 1.239 MeV was identified as a proton using $\Delta E \cdot T$ techniques as described in Chapter 7. Its half-life was measured as 85 ms, as shown in Figure 8.5. The decay was assigned to the isotope ^{151}Lu based on a series of indirect arguments; unfortunately, reactions such as this produce many different products, and it is often a difficult task to identify the source of the observed radiations. This experiment thus provides evidence for the decay $^{151}\text{Lu} \rightarrow {}^{150}\text{Yb} + \text{p}$.

Study of decays such as this enables us to extend our knowledge of nuclear mass systematics far beyond the previous limits; for instance, at the time of this work ^{151}Lu was three protons further from stability than the previous last known isobar (^{151}Er). Figure 8.6 shows the Q_p values deduced from known masses and from extrapolations based on systematics. The value for ^{151}Lu lies right on the theoretical calculation, giving confidence to both the identification of the isotope and to the theoretical calculation.

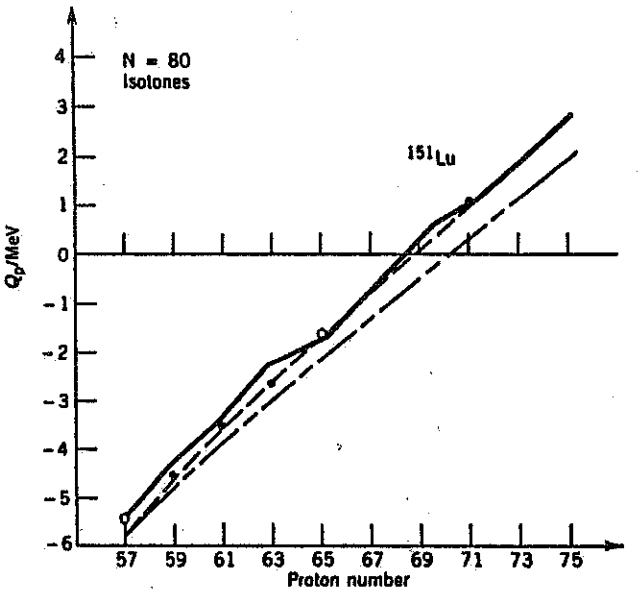

Figure 8.6 Proton-decay energies of $N = 80$ isotones. The solid lines are theoretical calculations based on nuclear mass formulas (somewhat like the semiempirical mass formula). Only for ^{151}Lu is the decay energy positive. From S. Hofmann et al. *Z. Phys. A* **305**, 111 (1982).

Using Equation 8.18 for the half-life gives a value of about 1.7 μs, too small by nearly 5 orders of magnitude. For this reason, it has been proposed that the decay is inhibited by differences in the nuclear structure of the initial and final states (or possibly by a large angular momentum change in the decay, examples of which are discussed in the next section).

8.5 ANGULAR MOMENTUM AND PARITY IN α DECAY

We have up to this point neglected to discuss the angular momentum carried by the α particle. In a transition from an initial nuclear state of angular momentum I_i to a final state I_f, the angular momentum of the α particle can range between $I_i + I_f$ and $|I_i - I_f|$. The nucleus ^{4}He consists of two protons and two neutrons all in 1s states and all with their spins coupled pairwise to 0. The spin of the α particle is therefore zero, and the total angular momentum carried by an α particle in a decay process is purely orbital in character. We will designate this by ℓ_α. The α particle wave function is then represented by a $Y_{\ell m}$ with $\ell = \ell_\alpha$; thus the parity change associated with α emission is $(-1)^{\ell_\alpha}$, and we have a parity *selection rule*, indicating which transitions are permitted and which are absolutely forbidden by conservation of parity: if the initial and final parities are the same then ℓ_α must be even; if the parities are different, then ℓ_α must be odd.

To study the applications of these rules, we must recognize that we have also neglected one very significant feature of α decay—a given initial state can populate many different final states in the daughter nucl This property

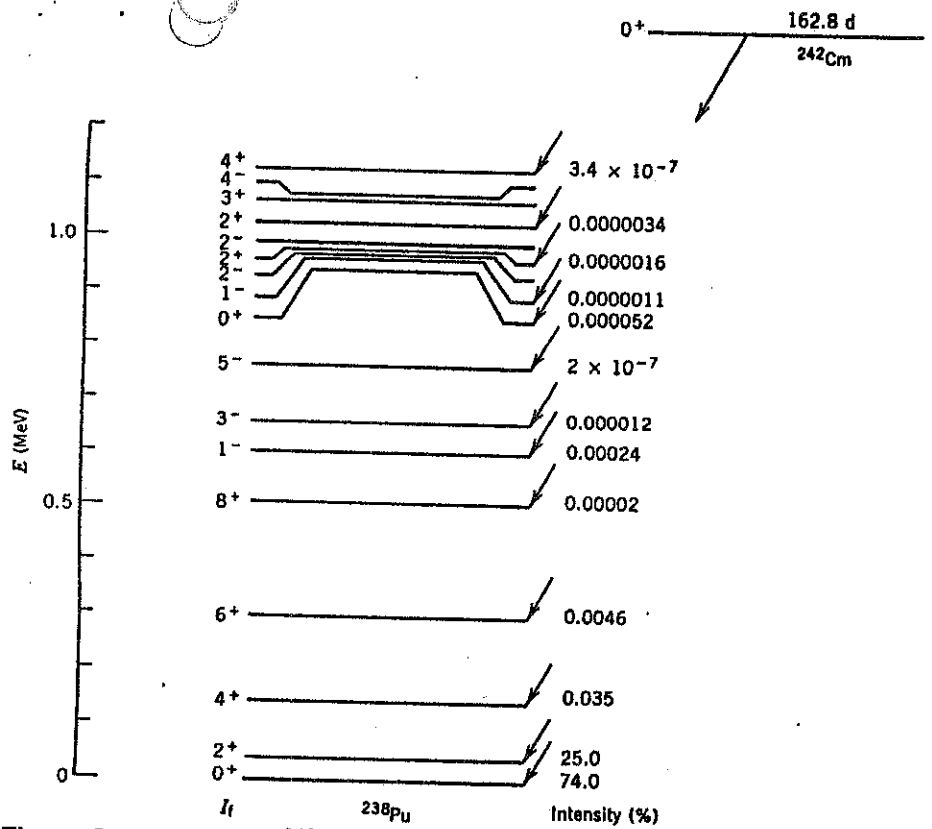

Figure 8.7 α decay of ^{242}Cm to different excited states of ^{238}Pu. The intensity of each α-decay branch is given to the right of the level.

sometimes known as the "fine structure" of α decay, but of course has nothing whatever to do with atomic fine structure. Figure 8.7 shows the α decay of ^{242}Cm. The initial state is spin zero, and thus the angular momentum of the α particle ℓ_α is equal to the angular momentum of the final nuclear state I_f. You can see that many different states of ^{238}Pu are populated. The α decays have different Q values (given by the Q value for decay to the ground state, 6.216 MeV, less the excitation energy of the excited state) and different intensities. The intensity depends on the wave functions of the initial and final states, and also depends on the angular momentum ℓ_α. In Equation 2.60, it was shown how the "centrifugal potential" $\ell(\ell+1)\hbar^2/2mr^2$ must be included in spherical coordinates. This term, which is always positive, has the effect of raising the potential energy for $a < r < b$ and thus increasing the thickness of the barrier which must be penetrated. Consider for example the 0^+, 2^+, 4^+, 6^+, and 8^+ states of the ground-state rotational band. The decay to the 2^+ state has less intensity than the decay to the ground state for two reasons—the "centrifugal potential" raises the barrier by about 0.5 MeV, and the excitation energy lowers Q by 0.044 MeV. The decay intensity continues to decrease for these same reasons as we go up the band to the 8^+ state. If we use our previous theory for the decay rates, taking into account the increasing effective B and decreasing Q, we obtain the following estimates for the relative decay branches: 0^+, 76%; 2^+, 2[illegible]; 4^+, 1.5%; 6^+, 0.077%; 8^+, 8.4×10^{-5}%. These results are not in exact agreement with the observed decay intensities, but they do give us a rough idea of the origin of the decrease in intensity.

Once we go above the ground-state band, the α decay intensities become very small, of the order of 10^{-6}% of the total decay intensity. This situation results from the poor match of initial and final wave functions—many of these excited states originate with vibrations or pair-breaking particle excitations, which are not at all similar to the paired, vibrationless 0^+ ground state of ^{242}Cm. You should note that there are some states for which there is no observed decay intensity at all. These include the 2^- states at 0.968 and 0.986 MeV, the 3^+ state at 1.070 MeV, and the 4^- state at 1.083 MeV. Alpha decay to these states is absolutely forbidden by the parity selection rule. For example, a $0 \rightarrow 3$ decay must have $\ell_\alpha = 3$, which must give a change in parity between initial and final states. Thus $0^+ \rightarrow 3^-$ is possible, but not $0^+ \rightarrow 3^+$. Similarly, $0 \rightarrow 2$ and $0 \rightarrow 4$

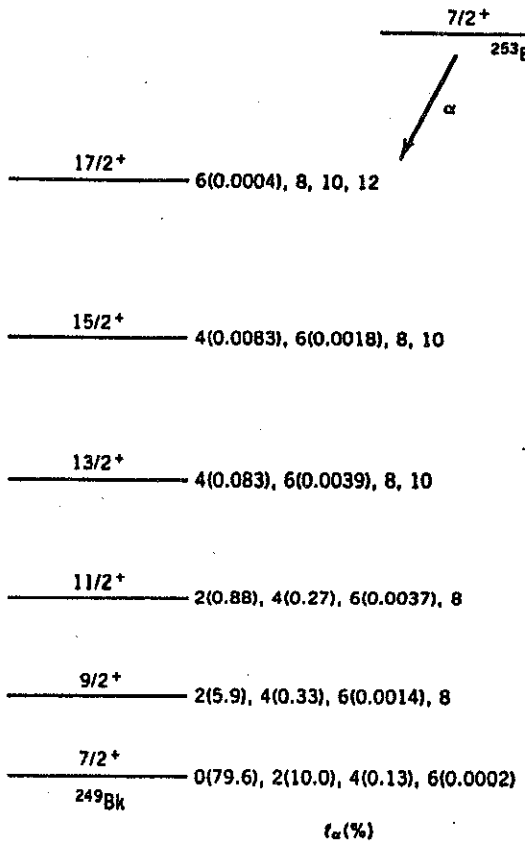

Figure 8.8 Intensities of various α-decay angular momentum components in the decay of ^{253}Es. For $\ell_\alpha = 8$ and higher, the intensities are not known but are presumably negligibly small. From the results of a study of spin-aligned α decays by A. J. Soinski et al., *Phys. Rev. C* 2, 2379 (1970).

decays cannot change the parity, and so $0^+ \rightarrow 2^-$ and $0^+ \rightarrow 4^-$ are not permitted.

When neither the initial nor the final states have spin 0, the situation is not so simple and there are no absolutely forbidden decays. For example, the decay $2^- \rightarrow 2^+$ must have odd ℓ_α (because of the change in parity), and the angular momentum coupling rules require $0 \leq \ell_\alpha \leq 4$. Thus it is possible to have this decay with $\ell_\alpha = 1$ or 3. The next question that occurs is whether $\ell_\alpha = 1$ or $\ell_\alpha = 3$ is favored and by how much. Our previous discussion would lead us to guess that the $\ell_\alpha = 1$ intensity is roughly an order of magnitude greater than the $\ell_\alpha = 3$ intensity. However, measuring only the energy or the intensity of the decay gives us no information about how the total decay intensity is divided among the possible values of ℓ_α. To make the determination of the relative contributions of the different ℓ values, it is necessary to measure the angular distribution of the α particles. The emission of an $\ell = 1$ α particle is governed by a $Y_1(\theta, \phi)$, while an $\ell = 3$ α decay is emitted with a distribution according to $Y_3(\theta, \phi)$. If we determine the spatial distribution of these decays, we could in principle determine the relative amounts of the different ℓ values.

To do this experiment we must first align the spins of our α-radioactive nuclei, such as by aligning their magnetic dipole or electric quadrupole moments in a magnetic field or in a crystalline electric field gradient. Keeping the spins aligned requires that the nuclei must be cooled to a temperature at which the thermal motion is not sufficient to destroy the alignment; generally temperatures below 0.01 K are required (that is, less than 0.01 degree above the absolute zero of temperature!).

As an example of such an experiment, we consider the decay of ^{253}Es to states of the ground-state rotational band of ^{249}Bk. The possible ℓ values are indicated in Figure 8.8, and the results of measuring the α-particle angular distributions help us to determine the relative contribution of the different values of ℓ_α.

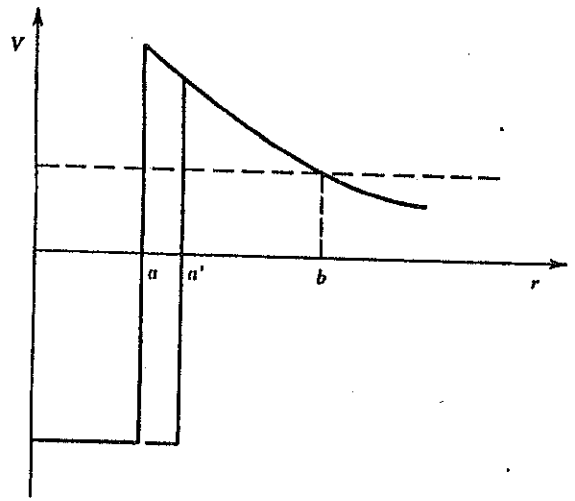

Figure 8.9 In a deformed nucleus, α particles escaping from the poles enter the Coulomb barrier at the larger separation a', and must therefore penetrate a lower, thinner barrier, therefore more probable to observe emission from the poles than from the equator.

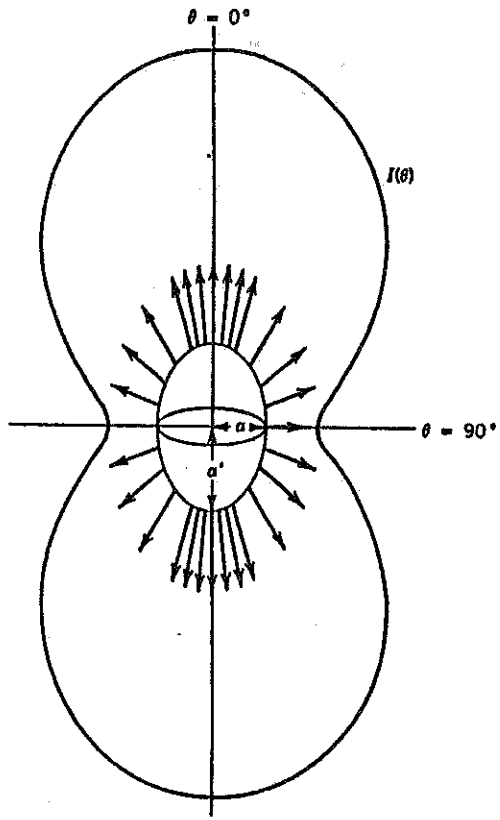

Figure 8.10 Intensity distribution of α particles emitted from the deformed nucleus at the center of the figure. The polar plot of intensity shows a pronounced angular distribution effect.

Since many α-emitting nuclei are deformed, these angular distribution measurements can also help us to answer another question: if we assume a stable prolate (elongated) nucleus, will more α's be emitted from the poles or from the equator? Figure 8.9 suggests a possible answer to this question: at the large radius of the poles, the α particle feels a weaker Coulomb potential and must therefore penetrate a thinner and lower barrier. We therefore expect that polar emission ought to be more likely than equatorial emission. Figure 8.10 shows the angular distribution of α emission relative to the symmetry axis. You can see that emission from the poles is 3–4 times more probable than emission from the equator, exactly as we expect on the basis of the potential.

8.6 α DECAY SPECTROSCOPY

The final topic in our discussion of α decay is this: What can we learn about the energy levels of nuclei by studying α decay?

Let's consider, for example, the 5.3-h decay of ^{251}Fm to levels of ^{247}Cf. (The levels of ^{247}Cf are also populated in the beta decay of ^{247}Es, but the half-life of that decay is so short, 4.7 min, that it is more difficult to use for a detailed probe of the level structure of ^{247}Cf.)

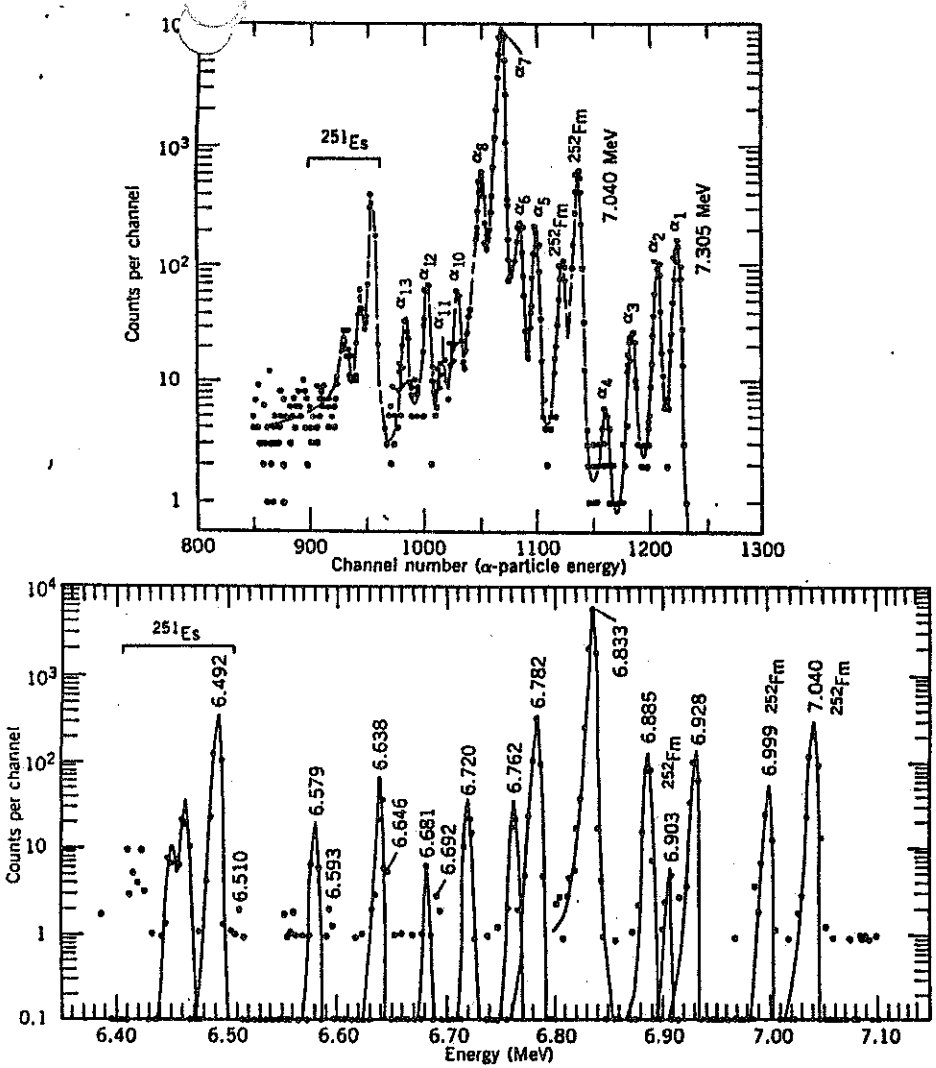

Figure 8.11 α spectrum from the decay of ^{251}Fm. The top portion shows the spectrum as observed with a Si detector. The bottom shows a portion of the same spectrum observed with a magnetic spectrometer, whose superior energy resolution enables observation of the 6.762-MeV decay, which would be missed in the upper spectrum. From Ahmad et al., *Phys. Rev. C* 8, 737 (1973).

Figure 8.11 shows the energy spectrum of α decays from the decay of ^{251}Fm. As you can see, there are 13 distinct groups of α particles; each group presumably represents the decay to a different excited state of ^{247}Cf. How can we use this information to construct the level scheme of ^{247}Cf? Based on the α spectrum, we first must find the energy and intensity of each α group. The energy is found by comparing with decays of known energy (the impurity decays from the ^{252}Fm contaminant are helpful for this) and the intensity is found from the area of each peak. The result of this analysis is shown in Table 8.3, along with the uncertainties that come mostly from the counting statistics for each peak. (Notice that the strongest peaks have the smallest *relative* uncertainties.) To find the decay energies (that is, the relative energies of the nuclear states), we must use Equation 8.7, since the measured α energies are only the kinetic energies. These are also shown in Table 8.3.

Table 8.3 α Decays from ^{251}Fm

α Group	α Energy (keV)	Decay Energy (keV)	Excited-State Energy (keV)	α Intensity (%)
α_1	7305 ± 3	7423	0	1.5 ± 0.1
α_2	7251 ± 3	7368	55	0.93 ± 0.08
α_3	7184 ± 3	7300	123	0.29 ± 0.03
α_4	7106 ± 5	7221	202	~ 0.05
α_5	6928 ± 2	7040	383	1.8 ± 0.1
α_6	6885 ± 2	6996	427	1.7 ± 0.1
α_7	6833 ± 2	6944	479	87.0 ± 0.9
α_8	6782 ± 2	6892	531	4.8 ± 0.2
α_9	6762 ± 3	6872	552	0.38 ± 0.06
α_{10}	6720 ± 3	6829	594	0.44 ± 0.04
α_{11}	6681 ± 4	6789	634	0.07 ± 0.03
α_{12}	6638 ± 3	6745	678	0.56 ± 0.06
α_{13}	6579 ± 3	6686	738	0.26 ± 0.04

The different ^{247}Cf excited states will quickly decay to the ground state by emitting γ-ray photons, so in constructing the decay scheme it is helpful to have the energies and intensities of the γ rays as well. Figure 8.12 shows the observed γ rays and Table 8.4 shows the deduced energies and intensities.

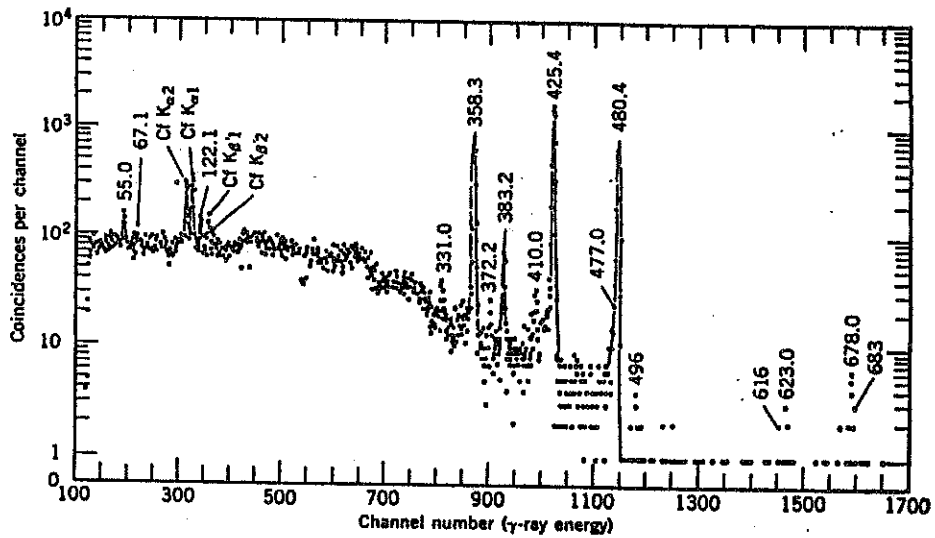

Figure 8.12 γ-ray spectrum of ^{251}Fm in coincidence with all α decays in the range 6.0 to 7.7 MeV. The spectrum was obtained with a Ge(Li) detector.

Table 8.4 γ Rays in ^{247}Cf following α Decay of ^{251}Fm

Energy (keV)	Intensity (% of decays)	Energy (keV)	Intensity (% of decays)
55.0 ± 0.2	0.58 ± 0.08	425.4 ± 0.1	51 ± 4
67.1 ± 0.2	0.28 ± 0.05	477.0 ± 0.3	0.54 ± 0.08
22.1 ± 0.2	0.28 ± 0.05	480.4 ± 0.1	21 ± 2
331.0 ± 0.3	0.35 ± 0.07	496 ± 1	~ 0.08
358.3 ± 0.1	17 ± 1.5	616 ± 1	~ 0.05
372.2 ± 0.4	0.25 ± 0.05	623.0 ± 0.8	0.07 ± 0.02
382.2 ± 0.3	1.2 ± 0.13	678.0 ± 0.8	0.26 ± 0.06
410.0 ± 0.3	0.50 ± 0.07	683 ± 1	~ 0.04

Now the detective work comes. Let's assume (and here we must be very careful, as we see in the next example) that the highest energy α decay populates the ground state of ^{247}Cf. (In an even-even nucleus, this would be a very good assumption, because $0^+ \rightarrow 0^+$ α decays are very strong and not inhibited by any differences between the wave functions of the initial and final nuclear states. In an odd-A nucleus, the initial and final ground states may have very different characters so that the decay to the ground state may be very weak or even vanishing.) The decay just lower in energy differs from the ground-state decay by about 55 keV. Assuming this to populate the first excited state, we are pleased to find among the γ transitions one of energy 55 keV, which presumably represents the transition between the first excited state and the ground state. The next α decay populates a state at 123 ± 3 keV above the ground state, and we find among the γ rays one of energy 122.1 keV, which corresponds to a transition from the second excited state to the ground state. We also find a transition of energy 67.1 (= 122.1 − 55.0) keV, which results from transitions between the second and first excited states.

Let's guess that these three states (with assumed energies 0, 55.0 keV, 122.1 keV) form a rotational band whose states, we recall from the discussion of odd-A deformed nuclei in Section 5.3, have angular momenta $I = \Omega, \Omega + 1, \Omega + 2, \ldots$, where Ω is the component of the angular momentum of the odd particle along the symmetry axis. The energy difference between the first excited state and ground state should then be

$$\Delta E_{21} \equiv E_2 - E_1 = \frac{\hbar^2}{2\mathcal{I}}[(\Omega + 1)(\Omega + 2) - \Omega(\Omega + 1)] = \frac{\hbar^2}{2\mathcal{I}} 2(\Omega + 1) \tag{8.19}$$

where we have used $E = (\hbar^2/2\mathcal{I})I(I + 1)$ for the energy of rotational states. Similarly, the difference between the ground state and second excited state is

$$\Delta E_{31} \equiv E_3 - E_1 = \frac{\hbar^2}{2\mathcal{I}}[(\Omega + 2)(\Omega + 3) - \Omega(\Omega + 1)] = \frac{\hbar^2}{2\mathcal{I}} 2(2\Omega + 3) \tag{8.20}$$

Combining these results with the experimental values, $\Delta E_{21} = 55.0$ keV and $\Delta E_{31} = 122.1$ keV, we conclude $\Omega = 3.5 \pm 0.2$ (that is, $\Omega = \frac{7}{2}$) and $\hbar^2/2\mathcal{I} = 6.11 \pm 0.02$ keV. These three states thus seem to form a rotational band with $I = \frac{7}{2}, \frac{9}{2}, \frac{11}{2}$. With our deduced values we can predict the energy of the $\frac{13}{2}$ state:

$$\Delta E_{41} = \frac{\hbar^2}{2\mathcal{I}}\left[\frac{13}{2}\cdot\frac{15}{2} - \frac{7}{2}\cdot\frac{9}{2}\right] = 201.6 \text{ keV}$$

and the $\frac{15}{2}$ state

$$\Delta E_{51} = \frac{\hbar^2}{2\mathcal{I}}\left[\frac{15}{2}\cdot\frac{17}{2} - \frac{7}{2}\cdot\frac{9}{2}\right] = 293.3 \text{ keV}$$

Apparently, the $\frac{11}{2}$ state is populated by the very weak α_4 decay, but its γ decays may be too weak to be seen in the spectrum of Figure 8.12. The decay to the $\frac{15}{2}$ state is not observed.

The interpretation of the remaining states is aided by α-γ coincidence studies, in which we electronically select only those γ transitions that follow a given α decay within a certain short time interval (in this case 110 ns). Since this time is long compared with typical lifetimes of nuclear states, all γ rays that follow the α decay will be recorded, even those that follow indirectly (such as the case in which two γ's are emitted in cascade, one following the other). The following coincidence relationships were observed:

Coincidence Gate	γ Rays (keV)
α_5	383.2
α_6	372.2, 383.2
α_7	55.0, 67.1, 122.1, 358.3, 425.4, 480.4
α_8	331.0, 358.3, 410.0, 425.4, 477.0, 480.4
α_{12}	623.0, 678.0

The decay α_5 goes to a state at 383.2 keV, which then goes directly to the ground state by emitting a single γ ray. The decay α_6 populates a state at about 427 keV. There is no coincident γ ray of that energy, which indicates no direct transition to the ground state, but there is a transition of energy 372.2 keV which, when added to 55.0 keV, gives 427.2 keV, very close to the energy of the state. We therefore conclude that this state, at 427.2 keV, decays to the first excited state at 55.0 keV. There is also a coincident transition at 383.2 keV, and thus this state at 427.2 keV must decay to the previously established state at 383.2 keV, by emitting a γ ray of energy 427.2 − 383.2 = 44.0 keV; this γ ray is not observed. The decay α_7 to the state at 480.4 keV shows decays to the ground state and to the 55.0 and 122.1 keV states (425.4 + 55.0 = 480.4; 358.3 + 122.1 = 480.4). Similarly, the decay α_8 to a state of 532.0 keV shows direct transitions to the lower states (331.0 + 201.0 = 532.0; 410.0 + 122.1 = 532.1; 477.0 + 55.0 = 532.0) but not directly to the ground state. It also shows coincident transitions that originate from the 480.4-keV level, so there must be a transition of energy 51.6 keV (= 532.0 − 480.4). In a similar fashion we analyze the other α and γ decays, and Figure 8.13 shows the resulting decay scheme.

For the states above the ground-state band, the assignment of spins and intrinsic angular momentum Ω is not as easy as it was for the states of the

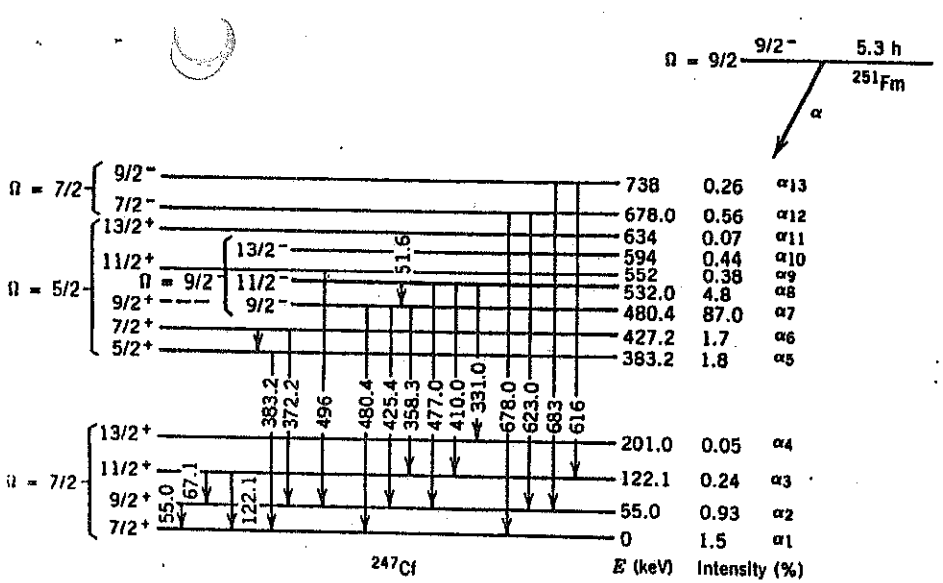

Figure 8.13 The decay scheme of ^{251}Fm to levels of ^{247}Cf deduced from α and γ spectroscopy. The spin assignments for the higher levels are deduced using γ-ray and internal conversion techniques described in Chapter 10.

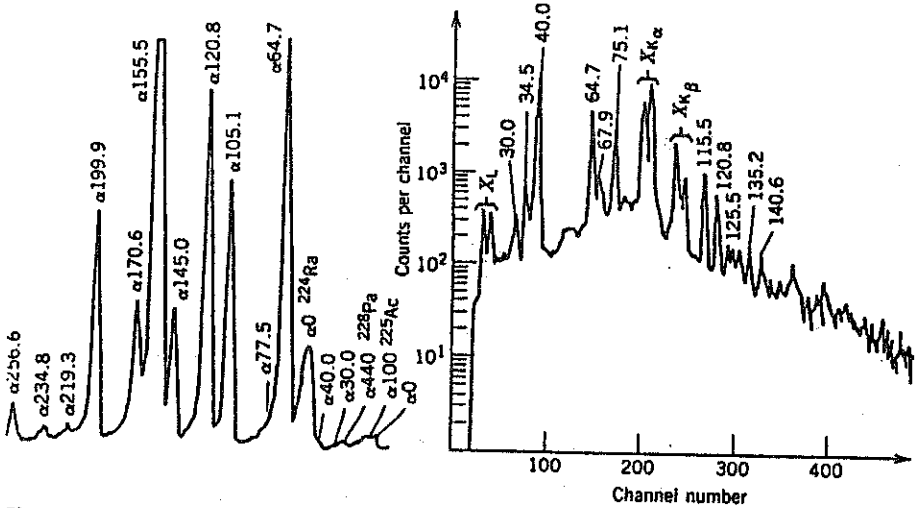

Figure 8.14 α (left) and γ (right) spectra from the decay of ^{229}Pa to ^{225}Ac. The α peaks are labeled according to the excited state populated in ^{225}Ac; thus α105.1 indicates the decay leading to the excited state at 105.1 keV. Prominent peaks from impurities are also indicated. The γ spectrum is taken in coincidence with all α's. From P. Aguer et al., *Nucl. Phys. A* **202**, 37 (1973).

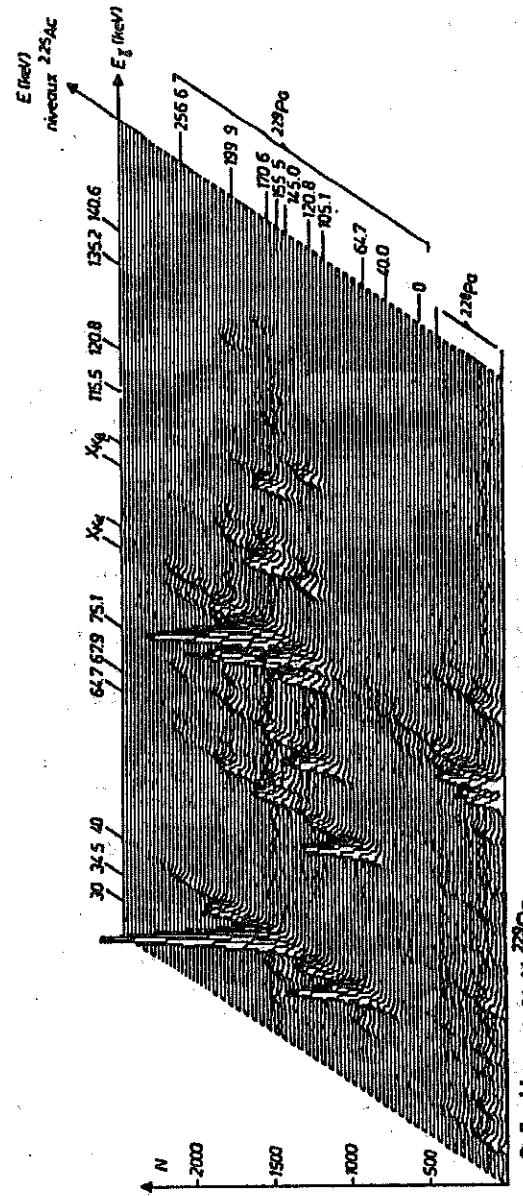

Figure 8.15 Three-dimensional (sometimes called two-parameter) representation of α-γ coincidences in the decay of ^{229}Pa. The horizontal axis shows γ-ray energies, labeled along the top. The oblique axis gives α-decay energies, labeled to indicate the ^{225}Ac state populated in the decay. The vertical axis gives the intensity of the coincidence relationship.

ground-state rotational band. To make these assignments, we need additional information from the γ decays; these measurements are discussed in Chapter 10.

Notice the strong α branch to the state at 480.4 keV. This occurs because the wave functions of the initial and final states are identical—both come from the same $\Omega = \frac{9}{2}$ deformed single-particle state—and the result is that more than 93% of the decay intensity goes to states of that so-called "favored" band. The observed decay rates can be compared with values calculated for various deformed single-particle states using the Nilsson wave functions, and in general there is good agreement between the measured and calculated results, both for the favored and unfavored decays. It is such comparisons between theory and experiment that allow us to assign the single-particle states because the intrinsic Ω and Nilsson assignments are not directly measurable.

The data for this discussion were taken from I. Ahmad, J. Milsted, R. K. Sjoblom, J. Lerner, and P. R. Fields, *Phys. Rev. C* 8, 737 (1973). Theoretical calculations of α transition amplitudes for states in even-A and odd-A deformed nuclei of the actinide region can be found in J. K. Poggenburg, H. J. Mang, and J. O. Rasmussen, *Phys. Rev.* 181, 1697 (1969).

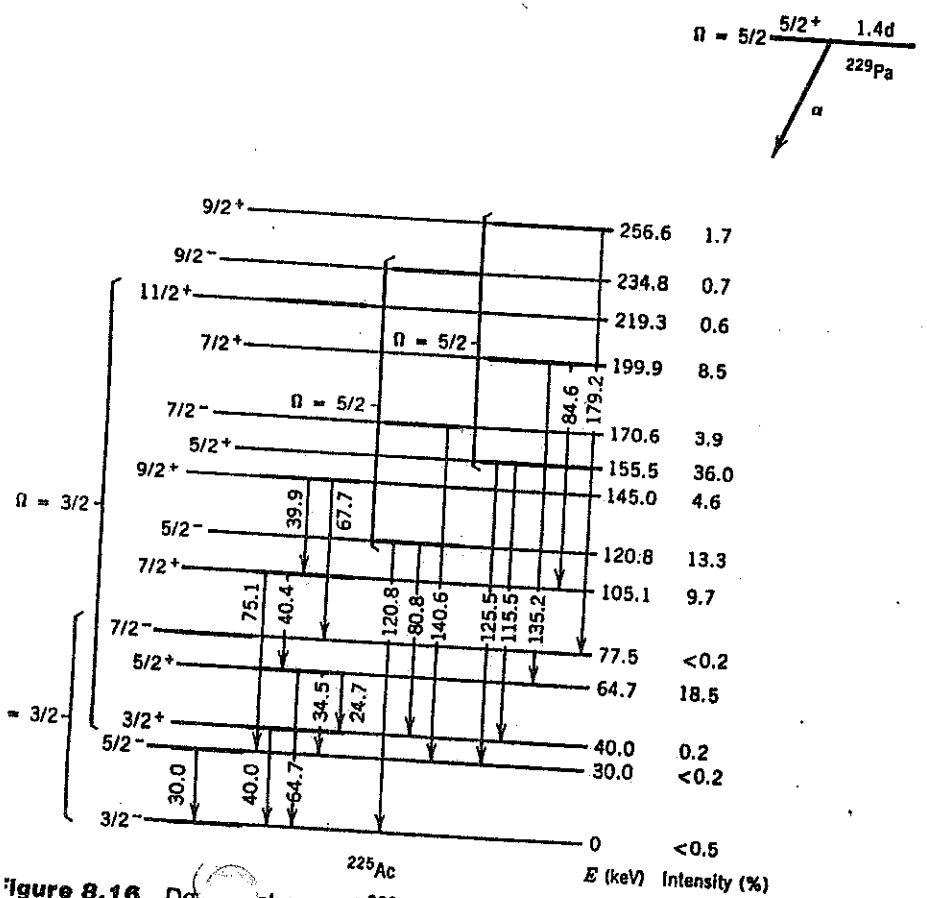

Figure 8.16 Decay scheme of ^{229}Pa deduced from α and γ spectroscopy.

Another example of the study of nuclear spectroscopy through α decay is illustrated in Figures 8.14–8.16. Figure 8.14 shows the α and γ spectra from the decay $^{229}\text{Pa} \rightarrow {}^{225}\text{Ac}$, and you can see that the decay to the ground state (labeled α_0) cannot be verified. Again, the α-γ coincidences help to elucidate the decay scheme, and a particularly instructive way to illustrate the coincidences is shown in Figure 8.15. Each peak in this three-dimensional spectrum represents a definite coincidence relationship between the α and the γ that label the axes. The information derived from the coincidence studies is used to make the decay scheme shown in Figure 8.16. Four rotational bands are identified in ^{225}Ac, positive and negative parity bands with $\Omega = \frac{1}{2}$ and $\frac{5}{2}$. The decaying ^{229}Pa is assigned $\frac{5}{2}^+$, so in this case the favored decay to the $\frac{5}{2}^+$ band in the daughter has about 46% of the decay intensity. The decay to the $\frac{1}{2}^-$ ground-state rotational band is strongly inhibited by the nuclear wave functions, resulting in the very weak (and possibly nonexistent) decay to the ground state. In this case it would lead to errors if we had assumed that the highest energy observed α group ($\alpha_{64.7}$, or $\alpha_{40.0}$ if we looked carefully) corresponded to transitions to the ground state.

The data for the ^{229}Pa decay come from P. Aguer, A. Peghaire, and C. F. Liang, *Nucl. Phys. A* 202, 37 (1973).

REFERENCES FOR ADDITIONAL READING

Somewhat more extensive discussions of α decay can be found in Chapter 16 of R. D. Evans, *The Atomic Nucleus* (New York: McGraw-Hill, 1955), and in Chapter 13 of I. Kaplan, *Nuclear Physics* (Reading, MA: Addison-Wesley, 1955). For surveys of α-decay theory, see H. J. Mang, *Ann. Rev. Nucl. Sci.* 14, 1 (1964), and J. O. Rasmussen, "Alpha Decay," in *Alpha-, Beta- and Gamma-Ray Spectroscopy*, edited by K. Siegbahn (Amsterdam: North-Holland, 1965), Chapter XI. A discussion of the use of α decay for nuclear spectroscopy is that of F. S. Stephens, in *Nuclear Spectroscopy*, part A, edited by F. Ajzenberg-Selove (New York: Academic, 1959), Section I.E.2.

PROBLEMS

1. Find the Q values of the following decays:
   (a) $^{247}\text{Bk} \rightarrow {}^{243}\text{Am} + \alpha$; (b) $^{251}\text{Cf} \rightarrow {}^{247}\text{Cm} + \alpha$; (c) $^{230}\text{Th} \rightarrow {}^{226}\text{Ra} + \alpha$.
2. For each decay given in Problem 1, calculate the kinetic energy and velocity of the daughter nucleus after the decay.
3. From the known atomic masses, compute the Q values of the decays:
   (a) $^{242}\text{Pu} \rightarrow {}^{238}\text{U} + \alpha$
   (b) $^{208}\text{Po} \rightarrow {}^{204}\text{Pb} + \alpha$
   (c) $^{208}\text{Po} \rightarrow {}^{196}\text{Pt} + {}^{12}\text{C}$
   (d) $^{210}\text{Bi} \rightarrow {}^{208}\text{Pb} + {}^{2}\text{H}$
4. In the decay of ^{242}Cm to ^{238}Pu, the maximum α energy is 6112.9 ± 0.1 keV. Given the mass of ^{238}Pu, find the mass of ^{242}Cm.
5. The highest energy α particle emitted in the decay of ^{238}U to ^{234}Th is 4196 ± 4 keV. From this information and the known mass of ^{238}U, compute the mass of ^{234}Th

Simple relation for alpha decay half-lives

B. Alex Brown
National Superconducting Cyclotron Laboratory
and Department of Physics and Astronomy, Michigan State University, East Lansing, Michigan 48824
(Received 23 March 1992)

The experimental values of $\log_{10}T_{1/2}$(sec) plotted vs $Z_d^{0.6}/\sqrt{Q_\alpha}$ are shown to fall on a nearly universal straight line with $\log_{10}T_{1/2}(\text{sec})=(9.54Z_d^{0.6}/\sqrt{Q_\alpha})-51.37$, where Z_d is the charge number of the daughter nucleus and Q_α is expressed in units of MeV. This behavior also numerically comes out of the semiclassical WKB calculation of the barrier penetration factor. The fine structure in the ratio of experiment over theory is briefly discussed.

PACS number(s): 23.60.+e

The earliest law for the systematics of α decay lifetimes was formulated by Geiger and Nuttall [1]. This was the observation that $\log_{10}T_{1/2}$(sec) plotted vs $1/\sqrt{Q_\alpha}$, where Q_α is the α decay Q value, empirically formed straight lines for a series of nuclei with the same charge number. In Fig. 1(a), I show a modern version of this plot for the $J_i^\pi=J_f^\pi=0^+$ α decay data tabulated in Ref. [2]. There are 119 data points for a range of Z_d from 74 to 106, where Z_d is the charge number of the daughter nucleus. Even though the data for a given Z_d value fall on roughly a straight line, there is a large scatter between the lines for different Z_d values.

It is well known that this trend can be understood in terms of the semiclassical approximation for the decay rate

$$W=PW_cT\ , \tag{1}$$

where P is the preformation probability, W_c is the collision rate of the α particle with the nuclear surface, and T is the barrier penetration factor given for $l=0$ decays in the WKB approximation by

$$T=\exp\left\{-2\int_{R_t}^{R_c}\sqrt{2\mu[V(r)-Q_\alpha]/\hbar^2}dr\right\}\ . \tag{2}$$

In this expression R_t is the "touching" radius. $R_t=R_\alpha+R_d$, where R_α and R_d are the hard-sphere radii for the α and daughter nuclei, respectively. The potential is given by $V(r)=Z_\alpha Z_d e^2/r$, where $Z_\alpha=2$, and R_c is the classical turning point, $R_c=Z_\alpha Z_d e^2/Q_\alpha$. The reduced mass is $\mu=M_\alpha M_d/(M_\alpha+M_d)$. Equation (2) can be integrated exactly to give

$$T=\exp\{-2Z_\alpha Z_d e^2\sqrt{2\mu/Q_\alpha\hbar^2}\times[\cos^{-1}(x)-x\sqrt{1-x^2}]\}\ , \tag{3}$$

where $x=\sqrt{R_t/R_c}$. The last part of Eq. (3) can be expanded in a power series in x:

$$\cos^{-1}(x)-x\sqrt{1-x^2}=(\pi/2)-2x+x^3/3-\cdots\ . \tag{4}$$

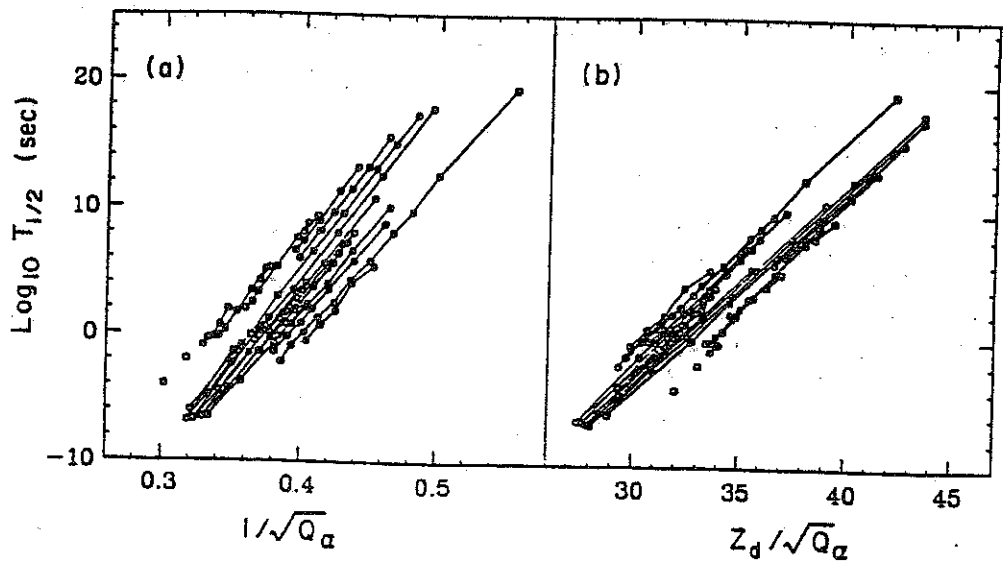

FIG. 1. (a) On the left-hand side, the experimental values for $\log_{10}T_{1/2}$(sec) are plotted vs $1/\sqrt{Q_\alpha}$, where the data for $T_{1/2}$ and Q_α are taken from Ref. [2]. (b) On the right-hand side, the experimental values for $\log_{10}T_{1/2}$(sec) are plotted vs $Z_d/\sqrt{Q_\alpha}$. The points for a given value of Z_d are connected by lines.

 ©1992 The American Physical Society

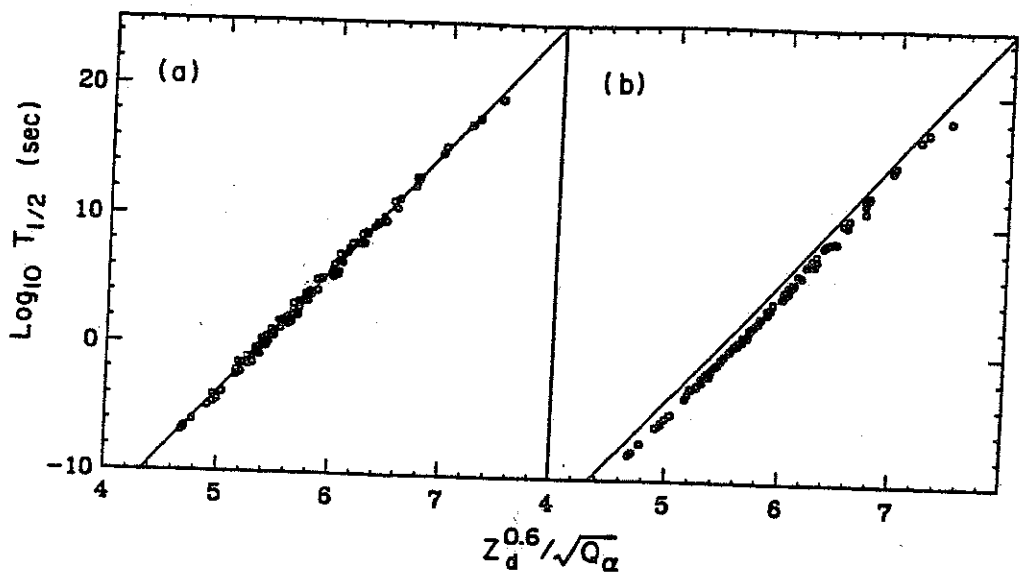

FIG. 2. (a) On the left-hand side, the experimental values for $\log_{10}T_{1/2}(\text{sec})$ are plotted vs $Z_d^{0.6}/\sqrt{Q_\alpha}$. The straight line represents a best fit to the data. (b) On the right-hand side, the theoretical values for $\log_{10}T_{1/2}(\text{sec})$ from Eq. (1) are plotted vs $Z_d^{0.6}/\sqrt{Q_\alpha}$ and compared to the best fit line from (a).

The x^3 term is often dropped in the discussion of this expansion, but it is important at the level of about 1 order of magnitude in the half-life. The next-order term in x^5 is not important at the present level of experimental and theoretical uncertainty. The barrier penetration factor in terms of the power series expansion is

$$T=\exp\left[-2\sqrt{2\mu/\hbar^2}\left[\frac{\pi Z_\alpha Z_d e^2}{2\sqrt{Q_\alpha}}-2\sqrt{Z_\alpha Z_d e^2 R_t}+\frac{Q_\alpha R_t^{3/2}}{3\sqrt{Z_\alpha Z_d e^2}}\right]\right]. \quad (5)$$

The original Geiger-Nuttall rule emerges from the first term in this expansion together with the fact that the second term does not depend on Q_α. Further, as previously noted [3], this result suggests that $\log_{10}T_{1/2}(\text{sec})$ vs $Z_d/\sqrt{Q_\alpha}$ may be a better way to plot the data. The result is shown in Fig. 1(b), where the data again form lines for a fixed Z_d value, and where the scatter as a function of Z_d is somewhat less than in Fig. 1(a). The scatter in Figs. 1(a) and 1(b) is due mainly to the second term on the left-hand side of Eq. (5).

Here I point out that there is an interesting interpolation between Figs. 1(a) and 1(b). Namely, if one plots $\log_{10}T_{1/2}$ vs $Z_d^{0.6}/\sqrt{Q_\alpha}$ as shown in Fig. 2(a), the points fall on a nearly universal straight line. Also shown in this figure is a straight line which represents a best fit to the data. It is given by

$$\log_{10}T_{1/2}(\text{sec})=(9.54Z_d^{0.6}/\sqrt{Q_\alpha})-51.37\ ,$$

where Q_α is expressed in units of MeV. The rms deviation of the experimental values of $\log_{10}T_{1/2}(\text{sec})$ from this straight line is 0.33. The rms deviation of the straight-line fit as a function of the power of Z_d is shown in Fig. 3 and is seen to have a sharp minimum at a value of about 0.6.

It is not obvious that this should follow from Eq. (1); however, numerically it does. In Fig. 2(b) I show $\log_{10}T_{1/2}(\text{sec})=\log_{10}(\ln 2/W)$ vs $Z_d^{0.6}/\sqrt{Q_\alpha}$, where W is calculated from Eq. (1) and the experimental Q_α are used. The theoretical results are compared to the best-fit line from Fig. 2(a). I have used $P=1$, $R_\alpha=2.15$ fm, $R_d=r_0A_d^{1/3}$, with $r_0=1.2$ fm, and the classical value for W_c given by

$$W_c=(1/2R_t)\sqrt{2Q_\alpha/\mu}\ , \quad (6)$$

which follows from the classical motion of an α particle in the nucleus in a potential $V(r)=0$ for $r<R_t$. [The results are, however, relatively insensitive to the value assumed for $V(r)$ inside the nucleus.] The radii R_α and R_d used above are the uniform sphere radii which are related to the rms charge radii r_{ch} by $R=\sqrt{5/3}r_{ch}$ ($r_{ch}=1.67$ fm for the α particle). The theoretical points from the semi-

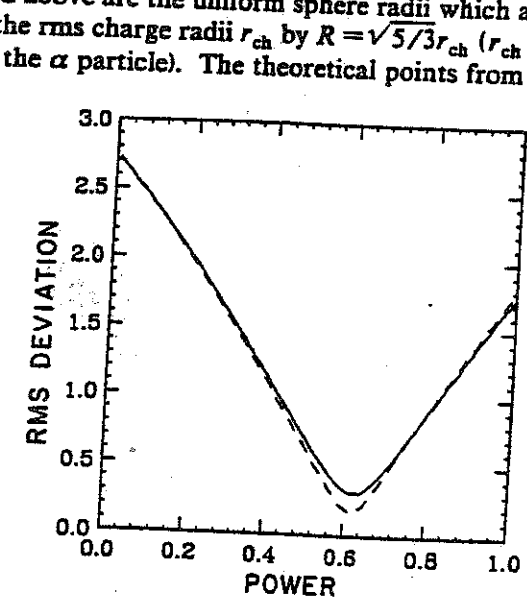

FIG. 3. rms deviation of the straight-line fit to $\log_{10}T_{1/2}(\text{sec})$ vs $Z_d^x/\sqrt{Q_\alpha}$ as a function of the power x. The solid line is the fit to the experimental data and the dashed line is the fit to the semiclassical WKB calculation.

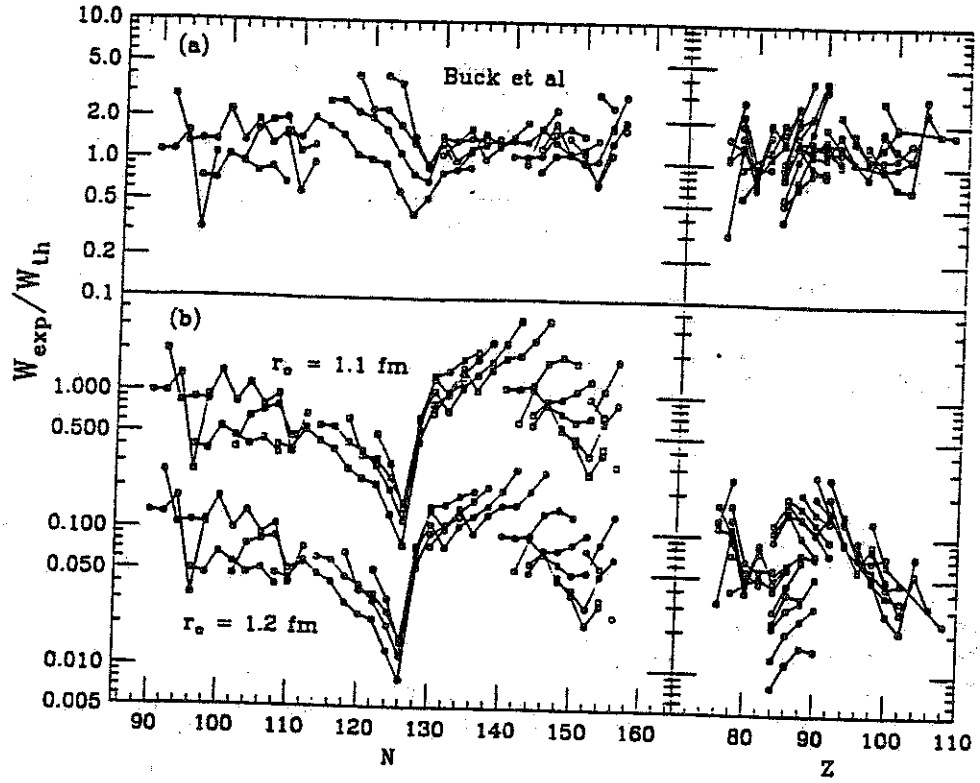

FIG. 4. (a) On the top, the ratio of the experimental and theoretical decay rate for α decay (circles) is shown with the theoretical decay rate taken from Ref. [2]. On the left-hand side the points are plotted vs neutron number $N=N_d+2$, and those for a given proton number $Z=Z_d+2$ are connected by a line. On the right-hand side the points are plotted vs Z, and those for a given N value are connected by a line. (b) On the bottom, the ratio of the experimental and theoretical decay rate for α decay is shown with the theoretical decay rate obtained from the present calculations with $r_0=1.2$ fm (circles) and $r_0=1.1$ fm (squares).

classical WKB approximation follow the straight-line dependence even a little better than the data (rms=0.20, see Fig. 3).

The deviation between experiment and theory can be seen in more detail in the usual way [4] by plotting the preformation factor P, as deduced from the ratio of the experimental and theoretical decay rates versus neutron and proton number as in Fig. 4(b). The well-known fine structure in P vs neutron number N can easily be seen with the dominant effect being a dip to $P=0.01$ at $N=126$. The top set of points in Fig. 4(b) obtained with a value of $r_0=1.1$ fm illustrates the strong correlation between r_0 and P. The decrease in P at $N=126$ is correlated with a decrease in the measured rms charge radii at $N=126$ [5]. However, the radius variation is only about 2%, whereas a dip of 1 order of magnitude in P would require about a 10% radius change if this were the only thing responsible. Buck, Merchant, and Perez [2] have postulated that the radius to be used for R_t should be determined not from the charge radius but by the Bohr-Sommerfeld condition for an α-particle wave function inside the nucleus with a fixed well depth and a fixed number of nodes. In addition, they postulate that there is a 10% increase in the number of nodes at $N=126$ due to the change of valence shell structure. This increases the radius by 10% and thus accounts for the discontinuity at $N=126$. The P values obtained from their assumption about R_t as shown in Fig. 4(a) show about a factor of 2–3 improvement in the scatter, and the discontinuity at $N=126$ is mostly accounted for.

Another way to interpret the results of Buck *et al.* is to relate R_t for the α cluster to the radius of the valence orbits. There is about a 10% increase in the rms radius of the valence neutrons when they change from the $(0h_{9/2},1f_{7/2},1f_{5/2},2p_{3/2}2p_{1/2},0i_{13/2})$ major shell below $N=126$ to the $(0i_{11/2},1g_{9/2},1g_{7/2},2d_{5/2},2d_{3/2}3s_{1/2},0j_{15/2})$ major shell above $N=126$. There should be a similar effect when the valence protons cross $Z=82$. The empirical Z dependence is shown on the right-hand side of Fig. 4. The lines which cross $Z=82$ are for neutron numbers around ^{194}Pb ($N=112$) and surprisingly do not show a discontinuity at $Z=82$, perhaps because $Z=82$ is not a good magic number for these very light Pb isotopes. Other lines on the right-hand side of Fig. 4 start at $Z=84$ (the Po isotopes) and show about the same trend from $Z=84$ to 90 as for the neutron points between $N=128$ and 140 on the left-hand side of Fig. 4. Thus, in summary, the comparison in Fig. 4(b) indicates a discontinuity in both N and Z centered only on the doubly magic nucleus ^{208}Pb. The orbit occupations of the valence protons and neutrons also influence the amount of proton-neutron correlation and hence the preformation probability. Quantitative calculations based on microscopic models have been difficult and controversial [6] and have thus far been limited mainly to the one case ^{212}Po α decay.

In summary, I have shown that the experimental values of $\log_{10}T_{1/2}(\text{sec})$ plotted vs $Z^{0.6}/\sqrt{Q_\alpha}$ fall on a nearly universal straight line. These systematics

should be useful for extrapolations to more exotic nuclei and to superheavy nuclei. I also have shown that this behavior comes out numerically from the semiclassical WKB approximation. It may be useful to consider whether or not there is any simpler underlying physical interpretation of this simple functional dependence of the decay rate on Z_d.

Note added in proof. Other simple relations have been proposed, which are similar in spirit to mine but not the same in form. These are summarized in Ref. [7]. In particular, the form of Wapstra *et al.* [8] can be fitted to the data set considered here with the result $\log_{10}T_{1/2}(\text{sec})=[(1.001Z_d+51.89)/\sqrt{Q_\alpha}]-51.37$, with an rms deviation of 0.31. The form of Taagepera and Nurmia [9] and Keller and Munzel [10] can be fitted to the data set considered here with the result, $\log_{10}T_{1/2}(\text{sec})=1.598[(Z_d/\sqrt{Q_\alpha}-Z_d^{2/3}]-19.94$, and with an rms deviation of 0.33.

This work was supported in part by U.S. National Science Foundation Grant No. PHY-90-17077.

[1] H. Geiger and J. M. Nuttall, Philos. Mag. 22, 613 (1911); H. Geiger, Z. Phys. 8, 45 (1921).
[2] B. Buck, A. C. Merchant, and S. M. Perez, Phys. Rev. Lett. 65, 2975 (1990); J. Phys. G 17, 1223 (1991).
[3] For example, S. S. M. Wong, *Introductory Nuclear Physics* (Prentice-Hall, Englewood Cliffs, NJ, 1990).
[4] For example, K. S. Toth *et al.*, Phys. Rev. C 45, 856 (1992); Y. Hatsukawa, H. Nakahara, and D. C. Hoffman, *ibid.* 42, 574 (1990).
[5] B. A. Brown, C. R. Bronk, and P. E. Hodgson, J. Phys. G 10, 1683 (1984).
[6] T. Fliessbach and S. Okabe, Z. Phys. A 320, 289 (1985); A. Watt, D. Kelvin, and R. R. Whitehead, J. Phys. G 6, 31 (1980); I. Tonozuka and A. Arima, Nucl. Phys. A323, 45 (1979).
[7] D. N. Pomenaru and M. Ivascu, J. Phys. (Paris) 44, 791 (1983).
[8] A. H. Wapstra *et al.*, in *Nuclear Spectroscopy Tables* (North-Holland, Amsterdam, 1959).
[9] R. Taagepera and M. Nurmia, Ann. Acad. Sci. Fenn. Ser. A78 (1961).
[10] K. A. Keller and H. Z. Munzel, Z. Phys. 255, 419 (1972).